Diffusie-MRI-biomerkers voor cognitieve training
in een ratmodel voor mild traumatisch hersenletsel

Towards Diffusion MRI Biomarkers for Cognitive Training
in a Mild Traumatic Brain Injury Rat Model

Kim Braeckman

Promotoren: prof. dr. C. Vanhove, dr. B. Descamps, prof. dr. K. Caeyenberghs
Proefschrift ingediend tot het behalen van de graad van
Doctor in de ingenieurswetenschappen: biomedische ingenieurstechnieken

UNIVERSITEIT
GENT

Vakgroep Elektronica en Informatiesystemen
Voorzitter: prof. dr. ir. K. De Bosschere
Faculteit Ingenieurswetenschappen en Architectuur
Academiejaar 2018 - 2019

ISBN 978-94-6355-277-6
NUR 954
Wettelijk depot: D/2019/10.500/85

Department of Electronics and Information Systems
Faculty of Engineering and Architecture
Ghent University

UNIVERSITEIT
GENT

Infinity Lab - MEDISIP
Corneel Heymanslaan 10
Entrance 36, floor 5
9000 Ghent
Belgium

Promotors
prof. dr. ir. Christian Vanhove
dr. Benedicte Descamps
prof. dr. Karen Caeyenberghs

Examination board
prof. dr. ir. Gert De Cooman, Universiteit Gent, *chairman*
prof. dr. ir Roel Van Holen, Universiteit Gent, *secretary*
prof. dr. Karel Deblaere, Universiteit Gent
prof. dr. Guy Vingerhoets, Universiteit Gent
prof. dr. Alexander Leemans, Universitair Medisch Centrum Utrecht
dr. Stephan Missault, Universiteit Antwerpen

Dankwoord

Het duurt nog een half vooraleer mijn trein toekomt (*die uiteraard niet op tijd rijdt maar al zeker vijf minuten vertraging heeft*) en gisteren heb ik mijn interne verdediging tot een goed eind gebracht. De treinrit van Aken naar Gent zal toch een goede twee uur duren en ik heb mijn gsm thuis vergeten. Een ideaal moment lijkt mij, om eens te mijmeren, terug te kijken op vier jaar doctoraal onderzoek en te overlopen aan wie ik dat allemaal te danken heb.

Professor Christian Vanhove en doctor Benedicte Descamps, of gewoon Chris en Bene voor de vrienden en zoals iedereen jullie kent. Ik zal nooit vergeten hoe de eerste kennismaking met jullie en het project verliep. Tijdens een voor jullie superdrukke dag, stond ik rond lunchtijd aan de deur (*ding dong ding dong, dong dong ding ding* – dat typische belgeluid dat ik ondertussen al uit de duizend herken). En dus, letterlijk tussen de soep en de patatten stelden jullie mij het project voor en maakten mij warm om dit onderzoek te beginnen. Op het einde van onze meeting kreeg ik een uitgebreide rondleiding in het labo van Chris die heel gepassioneerd vertelde (en echt bij elke rondleiding opnieuw) welke onderzoeken zoal lopen bij elk type scanner. Toen ik terug buiten stond wist ik het meteen: in een labo waar zo een ongedwongen vibe hangt wil ik graag werken. En zo geschiede. **MERCI**, Chris en Bene dat jullie in mij geloofden en deze kans aanboden, **MERCI**! Het deed ook telkens zoveel deugd te weten dat ik jullie nooit een vraag teveel kon stellen. Bene, je hebt een engelengeduld waar ik echt jaloers op ben. Steeds opnieuw zal je met een brede glimlach al mijn vragen beantwoorden. En Chris, het is zo fijn dat wanneer ik (en elke andere onderzoeker op Infinity) vraag of je straks eens even tijd hebt, je altijd antwoordt

met: *"Ja hoor, ... anders nu?"* Daarom nog eens, **MERCI**! Naast Chris en Bene is er ook Professor Karen Caeyenberghs die het project heeft uitgeschreven en ondertussen naar Australië is verhuisd. Karen, hoewel onze eerste kennismaking via skype verliep merkte ik al meteen dat ook jij steeds met veel enthousiasme klaar zou staan om mijn vragen te beantwoorden en met veel geduld en kritische blik mijn papers zou nalezen. Daarom, **MERCI**, om ondanks de groooooooooooote afstand en het groooooooooooote tijdsverschil steeds bereikbaar te zijn vanuit Melbourne, **MERCI**!

Naast de drie promotoren stonden er natuurlijk ook tal van collega's klaar voor de nodige input... en output! Eens goed ventileren als het niet goed gaat is o zo belangrijk. Ik denk dat Inge en de bureaus aan de andere kant van de gang wel af en toe eens zullen gedacht hebben *"Oei oei, is alles daar wel ok?"* bij het herhaaldelijk horen van *"G*dverdoeme hé"*. Langs de andere kant waren er vaak koffie (*Euhnee! Ik bedoel natuurlijk*) research breaks met de PhD studenten. Hier werd er (wel degelijk) over ons onderzoek gediscussieerd maar steeds met een lekkere taart of zelfgemaakte koekjes erbij. Zo zal ik ook nooit vergeten hoe Mariele – uit Duitsland – een alternatieve methode voor euthanasie voorstelde die gebruikt maakt van gas. Je begrijpt wel dat er nadien niet veel serieuze vragen meer kwamen en we nog de hele namiddag gelachen hebben. Further, I would like to thank all the (former) PhD students at MEDISIP who, although I do not thank them explicitly, were certainly not less important during the last 4 years. **MERCI**, Nathalie, Carmen, Lara, Ester, Stijn, Willeke, Thibault, Radek, Jens, Prakash, Gwenaëlle, Mariele, Paulo, Emma, Tim, Milan, Jolan, Marec and Charlotte for being my colleagues, **MERCI**! And for the ones who still need to finish their book and PhD: do not panic, it will all be ok and I'm convinced it will be fabulous! Also, Paulo, I wish you all the best with your very soon to be born daughter. I'm so happy for you! Maar in het bijzonder wil ik zeker mijn bureaugenootjes bedanken. Willeke, Thibault en Jens: the first generation. Bij jullie kwam ik terecht toen het in de kelder van Infinity toch een beetje te eenzaam was en ik heb zeker nooit spijt gehad van deze 'verhuis'. Jens, je bent een spraakwaterval waarbij gênante stiltes nooit of te nimmer voorvallen. Ik vind het ook geweldig grappig om je te zien giechelen vanuit mijn linkerooghoek telkens je een grappig

filmpje bekijkt of sms ontvangt. Hoewel je niet vaak aanwezig was in onze bureau had je toch de gave om je aanwezigheid zeker niet ongemerkt te laten en iedereen aan te steken met je positivisme en gewoon algemene leutigheid. Willeke, je bent nu al even weg maar ik weet nog dat ik zeer blij was dat jij ook naar OHBM in Vancouver zou gaan. Mijn eerste grote congres en dan nog eens aan de andere kant van de wereld. Want met twee is altijd leuker dan alleen. Ik weet ook nog hoe jaloers we waren dat onze beide lieven een upgrade hadden gekregen naar business class toen ze na het congres over kwamen gevlogen en wij ocharme negen uur in het middelste stoeltje van economy class hadden gezeten. Thibault, hoewel ik zeker niet alles begreep van je onderzoek vond ik het echt inspirerend hoe jij op zo een rustige manier en met warme vertelstem je onderzoek zo begrijpelijk kon uitleggen. Het was echt een plezier om naar jou te luisteren en je hebt de lat voor ons – de achterkomers – hoger gelegd. Ik hoop dat ik het tijdens mijn verdediging vandaag even goed doe. En dan de bureaugenoten: the next generation. (*Vreemd genoeg doet dit me denken aan Pokémon en Jens die iedereen op het labo aanstak om Pokémons te vangen op het UZ. Wat doe je anders op vrijdag namiddag, hé?*) Emma, ik was erg blij dat er iemand het preklinisch team kwam versterken en jij je ook in het diffusiewereldje stortte. Ik denk dat we samen die tractografiepipeline toch goed hebben uitgewerkt (en dit zonder de servers te doen crashen). Ik wens je nog heel veel succes met de verwerking van de talrijke diffusiedatasets en weet dat je echt iets geweldig mooi zal maken van je werk. Milan, het spijt mij om te moeten toegeven dat ik nog steeds niks begrijp van neural networks en artificial intelligence, ook al leg je het bij iedere presentatie zo bevattelijk mogelijk uit. Trouwens, ging er geen workshop komen? (*knipoog knipoog*). Maar ik ben ervan overtuigd, met die fancy game (*euh*) research computer van jou zal je nog zotte dingen doen en zeer mooie resultaten creëren. Tim, ik weet dat je binnenkort je presentatie moet geven om een FWO beurs te halen en na het luisteren van je proefpresentatie ben ik zeker dat jij "the right man in the right place" bent. Suuuuuuperveel succes gewenst en go get 'em tiger! En dan, mijn metekindje, Jolan, jou kan ik toch niet vergeten. En de vele koffietjes die je drinkt. En het feit dat jij Charlotte uit 'den andere bureau' altijd aantrekt waardoor iedereen zijn concentratie plots weg is (mopje hé Charlotte, ik ben zeer blij dat jij in mijn team zit en zal blijven zitten!). **MERCI**, nog eens om in mijn team

te zitten, **MERCI**! Saskia en Inge, **MERCI**, om het administratieve PhD leven zoveel gemakkelijker te maken. En Jurgen, **MERCI**, om mij van zo een mooi TBI model te voorzien. Ik denk dat het nog vele jaren dienst zal kunnen doen. Tot slot wil ik ook nog de collega's aan 'den overkant van de gang' of te Biomedda bedanken. **MERCI**, voor de vele leuke geanimeerde discussies tijdens de middagpauzes.

Omdat Infinity zoveel verschillende onderzoeksdisciplines samenbrengt had ik ook vele collega's buiten MEDISIP. **MERCI**, Sara, Nick, Stef, Jeroen, Glenn, Tristan, Tessa en Sarah van de Radiofarmacie, Valerie van de Radiologie en Julie en Sam van Nucleaire Geneeskunde, **MERCI**! De dagen dat we allemaal in het labo druk scanden en er dus veel leven in de brouwerij was, waren er van de leukste maar ook buiten het labo heb ik zoveel onvergetelijke momenten beleefd tijdens sportdagen, etentjes, drinks of congressen. En ik hoop dat jullie nog weten: "What happens in San Sebastian, stays in San Sebastian". Maar ik wil jullie ook oprecht bedanken omdat ik tijdens mijn trainingsexperimenten op jullie kon rekenen: voor het wegen en eten geven van de ratjes tijdens het weekend en omdat jullie bereid waren te assisteren bij het induceren van de milde TBI. Verder wil ik ook Sara in het bijzonder bedanken want het is dankzij jou dat ik Infinity ben binnengerold en de kans heb gekregen om verder te doctoreren. Ik vond onze samenwerking altijd heel fijn en ben dan ook erg blij om deze samenwerking binnenkort verder te zetten bij Molecubes.

Ook wil ik mijn thesisstudenten Arne, Sam, Hannah en Ine bedanken voor hun hulp tijdens experimenten. Wat heb ik geluk gehad om zo een gemotiveerde studenten te mogen begeleiden.

Gelukkige heb ik naast al mijn fantastische collega's ook heel wat vrienden die steeds klaarstaan en die ik hier graag wil bedanken. Stijn, fantastisch gewoon dat we al sinds dag 1 in het middelbaar (en dus al ruim 15 jaar) steeds bij mekaar terecht kunnen voor vragen over lessen, practica, problemen tijdens experimenten,... Hoewel jij de immunologie richting uitging (iets wat mij niet zo ligt, *"help hoe zat dat nu weer met die T- en B-cellen?!"*) heb ik altijd met heel veel interesse geluisterd naar jouw onderzoek tijdens onze lunchpauzes op het UZ. Of

natuurlijk naar de frustraties van onderzoek, het vallen en opstaan, ... Maar ook de totaal absurde van de pot gerukte conversaties blijven echt een van mijn favoriete lunch momentjes. Kaat, Eve, Jelle, Yarne en Stijn of beter gekend als de facebookgroep 'NOg ter discussie'. Wat is het heerlijk om een groep te hebben waar je je niet moet generen voor het maken van typfouten of andere persoonlijke 'flaws' (*ik zal maar zwijgen over Kathedralen zeker...?*). Waar 'soel soel' en 'poepers' gekende termen zijn, feestjes in Ibiza zeker nooit saai zijn en je nooit 'Sorry voor alles' moet zeggen. **MERCI**, om die zot samengestelde bende te zijn, **MERCI**! Misschien weet niet iedereen dit maar ik heb ook al een lange Chirocarrière achter de rug. En daarbij mag ik echt terugkijken op enorm mooie momenten met enorm mooie mensen. Jullie hier daarvoor allemaal bedanken zou ons iets te ver brengen en misschien voor natte bladzijden zorgen dus dat houden we voor een andere keer. Maar oprecht, **MERCI**, voor de gezellige kampvuurtjes, camionfeestjes, fuiven, etingen,... die echt een ideale ontspanning zijn als het onderzoek niet echt vordert. Ook **MERCI**, aan de Roowijven en -mannen (Eva, Emma, Lise, Davy, Simon, Leen en Jana) voor de leuke weekendjes, bbq's, de steeds aanwezige overdaad aan lekker eten en drinken, instuiven (*jaja we worden echt volwassen*), gezellige avondjes samen drinken omdat de drank op moet,... Ik denk dat ik wel mag zeggen dat we een bonte verzameling persoonlijkheden en karakters zijn maar dat we steeds op mekaar mogen rekenen niet alleen voor plezier maar ook voor steun, **MERCI**!

Ik heb ook het geluk een hechte familie te hebben en ik weet dat mijn oma haar deze avond zeker zal 'jeunen', opa met veel interesse zal luisteren en opa en marraine zeer trots zouden zijn. Ook al mijn tantes, nonkels, nichten en neven hebben altijd met aandacht geluisterd wanneer ik mijn onderzoek uitlegde hoewel ik dat misschien niet altijd even begrijpelijk deed. Ik heb ook twee fantastische ouders, mama en papa, die me steeds alle kansen hebben gegeven om te leren en studeren. Daarom in het bijzonder, **MERCI**, om op zolder net die ene bladzijde in een cursus te vinden die ik nodig had om een zin af te maken, om altijd naar jullie te kunnen bellen als ik me slecht voelde of panikeerde omdat ik nog nooit van Matlab en programmeren had gehoord (en ik dit moest kunnen voor een verplicht vak), om mij te komen halen als

ik niet thuis geraakte, om mijn teksten na te lezen, om telkens opnieuw naar mijn oefenpresentaties te luisteren, om het helmpje van het TBI model te solderen, ... om er gewoon altijd te zijn voor mij. **MERCI**! En dan last but certainly not least: diene Jelle, mijn lief, mijn beste vriend. **MERCI**, om met jouw ongelimiteerde positieve mindset mij steeds op te beuren als ik het niet meer zie zitten, om het gewoon cru te zeggen dat ik niet moet zagen maar het gewoon moet doen, maar ook om mij eten te geven, te wassen en naar het toilet te helpen toen ik even geen gebruik meer kon maken van mijn eigen armen (*en om mij Always discreet Boutique broekjes te kopen in plaats van Always maandverband, ik lach er mij nog steeds een breuk om, hebdem hebdem?*), om ook van mij een zachter persoon te maken die verdraagzamer is geworden - al zal jij beargumenteren dat dit niet zo is, om 'chiller' te zijn en meer het leven te nemen zoals het komt, om mijn zonnestraaltje te zijn die mij en het leven zoveel mooier maakt. **MERCI**!

Ik denk dat de meeste mensen wel zullen weten dat zoveel meligheid nogal abnormaal is voor mijn doen en 'een goe bierke en goe boefsel' meer mijn ding zijn (ik kom ten slotte uit 'een wel erg bourgondische Chiro'). Dus bij deze:

Santé mannen, en tot in den draai!

P.S.: Keep it simple but significant
– Don Draper

Samenvatting

Het doel van deze thesis is om een dieper inzicht te krijgen in de microstructurele veranderingen in de hersenen na het oplopen van een mild traumatisch hersenletsel (Engels: mild traumatic brain injury, mTBI) en cognitieve training met behulp van geavanceerde diffusie magnetische resonantie beeldvorming.

Traumatisch hersenletsel (TBI) is een grote oorzaak van een niet-aangeboren beperking in kinderen en volwassenen, en ieder jaar worden wereldwijd miljoenen mensen hierdoor getroffen. De meest voorkomende oorzaken van TBI zijn verkeersongevallen, een val of een sport gerelateerde impact en in ongeveer 70 - 90 % van de gevallen wordt een mild letsel opgelopen. Hoewel dit slechts een mild letsel is, kan het resulteren in een postcommotioneel syndroom wat wordt gekarakteriseerd door fysische klachten (bv. hoofdpijn), cognitieve moeilijkheden (zoals vermindering in verwerkingssnelheid, aandacht of geheugen) of gedragsproblemen (bv. prikkelbaarheid) en dit kan nog enkele jaren na het oplopen van het letsel blijven voortduren. Deze symptomen worden niet altijd gelinkt aan mTBI waardoor deze patiëntgroep vrij onzichtbaar blijft en amper erkend wordt. Hierdoor kreeg mTBI de stempel van 'stille epidemie'. Een andere uitdaging bij het vaststellen van mTBI is het gebrek aan radiologisch bewijs. Op het moment van impact worden de hersenen blootgesteld aan schurende en uitrekkende krachten die kunnen leiden tot diffuse axonale schade. Echter, conventionele medische beeldvormingstechnieken, zoals computertomografie (CT) of magnetische resonantie beeldvorming (Engels: magnetic resonance imaging, MRI), hebben maar een gelimiteerde sensitiviteit voor deze letsels wegens hun diffuse voorkomen en subtiele karakter. Dit heeft

geleid tot de ontwikkeling van meer geavanceerde MRI methoden zoals diffusie MRI, wat gevoeliger is in het detecteren van microstructurele schade ten gevolge van een mTBI.

Diffusie MRI is een beeldvormingstechniek dat veel interesse heeft verworven om microstructurele veranderingen in de hersenen te onderzoeken en wordt steeds meer gebruikt wegens de versterkte sensitiviteit voor veranderingen in de hersenen. De meest gebruikte diffusie beeldvormingstechniek voor TBI onderzoek is diffusie tensor beeldvorming (Engels: diffusion tensor imaging, DTI) en veranderingen in gemiddelde diffusiviteit (Engels: mean diffusivity, MD) en fractionele anisotropie (FA) - de twee meeste gebruikte parameters - zijn vaak vastgesteld. Echter, na een mTBI werden zowel toenames als afnames gerapporteerd en dus kan er geen consistent resultaat worden aangetoond. Bovendien, kunnen deze parameters beïnvloed worden door verschillende onderliggende biologische processen waardoor de parameters niet erg specifiek zijn. Bijvoorbeeld, een toename in FA kan wijzen op zowel axonale schade als een toename in myelinisatie. Als antwoord op deze non-specificiteit werden er andere diffusie modellen ontwikkeld zoals het diffusie kurtosis beeldvormings- (Engels: diffusion kurtosis imaging, DKI) model en het witte stof bundel integriteits- (Engels: white matter tract integrity, WMTI) model. In **Hoofdstuk 5**, was het eerste doel van deze thesis om de toegevoegde waarde van deze meer geavanceerde diffusie modellen, waarmee het microstructureel herstelproces geëvalueerd wordt, te onderzoeken in een ratmodel voor mild traumatisch hersenletsel. DKI is een extensie van het DTI model dat ook de mate van niet-Gaussiaanse diffusie schat, terwijl het biofysische WMTI model enkele voorgedefinieerde veronderstellingen inbouwt zodat de intra- en extra-axonale ruimtes beter worden gemodelleerd. Dit zal resulteren in een aantal extra parameters die meer specifiek kunnen zijn voor cellulariteit en intra- en extra-axonale kenmerken. Door gebruik te maken van een diermodel was het mogelijk om de veranderingen na mTBI te vergelijken met de normale hersenen in hetzelfde dier en om het ziekteproces op te volgen in de tijd. Wij hebben verminderde waarden van MD en radiale diffusiviteit (RD) kunnen aantonen één week na impact in respectievelijk, hippocampus en cingulum en dit was in overeenstemming met voorgaande humane studies bij patiënten met

een hersenschudding. Samen met een vermindering in radiale extra-axonale diffusiviteit (RadEAD) - een parameter uit het WMTI model - in het cingulum kan dit wijzen op cytotoxisch oedeem ten gevolge van neuroinflammatie. De vermindering was vooral gedreven door een sterke daling in de radiale component en in mindere mate de axiale component wat er kan op wijzen dat de axonale integriteit min of meer bewaard is gebleven in ons model. Dit duidt aan dat dit ratmodel dus een goed model is om mild traumatisch hersenletsel zonder zichtbare letsels op conventionele structurele scans te onderzoeken. Wij concludeerden dat de radiale parameters veelbelovende biomerkers kunnen zijn die sensitief zijn om microstructurele veranderingen te kunnen aantonen in de vroege fase na een milde en diffuse impact.

Bij diffusie tensor beeldvorming wordt de assumptie gemaakt dat één enkele voxel slechts één witte stof bundel bevat. In realiteit wordt deze assumptie vaak overtreden aangezien één enkele voxel meerdere bundels kan bevatten die kruisen, uitwaaieren of vermengen met elkaar waardoor er meestal een artificieel lage FA waarde ontstaat. Deze vermindering in FA interpreteren als een verlies van axonen en bundel integriteit zou in dit geval een misinterpretatie zijn van de onderliggende biologische processen. De techniek van beperkte sferische deconvolutie (Engels: constrained spherical deconvolution, CSD) kan meerdere bundel populaties onderscheiden binnen één enkele voxel (fixels genaamd) op een model- en assumptievrije manier en de morfologie van de individuele witte stof bundels kan onderzocht worden met behulp van een fixel-gebaseerde analyse (Engels: fixel-based analysis, FBA). In **Hoofdstuk 6**, onderzochten we of FBA meer specifieke informatie kan opleveren over de morfologieveranderingen van de bundels in een ratmodel voor mTBI. We hebben een significante toename in bundeldoorsnede (Engels: fiber cross-section, FC) kunnen vaststellen in het splenium van het corpus callosum, een grote witte stofbaan, van de mTBI ratten in vergelijking met de controle groep één week na impact. Dit resultaat is in overeenstemming met de resultaten van Hoofdstuk 5 en versterkt het idee van cytotoxisch oedeem en axonale zwelling in ons model. Hoewel we een significante toename in FC konden detecteren die kan wijzen op axonale zwelling, vermoeden we dat het voor toekomstige studies die een grotere steekproef grootte includeren, mogelijk moet zijn om meer wijdverspreide veranderingen te

detecteren waarmee we de kennis over witte stof schade na mTBI zullen vergroten.

Ondanks dat deze beeldvormingstechnieken zeker veelbelovend zijn, is het nog steeds nodig om de diffusie MRI veranderingen te valideren zodat we zeker kunnen zijn dat de veranderingen in de parameters wel degelijk een specifiek onderliggend biologisch proces voorstellen en hierin hebben preklinische proefdiermodellen een sleutelrol. In **Hoofdstuk 7**, hebben we de diffusie veranderingen, vastgesteld in Hoofdstuk 5, gevalideerd aan de hand van immunohistologische analyse met drie verschillende cellulaire merkers. Met anti-neurofilament en anti-synaptofysine evalueerden we of al dat niet respectievelijk de structuur (door het kleuren van de neurofilamenten) of synaps densiteit (door de synaptische vesikels aan te kleuren), was aangetast door de mTBI. Ook de astrocytaire respons, gelinkt aan neuroinflammatie en/of -plasticiteit, werd onderzocht met behulp van anti-gliaal fibrillair zuur proteïne (Engels: glial fibrillary acidic protein, GFAP). Onze resultaten waren drievoudig. Drie maand na impact observeerden we een correlatie tussen RD en MD, en histologische merkers die een vermindering in neurale structuur en gliale respons aantonen in de hippocampus. Meer specifiek waren verminderingen in diffusiviteit geassocieerd met meer gedefosforyleerde neurofilamenten, wat neurofilament compactie en reductie in axonale structuur kan aantonen. Ten tweede, toegenomen waarden in kurtosis drie maand na impact waren gecorreleerd met toegenomen GFAP reactiviteit en kan duiden op meer en/of hypertrofe astrocyten. Ten derde, hogere FA waarden één dag na impact waren gerelateerd aan hogere GFAP reactiviteit en toont aan dat FA mogelijks een predictieve merker zou kunnen zijn voor latere gliale activiteit. Hoewel we enkel associaties konden aantonen in de hippocampus en hierdoor dus geen WMTI parameters konden onderzoeken, zijn deze resultaten zeer bemoedigend om diffusie biomerkers te vinden die meer specifiek kunnen zijn voor het onderliggende biologische herstelproces.

Tot slot wouden we onderzoeken of het mogelijk is voor de diffusie parameters om microstructurele veranderingen ten gevolge van cognitieve training te kwantificeren in mTBI rattenhersenen. Het is reeds aangetoond dat cognitieve rehabilitatie kan helpen bij het verlichten

van klachten die TBI patiënten ervaren en het cognitief functioneren kan verbeteren. De laatste jaren zijn gecomputeriseerde cognitieve trainingsprogramma's populairder geworden om de getroffen cognitieve functies te trainen, maar we begrijpen de onderliggende biologische mechanismen nog niet volledig en meer onderzoek is nodig om ons inzicht te vergroten. Daarom hebben we twee verschillende types van cognitieve training (een geheugen- en een aandachtstraining) geëvalueerd in ons mTBI ratmodel met behulp van diffusie MRI als translationeerbare beeldvormingstechniek in **Hoofdstuk 8**. Verder, stelden we als hypothese dat de geheugentraining specifiek de TBI-geïnduceerde veranderingen in de hippocampus zou beïnvloeden, terwijl de aandachtstraining meer specifiek zou zijn voor het cingulum. Na de trainingsinterventie, hebben we een significante toename in FA kunnen demonstreren in het cingulum wat gepaard ging met stabiele waarden van diffusiviteit, terwijl de mTBI groep die geen training kreeg een significante toename in diffusiviteit vertoonde. Een toename in FA is reeds aangetoond in gezonde en oudere volwassenen nadat ze een cognitieve training volgden van 10 weken. Jammer genoeg, konden we de types training niet linken aan hun voorspelde doelregio en was er enkel een effect van training in het algemeen. Bovendien, waren verminderde waarden van diffusiviteit en toegenomen waarden in FA geassocieerd met gedragsverbeteringen zoals vastgesteld met een betere inhibitie controle. Tezamen, tonen deze resultaten voor het eerst aan dat cognitieve training met behulp van een touchscreen systeem het potentieel heeft om het secundaire ziekte proces te vertragen in ons mTBI ratmodel.

In conclusie, demonstreerden we dat meer geavanceerdere diffusie modellen, namelijk DKI en WMTI, sensitief zijn om microstructurele veranderingen na mTBI te detecteren zowel op het acute tijdspunt als het chronische tijdspunt en dat ze complementaire informatie kunnen verschaffen naast het meer gebruikte tensor model waardoor een dieper inzicht kan bekomen worden in het de pathofysiologie van mTBI. Bovendien, konden de veranderingen in diffusie parameters worden gelinkt aan het onderliggende biologische proces en toonden ze aan dat geactiveerde astrocyten (mogelijks gelink aan een neuroprotectieve respons met neuroinflammatie of -plasticiteit) een rol speelt in het secundaire ziekte proces dat leidt tot zwellen van de axonen maar zonder degeneratie

van de neuronen. Analyse met de FBA methode demonstreerde ook deze zwelling in het corpus callosum. Tot slot, was diffusie MRI in staat om aan te tonen dat een cognitieve training het potentieel heeft om het secundair ziekte proces te vertragen. Dus, deze resultaten tonen aan dat diffusie MRI een waardevolle beeldvormingsmethode is om de microstructurele status van de hersenen na een mTBI vast te stellen en dat het informatie kan aanleveren over de verbeteringen ten gevolge van cognitieve rehabilitatie op een objectieve en kwantitatieve manier.

Summary

The purpose of this dissertation is to provide a deeper understanding of the microstructural changes in the brain following mild traumatic brain injury (mTBI) and cognitive training therapy using advanced diffusion magnetic resonance imaging.

Traumatic brain injury (TBI) is a major cause of acquired disability in children and adults, and millions of people are affected worldwide every year. The main causes of TBI are road traffic accidents, falls or sport injuries and in about 70 - 90 % of the cases patients will suffer from a mild injury (mTBI). Though this is only a mild injury, it can result in post-concussion syndrome which is characterised by physical complaints (e.g., headaches), cognitive problems (such as deficits in processing speed, attention and memory) or behavioural changes (e.g., irritability) and can linger for several years after the injury. These symptoms are not always linked to mTBI making this patient group relatively invisible and highly unrecognised. Therefore, mTBI has been coined a 'silent epidemic'. Another challenge in the identification of mTBI is the lack of radiologic evidence. At the moment of injury, the brain is subjected to shear-strain forces which can lead to diffuse axonal injuries. However, conventional medical imaging techniques, such as computed tomography (CT) or magnetic resonance imaging (MRI), have limited sensitivity in detecting these injuries due to their diffuse and subtle nature. This has led to the development of more advanced MRI methods such as diffusion MRI which is more sensitive in detecting microstructural changes following mTBI.

Diffusion MRI is an imaging technique that has gained tremendous interest in investigating microstructural changes in the brain and is being used more often due to the enhanced sensitivity for the alterations in the brain. The most used diffusion imaging technique in TBI research is diffusion tensor imaging (DTI) and alterations in mean diffusivity (MD) and fractional anisotropy (FA) - the two most commonly used metrics - are widely established. However, both increases and decreases have been reported following an mTBI and thus no consistent outcome can be demonstrated. Furthermore, these metrics can be influenced by several underlying biological processes making the measures not very specific. For example, an increase in FA can be the result of both axonal swelling or an increase in myelination. In response to this non-specificity other diffusion models have been developed such as the diffusion kurtosis imaging (DKI) model and the white matter tract integrity (WMTI) model. In **Chapter 5**, the first goal of this dissertation was to investigate the added value of these more advanced diffusion models to evaluate the microstructural recovery process using a mild traumatic brain injury rat model. DKI is an extension of the diffusion tensor model which will also estimate the degree of non-Gaussian diffusion, whereas the biophysical WMTI model will build in some predefined assumptions to better model the intra- and extra-axonal spaces. This will result in several additional metrics that could be more specific for cellularity and intra- and extra-axonal features. By using an animal model, it was possible to compare the microstructural changes in the brain after induction of TBI with the normal brain in the same animal, as well as to monitor disease progression over time. In agreement with previous human studies in concussed patients we found decreased values of MD and radial diffusivity (RD) in the hippocampus and cingulum, respectively, one week post injury. Together with a decrease in the cingulum of the radial extra-axonal diffusivity (RadEAD) - a metrics derived from the WMTI model - this could be indicative of cytotoxic oedema as a result of neuroinflammation. The decrease in diffusivity was mainly driven by a strong decrease in the radial components and to a lesser extent the axial components suggesting that axonal integrity is more or less preserved in our model. This indicates that our rat model is a good model to study mild traumatic brain injuries where no lesions are visible with conventional structural imaging. We concluded that

radial diffusion measures might be promising biomarkers which could be sensitive to identify specific microstructural changes in the early phase after a mild and diffuse impact.

In diffusion tensor imaging the assumption is made that a single voxel contains one specific fibre population. In reality this assumption is frequently violated, since a single voxel can contain several fibre populations that cross, fan out or intermingle with each other, mostly leading to an artificially low FA value. Interpreting this decrease in FA as a loss of axons and fibre integrity would in this case be a misinterpretation of the underlying biological processes. The technique of constrained spherical deconvolution can estimate the different fibre populations within a voxel (i.e., fixels) in a model- and assumption-free manner and using the subsequent connectivity-based fixel enhancement analysis (or fixel-based analysis, FBA) the morphological changes within the individual white matter populations can be investigated better. In **Chapter 6**, we investigated whether FBA can provide more specific information of white matter bundle changes in a rat model of mild traumatic brain injury. We were able to demonstrate a significant increase in fibre cross-section (FC) in the splenium of the corpus callosum, a major white matter tract, of the TBI rats compared to the control group one week after impact. This result is in line with the results of Chapter 5 and strengthens the idea of cytotoxic oedema and axonal swelling in our model. Although we were able to detect a significant increase in FC which could indicate axonal swelling, we believe that future studies including a bigger sample size could be able to detect more widespread alterations and increase our understanding of white matter damage following mTBI.

Although these new techniques are certainly promising, validation of the observed diffusion metrics is still required to evaluate the link between these microstructural changes and the underlying biological process, where animal models also play a key role. In **Chapter 7**, we have validated the diffusion changes observed in Chapter 5 using an immunohistological analysis with three different cellular markers. With anti-neurofilament and anti-synaptophysin we evaluated whether or not the structure (by staining the neurofilaments) or synapse density (by staining the synaptic vesicles), respectively, was affected by the mTBI.

Also, the astrocytic response, related to neuroinflammation and/or -plasticity, was of interest and was investigated using anti-glial fibrillary acidic protein. Our results were threefold. We observed correlations between RD and MD, and histological markers indicative of a compromise in neural structure and glial response in the hippocampus three months post injury. More specifically reduced diffusivity values were associated with more dephosphorylated neurofilaments which could suggest neurofilament compaction and reduction in axonal structure. Secondly, increased values of kurtosis three months post injury were correlated with increased GFAP reactivity which is indicative of more and/or hypertrophic astrocytes. Thirdly, higher FA values one day post injury were also related to higher GFAP reactivity showing that FA could be a predictive biomarker for later glial activity. Although we could only demonstrate associations in the hippocampus and therefore could not investigate correlations with the WMTI model, these results are highly encouraging in finding diffusion biomarkers that could be more specific to the underlying biological recovery processes.

Lastly, we wanted to examine whether the diffusion metrics are able to quantify microstructural changes as a result of cognitive training on an injured brain. It has been shown that cognitive rehabilitation can help alleviate the complaints TBI patients experience and improve their cognitive functioning. In recent years computerized cognitive training programs have become more popular to train the affected cognitive functions, however, we do not fully understand the underlying biological mechanisms in TBI and more research is needed to increase our understanding. Therefore, we evaluated two types of cognitive training (a memory and an attention training) in our mTBI rat model using diffusion MRI as translational imaging method in **Chapter 8**. Furthermore, we hypothesised that the memory training would specifically alter TBI induced alterations in the hippocampus, whereas the attention training would be more specific for the cingulum. We were able to demonstrate a significant increase in FA in the cingulum following training intervention, which was accompanied by stable levels of diffusivity values, whereas the TBI group that did not receive training, showed significant increases in diffusivity. Increases in FA have been shown in healthy and elderly adults following 10 weeks of cognitive training. Unfortunately, we could

not link the type of training to their hypothesised target and there was only an effect of training in general. Furthermore, decreased values of diffusivity and increased values of FA were associated with behavioural improvements as witnessed by better inhibitory control. Together, the results show for the first time that cognitive training using a touchscreen system has the potential to slow down secondary disease progress in our mTBI rat model.

In conclusion, we demonstrated that more advanced diffusion models, namely DKI and WMTI, are sensitive in detecting microstructural alterations following mTBI both at the acute and more chronic time point and that they can provide complimentary information to the more widely used tensor model providing a deeper insight in the pathophysiology of mTBI. Furthermore, the changes in the diffusion measures could be linked to the underlying biological process and showed that activated astrocytes (possibly linked to a neuroprotective response with neuroinflammation and/or -plasticity) plays a role in the secondary disease progress leading to swelling of the axons but without degeneration of the neurons. Analysis with the FBA method could further demonstrate this swelling in the corpus callosum. Lastly, diffusion MRI was able to demonstrate that a cognitive training program has the potential to slow down secondary disease progress. Together, these findings show that diffusion MRI is a valuable imaging tool to assess microstructural status following mTBI and can provide information about the improvements induced by the cognitive rehabilitation in an objective, quantitative fashion.

List of abbreviations

AD	Axial Diffusivity
AK	Axial Kurtosis
AxEAD	Axial Extra Axonal Diffusivity
bTBI	Blast-induced TBI
CCI	Controlled Cortical Impact
CHI	Closed Head Injury
CNS	Central Nervous System
CPT	Continuous Performance Test
CSF	Corticospinal fluid
CT	Computed Tomography
CTE	Chronic Traumatic Encephalopathy
DAI	Diffuse Axonal Injury
DKI	Diffusion Kurtosis Imaging
dMRI	Diffusion MRI
dMRI	Diffusion Weighted Magnetic Resonance Imaging
DTI	Diffusion Tensor Imaging

DWI	Diffusion Weighted Imaging
DWIs	Diffusion Weighted Images
EE	Environmental Enrichment
EPI	Echo Planar Imaging
FA	Fractional Anisotropy
FC	Fibre Cross-Section
FD	Fibre Density
FDC	Fibre Density and Cross-Section
FID	Free Induction Decay
FLAIR	Fluid Attenuated Inversion Recovery
FOD	Fibre Orientation Distribution
FPI	Fluid Percussion Injury
GCS	Glasgow Coma Scale
GFAP	Glial Fibrillary Acidic Protein
LFPI	Lateral Fluid Percussion Injury
MD	Mean Diffusivity
MK	Mean Kurtosis
MR	Magnetic Resonance
MRI	Magnetic Resonance Imaging
mTBI	Mild Traumatic Brain Injury
MWM	Morris Water Maze
PAL	Paired Associate Learning
PD	Proton Density

PGSE	Pulsed Gradient Spin Echo
RadEAD	Radial Extra Axonal Diffusivity
RARE	Rapid Acquisition with Refocused Echoes
RD	Radial Diffusivity
RF	Radiofrequency
RK	Radial Kurtosis
SNR	Signal-to-Noise Ratio
SWI	Susceptibility Weighted Imaging
TAI	Traumatic Axonal Injury
TBI	Traumatic Brain Injury
TE	Echo Time
TORT	Tortuosity
TR	Repetition Time
VOI	Volume-of-Interest
WMTI	White Matter Tract Integrity

List of publications

Journal Papers

1. Braeckman K, Descamps B, Vanhove C, Caeyenberghs K. **Exploratory relationships between cognitive improvements and training induced plasticity in hippocampus and cingulum in a rat model of mild traumatic brain injury: a diffusion MRI study**, 2019, Brain Imaging and Behaviour

2. Braeckman K, Descamps B, Vanhove C. **Advanced Diffusion Imaging in The Hippocampus of Rats with Mild Traumatic Brain Injury**, 2019. Journal of Visualized Experiments (150), e60012 (https://www.jove.com/video/60012/advanced-diffusion-imaging-hippocampus-rats-with-mild-traumatic-brain?status=a62018k)

3. Braeckman K, Descamps B, Pieters L, Vral A, Caeyenberghs K, Vanhove C. **Dynamic changes in hippocampal diffusion and kurtosis metrics following experimental mTBI correlate with glial reactivity**, 2019. NeuroImage:Clinical, 21, 101669.

4. Khalenkow D, Donche S, Braeckman K, Vanhove C, Skirtach A. **Added value of microscale Raman chemical analysis in mild traumatic brain injury (TBI) : a comparison with macroscale MRI**, 2018. ACS Omega, 3(12), 16806–16811.

Conference Abstracts

1. Braeckman K, Descamps B, Caeyenberghs K, Vanhove C. **Longitudinal DTI changes following cognitive training therapy in a mild traumatic brain injury rat model**, 2019. 4th Belgian Molecular Imaging Congress

2. Braeckman K, Descamps B, Caeyenberghs K, Vanhove C. **Longitudinal DTI changes following cognitive training therapy in a mild traumatic brain injury rat model**, 2019. 14th European Molecular Imaging Meeting

3. Braeckman K, Descamps B, Caeyenberghs K, Vanhove C. **Longitudinal DTI changes following cognitive training therapy in a mild traumatic brain injury rat model**, 2018. BMIC meets industry @ UCB

4. Braeckman K, Descamps B, Caeyenberghs K, Vanhove C. **Longitudinal DTI changes following cognitive training therapy in a mTBI rat model**, 2018. Belgian Brain Congress

5. Braeckman K, Descamps B, Caeyenberghs K, Vanhove C. **Characterisation of microstructural alterations in a weight drop mTBI rat model: a longitudinal diffusion MRI and histological analysis**, 2018. 13th annual meeting of the European Society for Molecular Imaging – ESMI

6. Braeckman K, Descamps B, Pieters L, Vral A, Caeyenberghs K, Vanhove C. **Characterisation of microstructural alterations in a weight drop mTBI rat model : a longitudinal diffusion MRI and histological analysis**, 2018. Abstract book : 10th annual meeting ISMRM Benelux Chapter, abstract P-72

7. Braeckman K, Descamps B, Vanhove C, Caeyenberghs K. **Characterizing microstructural alterations in a mTBI rat model: a multi-shell diffusion MRI analysis**, 2017. 2017 Organisation for Human Brain Mapping Annual Meeting.

8. Braeckman K, Descamps B, Caeyenberghs K, Vanhove C. **Characterizing microstructural alterations in rat model of mild**

traumatic brain injury : a longitudinal multi-shell diffusion MRI analysis, 2017. Abstract book : 9th annual meeting ISMRM Benelux Chapter,

9. Braeckman K, Descamps B, Caeyenberghs K, Vanhove C. **Characterizing microstructural alterations in a mTBI rat model: a multi-shell diffusion MRI analysis**, 2017. 12th meeting of the Belgian Neuroscience Society

10. Braeckman K, Descamps B, Caeyenberghs K, Vanhove C. **Characterizing microstructural alterations in a mTBI rat model: a multi-shell diffusion MRI analysis**, 2017. 3rd Belgian Molecular Imaging Congress

11. Braeckman K, Descamps B, Deblaere K, Caeyenberghs K, Vanhove C. **Characterizing microstructural alterations in a rat model of mild traumatic brain injury**, 2016. 15th Belgian National Day on Biomedical Engineering

Awards

- The BELNUC award for best oral presentation at BMIC 2019
- Oral presentation award 2018 at BMIC meets Industry @ UCB

Table of Contents

1 | Introduction

1.1 Situation

A trivial collision with the head of a fellow music festival visitor was enough to cause Belgian singer Coely to suffer from a mild traumatic brain injury. She described the following two weeks as "hard and painful" and one month after the impact she was still recovering. This happens to more persons than we would expect, and it is estimated that 250 000 individuals are suffering from an acquired brain injury in Flanders today. Nevertheless, as target group they remain relatively invisible due to the lack of knowledge and acceptance of mild traumatic brain injury. However, the impact on both the patient and the close circle of friends and family is not to be neglected.

When a person who sustained a traumatic brain injury arrives at the emergency department of a hospital - if ever -, a full range of evaluations will be performed to assess the severity of the injury, which can include medical imaging such as computed tomography (CT) and magnetic resonance imaging (MRI). Mild traumatic brain injury patients often show no medical imaging evidence of trauma and are therefore send home and simply need to rest and take pain killers to relief any possible headaches.

Following a mild traumatic brain injury an impairment in cognitive functioning can occur. It is common for traumatic brain injury patients to have problems with attention, concentration, speech and language, learning and memory, reasoning, planning and problem-solving. Usually these symptoms will resolve within a few days, however, there are

patients that still suffer from cognitive dysfunction several months to years after the injury. Cognitive training programs seem to alleviate these problems and have shown promising results in clinical studies, but it is poorly understood what happens in the brain.

To improve our understanding of the alterations in the brain following a mild traumatic brain injury and to progress our insight into the beneficial effects of cognitive training therapy, this dissertation aims to provide a deeper understanding of the microstructural changes in the brain using advanced magnetic resonance imaging techniques in a rat model of mild traumatic brain injury

1.2 Outline

In the next two chapters (**Chapter 2 and 3**), we will give a general introduction on the different dimensions of traumatic brain injury and on diffusion weighted magnetic resonance imaging, the imaging technique that will be used in this dissertation.

In **Chapter 4**, the overall aim of the research outlined in this dissertation is summarized and the specific research questions are listed.

In **Chapter 5**, the results of a longitudinal, multi-shell diffusion weighted magnetic resonance imaging study in a rat model of mild traumatic brain injury are presented. We used three different diffusion models and were able to demonstrate that diffusion weighted magnetic resonance imaging is sensitive in detecting longitudinal microstructural changes after mild traumatic brain injury.

Because of limitations to the models used in Chapter 5, we will evaluate the potential of a recently established diffusion model that can provide information on the different fiber populations of white matter pathways in the brain. This longitudinal study in rats with mild traumatic brain injury is outlined in **Chapter 6**.

Although the presented diffusion models are helpful for interpreting the alteration in the brain following a traumatic brain injury, their

validity still needs to be investigated so that we can be sure that the detected diffusion changes are representative for the underlying structural changes. In **Chapter 7**, we will examine whether the diffusion changes can be linked to specific microstructural processes.

After establishing possible biomarkers that can follow up alterations in the brain following mild traumatic brain injury, these can be used to investigate the influence of cognitive training to improve cognitive functioning in an objective manner. Therefore, in **Chapter 8**, we will investigate whether two training tasks can alter the mTBI-induced brain changes in rats after an intense training intervention of 12 weeks using diffusion magnetic resonance imaging.

Finally, **Chapter 9 and 10** will provide a general discussion and conclusion of the presented results, place them in a broader context and reflect on the future perspectives of research on mild traumatic brain injury.

2 The brain, traumatic brain injury and cognitive training

2.1 Anatomy and structure

2.1.1 From macro to micro

The brain has a complex layered anatomy and is the biggest part of the Central Nervous System (CNS). It is an extremely fast and reliable computing system that processes incoming information and drives and manages all outgoing responses of the body. From the outside three major parts of the brain can be distinguished: the cerebrum, cerebellum and brainstem. The dominant part, the cerebrum, is a symmetric structure that is separated along the midline in a left and right hemisphere. In its turn, each hemisphere can be subdivided into a frontal, temporal, parietal and occipital lobe (Figure 2.1) [1].

On the exterior, the cerebrum has a wrinkly appearance due to the many folded gyri that increase the surface area. They make up the cerebral cortex and consist of the bodies of the neurons and dendrites, organised in layers, which gives the cortex a pink-grey appearance, hence the name grey matter. Below the cortical layers there is a central core of white matter made up of fibres that form connections between different grey matter regions. Because the fibres are mostly myelinated (fatty substance) they appear white. The myelinated fibres make it possible to send signals from one region to another with high efficiency.

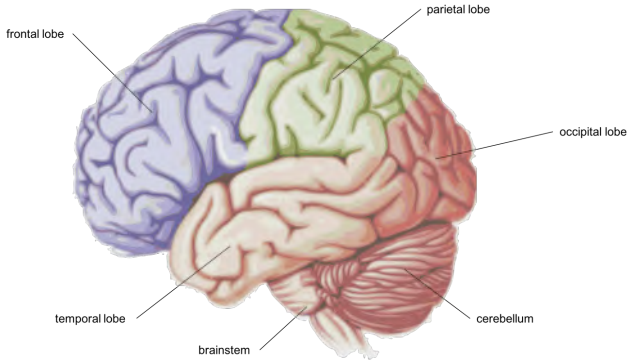

Figure 2.1: The cerebrum devided in the frontal, parietal, occipital and temporal lobe. Also the cerebellum and brainstem are indicated. Figure adapted from [1].

Connections between regions can occur within the same hemisphere and thus be rather short (association fibres), between the two hemispheres (commissural fibres) or even away from the brain to the spinal cord (projection fibres) and makes an efficiently working network essential [2].

Microstructurally, the nerve cells, or neurons, are the most important elements in the brain and are specialised in receiving and transmitting information (Figure 2.2). They have characteristic features - the neurites - that are extensions of the cell body or soma. These neurites are called dendrites when they receive incoming information and axons when they are used to transmit the information to the next cell. One neuron has several rather short dendrites but mostly one long axon. To ensure an efficient information transfer over a long distance, the axon is covered with myelin sheets which act as insulation on an electrical wire. To communicate with each other, the neurons make use of specialised cell junctions, known as synapses. The information transfer can be done electrically where ions or small molecules traverse through small channels in the neighbouring cells, or chemically involving one cell to release neurotransmitters into the synaptic cleft where they can bind to receptors on the next cell [3].

In addition to neurons, the brain microstructure consists of many

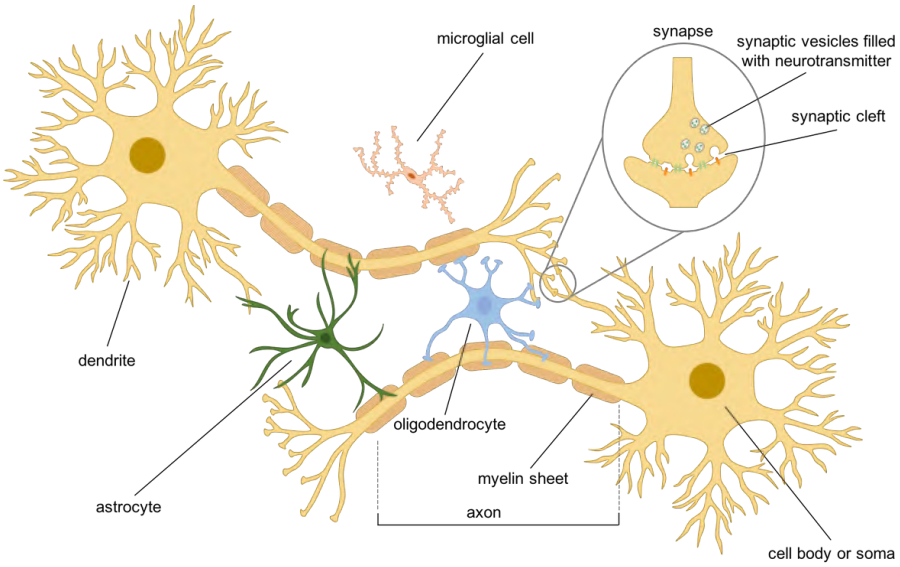

Figure 2.2: Brain microstructure, image made with Motifolio Illustration Toolkit

support cells, or glia cells, which assist and facilitate proper functioning of the neurons. Astroglia are stellate-shaped cells that extend between the neurons and vascular elements occupying most of the extracellular space in the CNS. They have numerous functions and help to maintain homeostasis. In attempting to repair damage to the CNS they can form glial scar tissue. Myelination of the axons is achieved by oligodendrocytes. The smallest glia cells are the microglia, hence the name, and they function in the phagocytosis of damaged tissue and participate in inflammatory responses [3].

2.1.2 Rat brain anatomy

The rodent is the most often used animal for research in mammalian neuroscience and although there are a lot of similarities with the structures of the human brain, there are also differences. Apart from the obvious difference in brain size there are also some white matter tracts that are present in the human brain but cannot be found in a rat brain.

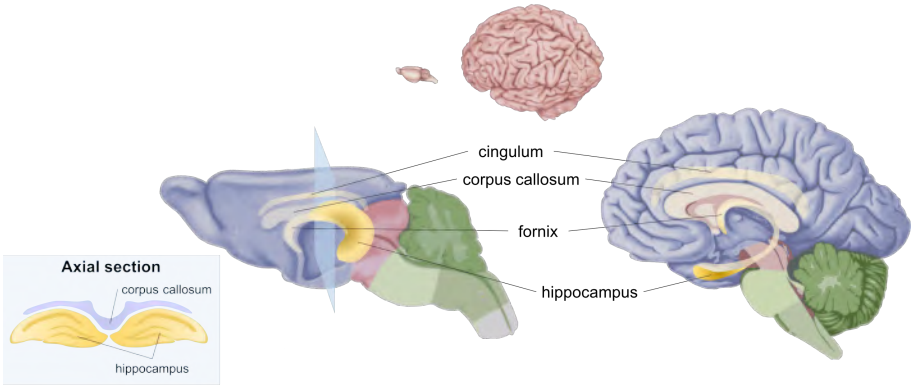

Figure 2.3: Top: Difference in size between a rat brain and a human brain. Bottom: Comparison of structures of interest in rat and human brain. Figure adapted from [1]

Therefore, in the next section, we will make a small comparison of structures found both in human and rat brain, and focus on structures important for cognitive functioning.

Similar to humans, the corpus callosum is the largest bundle of white matter fibres and connects the two hemispheres of the brain like a strong bridge to ensure that the two hemispheres function together as a coordinated whole (Figure 2.3). Also similar to the human brain are the two cingulum bundles (left and right hemisphere) which are situated on top of the corpus callosum and project in the anterior-posterior direction. Unlike the human brain, the hippocampus of the rat brain is a big structure that cannot be overlooked. On axial sections it can be recognised as a 'moustache'-like structure but as a volume it is comprised of two horn-like shapes. In humans on the other hand, the hippocampus is a small structure in the medial temporal lobes. Comparable to humans, the fornix is a small white matter bundle that extents anteriorly from the hippocampus and relays information to the basal nuclei. Also the cingulum bundles are in connection with the hippocampus and have fibres running to the lower frontal lobe. The fornix, the cingulum and the hippocampus are part of the limbic system which is linked to a number of functions including memory, attention, behaviour control and decision making [4]. The function of the corpus

callosum is mostly deducted from studies in patients with no or only a partial corpus callosum present and patients with a callosotomy. These studies demonstrated that the corpus callosum can be important for bilateral motor coordination, language and facilitating cognitive and sensori-motor functioning [5].

2.2 Traumatic brain injury

Traumatic Brain Injury (TBI) can be defined as an alteration in brain function, or other evidence of brain pathology, caused by an external force [6]. This 'other evidence' can include information obtained from clinical imaging techniques such as Computed Tomography (CT) and Magnetic Resonance Imaging (MRI), or serum, Corticospinal fluid (CSF) or blood biomarkers. Additionally, the external force is mechanical in nature and caused by the head striking an object (e.g., blunt force trauma or sport injuries) or undergoing an acceleration/deceleration movement without visible trauma to the head (e.g., whiplash in road traffic accidents). Also, the head can be penetrated by a foreign body.

In Europe the incidence rate of TBI is estimated between 200 - 300 per 100 000 persons a year [7, 8]. However, this is most likely an underestimation since this estimate includes only TBI patients admitted to hospitals, resulting in underestimation of the frequency of milder TBI. Many of those milder injured patients do not seek help or disregard the subtle behavioural or neuropsychological changes which could be the only symptoms. Also, society is insufficiently aware of the impact of TBI. Therefore, the milder form of TBI has been termed as *silent epidemic* [9]. Especially young adults and elderly people are vulnerable age groups since they have a higher risk of road traffic accidents and falls [10].

2.2.1 Classification

To grade initial brain injury severity at the trauma scene or at emergency department admission, the Glasgow Coma Scale (GCS), which determines the level of consciousness, has been the primary clinical

Table 2.1: Glasgow coma scale

BEHAVIOUR	RESPONSE	SCORE
Eye opening response	Spontaneously	4
	To speech	3
	To pain	2
	No response	1
Best verbal response	Oriented to time, place and person	5
	Confused	4
	Inappropriate words	3
	Incomprehensible sounds	2
	No response	1
Best motor response	Obeys commands	6
	Moves to localised pain	5
	Flexion withdrawal from pain	4
	Abnormmal flexion (decortitate)	3
	Abnormal extension (decerbrate)	2
	No response	1

variable. The injury is graded in mild (GCS 13 - 15), moderate (GCS 9 - 12) or severe (GCS $\leq$ 8) according to a scoring system (Table 2.1)[11]. Depending on the severity of the injury, the consequences of the changes in brain structure can be temporary or permanent. The transient symptoms include headache, fatigue, anxiety, emotional lability and cognitive problems such as impaired memory, attention, concentration and executive functioning [12, 13].

The American Congress of Rehabilitation Medicine expanded the GCS and stated that a patient with a mild trauma should not loose consciousness longer than 30 minutes and not suffer from amnesia for more than 24 hours [14]. If this is not the case, one speaks of a moderate or severe trauma. The percentages of TBI severity are typically 80 % mild, 10 % moderate and 10 % severe [15]. Most Mild Traumatic Brain Injury (mTBI) patients recover within days or weeks, however about 10 - 15 % have persistent complaints after one year which is defined as post-

concussion syndrome and can include physical complaints (e.g., headaches), cognitive deficits (such as deficits in processing speed, attention or memory) or behavioural changes (e.g., irritability) [12].

In this work, we will focus on mTBI.

2.2.2 Pathophysiology of mTBI

TBI can result in focal and diffuse injuries. However, in reality both types arise and interact within the same individual making the pathophysiology of TBI very complex. Pathophysiology can be subdivided into primary injury, which is the direct result of the impact, and secondary injury which is the complex biochemical cascade initiated after trauma.

Primary injury

Injuries to the head can lead to many different types of structural damage ranging from large lesions that are easily detected (moderate-to-severe TBI) to microscopical damage (mTBI). In general, the parenchymal lesions will contain an epicentre of neurons, glial cells and vascular structures that sustain irreversible damage and can result in either focal or diffuse lesions [16]. Mostly there is not a lot of damage visible on the macroscopic level in mTBI. Damage can include scalp laceration and contusion, small haemorrhages, brain contusion and swelling of the brain, which all require no immediate intervention [17]. Microscopically, axons can be torn due to shear-strain forces which interrupt the neural transport. Also, destruction of the endothelial layer of small blood vessels, microporation of membranes and leaky ion channels can induce an imbalance in the water homeostasis causing either vasogenic or cytotoxic oedema [18].

Diffuse Axonal Injury (DAI), also termed Traumatic Axonal Injury (TAI), is an indirect injury caused by the shear-strain forces at the grey-white matter junction. It is characterised by multiple small lesions along the junction, the cortex or even subcortical structures when the impact is more severe [16]. The mechanical stretching of the brain parenchyma can tear the axonal connections and induce microhaemorrhages.

Secondary injury

Following the primary mechanical injury a complex cascade of neurochemical and neurometabolical events is initiated. The disruption of cell membranes, axonal stretching and leaky ion channels will cause uncontrolled and excessive release of excitatory neurotransmitters (e.g., glutamate by compromised astrocytes) which is toxic (excitotoxicity) [19]. In addition, the normal glutamate re-uptake by astrocytes is decreased or abolished due to destruction of neighbouring astrocytes. This will in turn lead to swelling of the remaining astrocytes. Furthermore, glutamate will bind to receptors that overactivate ion channels responsible for Na^{+} and Ca^{2+} influxes. This will further exacerbate the water homeostasis and induce Ca^{2+}-mediated damage such as dephosphorylation of intracellular components and activation of Ca^{2+}-dependent proteases [20]. The overflow of intracellular Ca^{2+} will also cause mitochondrial energy deficiencies, generation of free radicals and activation of the apoptotic breakdown process.

Surrounding the epicentre of primary injury there is often a penumbra with cells that have experienced reversible damage. In this penumbra most effects of the secondary biochemical cascade will occur during the early or late postraumatic period. This can result in ischaemic brain damage - whereby reduced blood flow and tissue oxygenation is present - and is often superimposed on the primary damage surrounding the epicentre and can be widespread [17].

2.2.3 Cognitive symptoms

Although the majority of TBI patients only suffer from a mild injury, it can result in a broad spectrum of post-concussive symptoms such as physical complaints (e.g., headaches), cognitive deficits (involving processing speed, memory or attention) or behavioural changes (e.g., irritability) [14]. Usually, these symptoms will resolve within the first few days, however, in up to 20 % of the cases the symptoms may become chronic and last for several months [21]. The development of long-lasting cognitive deficits is one of the most debilitating consequences of TBI and can negatively affect social functioning. For example, inappropriate or impulsive behaviour such as saying hurtful things and not realising

the social boundaries can be harmful for relationships [22]. Furthermore, executive functioning can be impaired following mTBI. Executive functioning can be defined as control processes that coordinate and regulate other cognitive (sub)processes or behaviours. These functions can include cognitive flexibility in the face of changing environment (in which dividing, switching and sustaining attention plays an important role) and organisation of dynamic, goal-directed behaviour [23]. More specifically, work productivity can be reduced when patients return to work and the person with TBI can have trouble remembering new information or planning and organising the execution of tasks. Further, impairments with reasoning, problem solving and judgement can cause the person to make more mistakes and to get less work done [24].

2.3 Animal models for mild traumatic brain injury

Since patients with traumatic brain injury show a tremendous variability and heterogeneity in many aspects (age, gender, type of trauma, other possible pathologies, ...), animal models play a key role in unravelling factors that prove a limitation in clinical research. For example, invasive studies for studying the cellular or molecular background are not possible for ethical reasons or can only be done after the person has passed away. Also, long serial studies prove to be a challenge. However, possible long-term effects of TBI may progress over time and not fully manifest until years after the injury. To better understand the underlying mechanisms of TBI, preclinical animal models are required because they allow a more detailed investigation of pathophysiological mechanisms following TBI within a highly controlled setting. Moreover, the development of novel prognostic or predicted biomarkers can be explored and validated, and new therapies can be investigated. A number of rodent models have been developed to mimic human TBI and in the following paragraphs we will give a short overview of these models, their morphological characteristics and imaging findings after injury. In this dissertation, we will focus on on a mTBI rat model.

2.3.1 Direct brain deformation models

Through an opening in the skull created by craniotomy, the brain can be displaced or deformed briefly, producing a more focal injury. Therefore, in general, the open head models produce more damage to the grey matter than to the underlying white matter.

Controlled cortical impact

The Controlled Cortical Impact (CCI) injury model is a well-known and widely used TBI model that has been around since the late 1980's [25]. Though it was originally developed in the ferret, it is most commonly used in rats and mice now. To induce the injury, a pneumatically or electromagnetically driven impactor is used that will transfer energy to the intact dura mater following craniotomy (Figure 2.4). This will cause focal damage to the underlying cortex, and sometimes the subcortical structures in cases of more severe injury. A key feature of CCI is that the mechanical factors such as velocity of impact, depth of resulting deformation and duration of impact can be controlled so that a broad range of TBI severities can be produced. A large majority of literature on CCI is focussed on the effects of moderate to severe TBI typically resulting in lesion cavitation and destruction of a large portion of the cortex which can easily be seen on MRI images not only immediately after impact but even one year post injury [26–30]. An increasing number of studies try to model mTBI by adjusting the mechanical parameters of the CCI model. A milder form of the injury can be achieved for example by reducing the velocity of impact or the impactor size. Ideally, in a mild injury minimal change in cortical volume should be present. However, there is no consensus what types of CCI are considered mild, moderate or severe and some articles claim a mild injury while destroying a large portion of the cortex [31, 32].

Fluid percussion injury

The midline Fluid Percussion Injury (FPI) model in the rat was developed around the same time as the CCI model [34]. In this model, the injury is inflicted by a pendulum striking the piston of a reservoir of

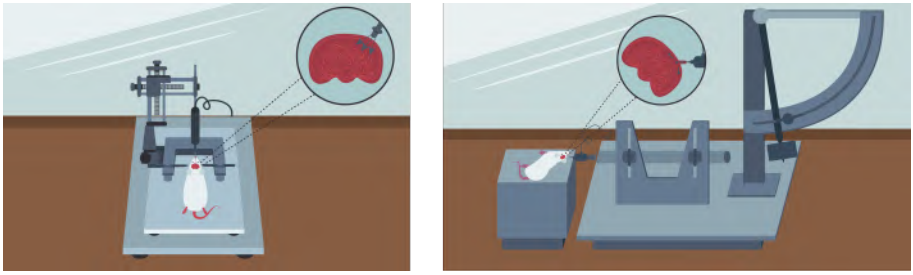

Figure 2.4: Schematic representation of the Controlled Cortical Injury model and the Fluid Percussion Injury model. Figure adapted from [33]

fluid that generates a fluid pressure pulse to the intact dura through a craniotomy (Figure 2.4). The severity of the injury depends on the force of the pressure pulse and has a mixed focal-diffuse pattern that closely mimics human closed head injury. A few years later, the Lateral Fluid Percussion Injury (LFPI) model was developed where the craniotomy site is moved from the vertex to a lateral position, hoping to induce a coup-contrecoup injury. Although it does not produce this type of injury, it does produce more consistent cell death to subcortical structures such as the hippocampus and thalamus, and avoids damage to the sagittal sinus [34]. In comparison with midline FPI where there is damage to both hemispheres, the LFPI model will inflict primarily unilateral cortical damage rarely involving the contralateral cortices. On MRI the most prominent morphological findings after moderate to severe FPI is the focal contusion of the cortex where the areas that were acutely damaged are replaced by CSF over time [35]. On the contrary, mild FPI does not induce such gross changes and there are no lesions visible using imaging technologies such as CT or MRI [36].

While the focal brain injury models have been useful in the study of TBI, the major drawback of these models is that they require a craniotomy. There is evidence that a craniotomy can affect the brain physiology and influence the TBI studies [37]. Also, in mTBI patients, skull fractures and craniotomies are uncommon, so when modelling mTBI in an animal, a craniotomy should be avoided.

2.3.2 Closed head models

Closed head injury models do not use craniotomy and therefore a focal injury is rare. On the contrary, these models try to induce wide spread damage throughout the brain and are sometimes termed diffuse injury models.

Controlled contusion injury model

The mouse or rat is placed in a stereotactic frame and the impact is delivered by use of an impactor but now onto a closed skull hoping to produce a diffuse injury. Most groups using this injury model do not report focal injuries and anatomical images do not show any lesions even after repeated injuries [38–40]. However, Maruichi et al. [41] observed minor bleeding in the inter-hemispheric fissure and lateral ventricles.

Weight drop model

Originally, the weight drop model was a cortical contusion injury model with craniotomy [42]. In this model, a weight is dropped through a cylinder onto a plate (footplate) which is in connection with the exposed dura mater to induce a focal injury. However, this model has become less popular and is not frequently used anymore. Later, a rodent model for Closed Head Injury (CHI) was developed. Briefly, a lightly anaesthetised rat is placed onto a hard surface with the skull exposed and a blunt-tipped rod is then released from a height of 1.5 - 2 cm onto the skull to induce a mild trauma. In the mild form of this model, skull fractures are usually avoided and no (or minimal) contusion sites are visible [43]. However, in the moderate to severe form, a large contusion site is present and the ventricles can be enlarged [44]. A few years later, Marmarou et al. [45] developed a weight drop model which induces a DAI pattern. In this model, the rat or mouse is placed on a foam matrass and has a helmet glued onto the skull, which will diffuse the impact of the weight dropped from a certain height through a guiding column (Figure 2.5). To induce a mTBI the weight is dropped from 1m. This rarely induces lesions visible on anatomical MRI. On the other hand, moderate to severe injuries (with a weight drop from 1.5 - 2 m) can induce haemorrhagic injuries in corpus callosum and cortex detectable

on MRI images [46]. Mostly, the weight drop model is used to induce a mild trauma with DAI and several recent studies have adapted the original model to further optimise the injury induction, e.g., by adjusting the weight to a lower mass and dropping the weight from a lower height [47]. In a different approach, the rat is placed on tinfoil suspended above a foam matrass whereby the rat will make a propelling movement at impact. This will induce acceleration/deceleration and rotational forces on the brain which mimics brain injury caused by a car accident [48]. In this work, we will use the Marmarou weight drop model to induce mTBI in rats. Because there is still no consensus on the definition of a mild injury in rodents, we used the absence of visible fracture or lesions on anatomical scans (CT or MRI) after trauma induction as a criterium for a mild trauma.

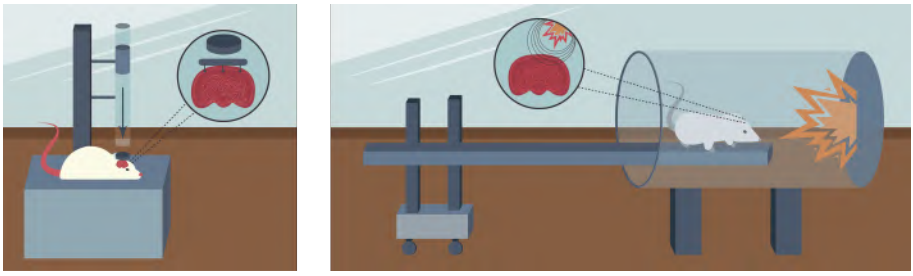

Figure 2.5: Schematic representation of the weight drop injury model and the blast injury model. Figure adapted from [33]

Blast injury model

Military personnel that has been exposed to a blast but without any visible injuries could suffer from Blast-induced TBI (bTBI) and there has been major interest in this subclass of TBI patients. To investigate effects of blast waves on the brain, various animal models try to simulate conditions associated with bTBI. The most frequently used models are open-field blast, blast tubes and shock tubes (Figure 2.5) [49]. In the first two models explosives are used to induce the blast, whereas in the latter compressed gas, such as helium, is used which is safer to use. Generally, in the milder forms of bTBI no injuries or lesions are visible in the brain parenchyma [50]. On the contrary, when the brain is exposed to multiple

blasts or more moderate to severe injury, there can be cortical contusions with or without subdural haemorrhages [51].

2.4 Cognitive remediation therapy in animals

As stated before, animal models are crucial to elucidate pathophysiological mechanisms following TBI and the exploration of therapy options. Over the past decades a myriad of behavioural assessments have been developed to evaluate cognitive functioning after mTBI. The Morris Water Maze (MWM) is one of the most widely used behavioural tests to demonstrate cognitive problems, more specifically spatial memory deficits [52]. However, the focus on cognitive training is a fairly new trend and adaptations of this swimming maze are now being used as training paradigm. Another neurorehabilitation therapy that has been developed to improve cognitive functioning in rodents is Environmental Enrichment (EE). However, both these types of cognitive training are not really translatable to human therapy. Additionally, standardisation of therapy is not easy to maintain and the extraction of outcome parameters is labour intensive. In recent years, computerized cognitive training programs have become more popular to train the affected cognitive functions in TBI patients [53, 54]. During training, the patient will typically perform a series of sessions increasing in task difficulty and systematically improve his cognitive functioning by repetitively performing neuropsychological exercises. Several recent studies have developed training paradigms to enhance memory or executive functioning for TBI patients [55–58] and reviews are modestly positive about the added value of such training programs [59, 60]. In response to the computerised testing and training in humans, touchscreen training systems for animal were developed.

2.4.1 Environmental enrichment

Environmental enrichment is an experimental strategy where housing is substantially different from that of usual experimental laboratory rats hoping to provide cognitive stimulation that will improve the cognitive functioning of the animal [61, 62]. In contrast to standard housing where a single rat or paired subjects live in traditional laboratory-sized cages

and receive only basic amenities (i.e., food and water), the EE cage has multiple levels and a wide array of sensory stimuli (e.g., balls, ramps, tubes, and nesting materials) (Figure 2.6). Typically 10 – 12 rats, which include both TBI and sham controls, are housed together in one cage to ensure equal conditions. This environment affords enrichment and integration of exploratory, physical, and social elements.

This training method has been studied extensively and has provided deeper insights in timing, duration and dosage of this therapy [61]. It has been demonstrated that EE for 6 hours is evenly beneficial for cognitive functioning as continuous enrichment and that enrichment for two weeks is sufficient to improve on a spatial learning task [63, 64]. Furthermore, it was shown that the cognitive benefits from a three week EE are maintained for at least 6 months post-rehabilitation [65].

Figure 2.6: Example of a housing cage used in environmental enrichment (left) and the pool used as Morris water maze (right). Figure adapted from [61, 66]

2.4.2 Maze training

There are only a few adaptation of the Morris water maze to engage the cognitive assessment method as a cognitive training. In the study by Brayer et al. [67] rats were trained implicitly beforehand on the MWM memory task to find a platform hidden under water that was moved

randomly in the four quarters of the pool (Figure 2.6). On the testing day, spatial cues were added to the walls to guide the rat in finding the hidden platform. Compared to the TBI rats that did not have this training stage, the TBI rats with training performed better (reduced platform and escape latency) and were able to incorporate the extra-maze cues into their search strategies. This method was further refined by adding a visual priming step whereby the rat is briefly exposed to the spatial cues during training [68].

2.4.3 Touchscreen based training

In response to the computerised testing and training in humans, Bussey et al. [69] developed the touchscreen training system for rats and was based on the Cambridge Neuropsychological Test Automated Battery (CANTAB) testing methods. The CANTAB itself originated in part from neuropsychological tests in rodents and monkeys and thus exemplifies translation in two ways [70]. This touchscreen testing method for rats, which has been thoroughly validated, allows graphic stimuli to be presented to a rodent and the rodent to respond to the computer screen via a nose-poke (Figure 2.7). In addition to facilitated translation between human and rodent tests, the system allows for a high degree of automation and standardisation and has the ability to deliver a battery of cognitive tasks. However, this touchscreen system has, to the best of our knowledge, never been used as cognitive training therapy. Contrary, the touchscreen systems have been used to investigate the influence of TBI on cognition and behaviour [71]. In the following sections, we will give a short overview of the two training tasks that will be used as cognitive training for mTBI rats in this dissertation.

PAL

The Paired Associate Learning (PAL) task finds it origins in studies on object-location association learning and had been linked to hippocampal functioning [70]. In animals this ability has been described as remembering 'what and where'. Rodent PAL is fundamentally similar to CANTAB-PAL in that it taps into object-location associations, namely the rat has to learn an association between a visual stimulus and its

Figure 2.7: Set up of the touchscreen training systems

location on the screen, demonstrated under cued-recall conditions [72]. More specifically for the rodent version will each visual stimulus (object: flower, spider or airplane) correspond to a specific location (Figure 2.8). On each trial, two different objects are presented, one in its correct location, the other in an incorrect location and the rat has to indicate which one is correct. The third location remains blank. The specific correct location of each object remains constant throughout training and only three object-location associations remain relevant throughout training, whereas in CANTAB-PAL novel object-location associations are used on each trial, requiring the encoding and maintenance of individual associations across a delay. Despite this difference, the rodent PAL task has generated patterns of results very much in line with observations from human research using CANTAB-PAL [70]. As mentioned before, the task has been linked to hippocampal functioning which has been confirmed in humans by lesions and functional MRI studies [73, 74]. Furthermore, the CANTAB-PAL has shifted from a research tool to a screening tool for Alzheimer's diseases in clinical practice as it is sensitive to performance decrements in patients with mild cognitive impairment and has predictive power in identifying patients that are likely to develop Alzheimer's disease [70]. Therefore, the rodent PAL has been studied to investigate pharmacological models of cognitive impairment [75].

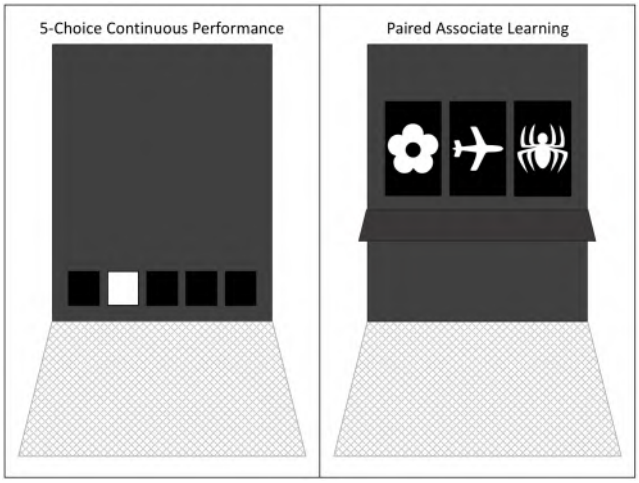

Figure 2.8: Schematic representation of the training tasks

5-CCP

The Continuous Performance Test (CPT) is widely established and the most commonly used measure of attention and response inhibition in both practice and research [76]. In essence the subjects must respond to target stimuli and be inhibited from responding to non- target stimuli. However, in rodents the original 5-Choice Serial Reaction Time Test omitted the element of non-target stimuli and thus it did not require response inhibition making it more a measure of attention and waiting impulsivity alone. Of note, variations of the 5CRTT have been successfully translated to human touchscreen platforms as well to investigate attentional deficits [77]. Today, the 5-Choice Continuous Performance test, an extension of the initial 5-CSRT task exists which more closely resembles the human versions of the test by including go and no-go trials [78]. More specifically, each trial a stimulus will be presented in one of the 5 windows (go trial) and the rat has to nose-poke that window (Figure 2.8). However, when the stimulus is presented in all 5 windows (no-go trial) the rat has to inhibit from a response. Additionally, the visual stimuli are presented at variable, unpredictable intervals to limit anticipation of the animal. In agreement with human data, the rodent CPT appears to relate on prefrontal and limbic cortical areas [77].

2.5 Imaging of TBI

Since TBI has such a complex pathology, visualisation of the full extent of the damage is not easy. In the acute phase, CT is of utmost importance to detect (focal) injuries that may require intervention (e.g., haematoma, skull fractures)[16]. In mTBI patients, CT can show intracranial lesions in only 20 % of the cases and usually it will only show subtle abnormalities such as petechial haemorrhages, mild oedema and/or small contusions that do not require surgical intervention (Figure 2.9.A)[79]. If the patient would deteriorate, a follow up CT scan is performed that can detect evolving secondary damages such as cerebral oedema, ischemia/infarction and herniation [16].

Although MRI has a far better sensitivity to certain types of brain lesions, it is rarely performed in the acute setting due to its complex logistics and lengthy scan times. Presently, conventional (anatomical) MRI is used to evaluate patients for whom CT fails to explain the neurologic status [16]. On T2-weighted and Fluid Attenuated Inversion Recovery (FLAIR) images, lesions can appear as hyperintense areas and can be indicative of oedema formation (Figure 2.9.B-C). However, because of its microscopic and diffuse nature, DAI is commonly undetected with anatomical MRI. Therefore, clinicians are shifting to using imaging techniques that are more sensitive to blood products that are associated with the microhaemorrhages present in DAI, such as $T2^*$ imaging and Susceptibility Weighted Imaging (SWI) of which SWI is highly superior in detecting lesions [81]. These scans will show little black dots at the location of the haemorrhages that are easily identifiable (Figure 2.9.D). Another imaging technique that is used more frequently to better identify mild axonal injury is Diffusion Weighted Imaging (DWI) and will be discussed in more detail in the next chapter.

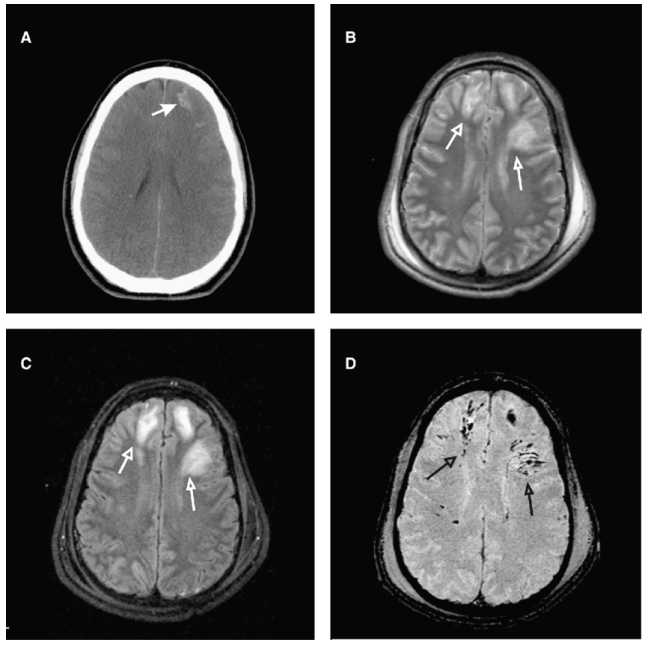

Figure 2.9: CT, T2, FLAIR, and SWI (A, B, C, and D, respectively) of a 40 - year-old male who suffered a TBI. CT demonstrates an ill-defined haemorrhage in the left frontal lobe (solid white arrow). T2 and FLAIR show a large lesion in the left frontal lobe and a smaller lesion in the right frontal lobe (open white arrows). While T2 and FLAIR show large areas of injury, SWI demonstrates numerous smaller foci of haemorrhage. SWI particularly identifies traumatic haemorrhage at the frontal gray-white matter junction that may be associated with diffuse axonal injury (open black arrows) [80].

3 Diffusion MRI and microscopy of the brain

3.1 Basic principles of MRI

3.1.1 Components of an MRI scanner

The magnetic resonance imaging (MRI) scanner has three major components that are essential to make an image (Figure 3.1). The large superconducting magnet is the most important part - and also the most expensive - and creates the static B_0 magnetic field around the patient which should be as homogeneous as possible [82]. Today, field strengths of 3 T are frequently used for human MRI scanners. The second component of the scanner are the gradient coils, these are necessary to influence the magnetic field in order to image certain parts of the patient [82]. Three pairs of coils make it possible to locally manipulate the magnetic field in x, y and z direction. Lastly, the Radiofrequency (RF) system will transmit the RF pulses to excite the tissue of the patient, and also receives the Magnetic Resonance (MR) signal from the same tissues.

3.1.2 Protons, spins and magnets

Protons are small positively charged particles in the nucleus of an atom and posses the intrinsic property of spin. We can represent this

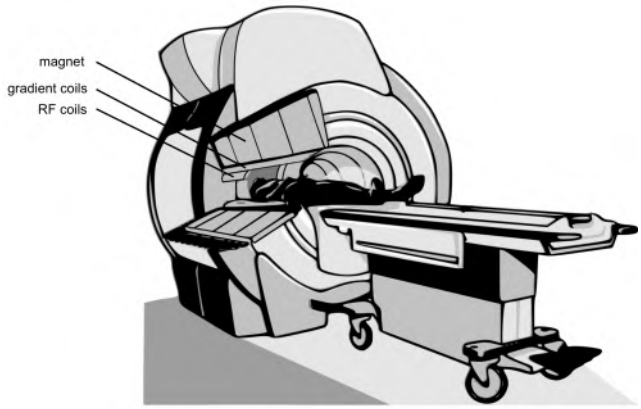

Figure 3.1: Schematic representation of an MRI scanner. Figure adapted from [83]

property by a charged particle that rotates around its own axis and this way inducing an electric current. Different atoms exhibit the spin property (^{1}H, ^{13}C, ^{19}F, ^{23}Na, ^{31}P, amongst others) all having one thing in common: an odd number of nucleons. In MRI mostly ^{1}H is used because there is an abundance of hydrogen atoms in the body coming from the fat and water molecules that are abundantly present in living tissue. Therefore, ^{1}H will provide a more intense MR signal in comparison with the other atoms. According to the laws of physics an electric current or a moving charge will induce a tiny magnetic field. Therefore, each proton will have a spin magnetic moment. In MRI this property is used to make images [84, 85].

The spin magnetic moment can be described by a vector μ. When the spins are not in an external magnetic field, the vectors will be oriented randomly. When they are brought into the B_0 magnetic field they will align to the field in a parallel or anti-parallel fashion (Figure 3.2). This is because there are two eigenstates of spin - spin up (parallel) or spin down (anti-parallel) - which have a low and high energy level, respectively. However, there is a slight excess ($\pm$ 3 ppm at 1 T) in the spin up state which will result in a small microscopic effect: the net magnetisation M_z which is aligned with the main magnetic field B_0 (figure 3.2.B). Furthermore, the spins precess around their own axis with a certain

frequency, the Larmor frequency ω_0. This frequency is dependent on the external magnetic field B_0 and a constant, the gyromagnetic ratio γ:

$$\omega_0 = \gamma \times B_0 \tag{3.1}$$

In the external magnetic field the spins will precess at the same frequency. However, they will all have a different phase. Therefore, the magnetic moments perpendicular to the magnetic field will cancel each other out and no net magnetisation will be detected.

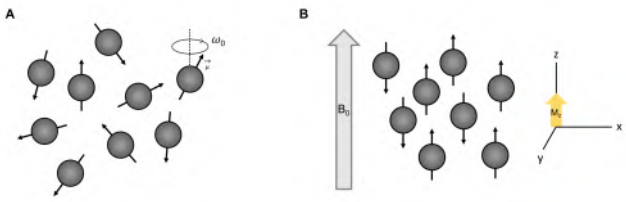

Figure 3.2: The spins are orientated randomly when they are not in an external magnetic field and therefore no net M_z will be present (A). However, when the spins are brought into an external field (B_0), the spins will align with the magnetic field in a spin up or spin down fashion, resulting in M_z (B).

To obtain a measurable signal an RF pulse is applied for a few milliseconds to stimulate the spins (Figure 3.3). The frequency of the RF pulse has to be the same as the Larmor frequency. Only then the spins can pick up the energy of the RF pulse. This is called resonance. Now, the spins start to precess with the same phase and this creates transverse magnetization M_T. Also, the spins tilt away from the longitudinal axis over a certain angle θ, depending on the energy of the RF pulse. In MRI, mostly a 90° pulse ($\theta = 90°$) is given which flips the magnetization completely from the longitudinal axis to the transverse axis. This transverse magnetization, spinning at the Larmor frequency, is responsible for the detectable MR signal. More transverse magnetisation leads to a stronger signal, however, the signal rapidly fades due to relaxation processes [84, 85]. This signal is called the Free Induction Decay (FID).

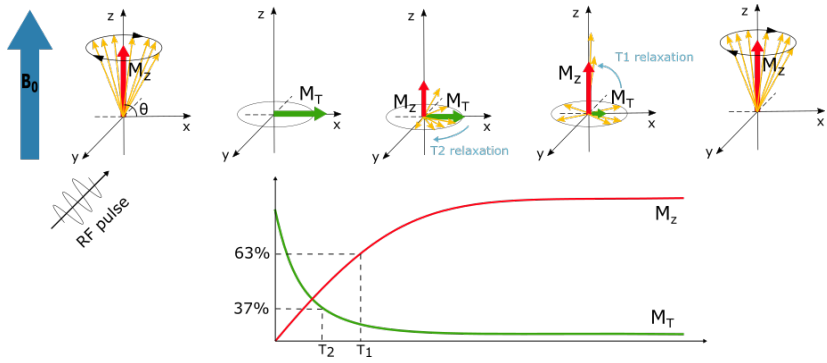

Figure 3.3: Before the application of the RF pulse the spins will be aligned to B_0 and precess with a different phase. After application of the RF pulse, the spins will be pushed into the xy-plain and all precess within the same phase, creating M_T which can be measured by the MR system. During relaxation the spins will gradually dephase (T_2 relaxation) and return back to the z-axis (T_1 relaxation) aligned with B_0. Both relaxation processes have an exponential course and are defined with a characteristic time constant, T1 and T2 respectively.

3.1.3 Spin relaxation

Relaxation after the 90° pulse will shift the spins back into the original energy state (aligned to B_0) very fast (Figure 3.3). Relaxation can be subdivided into two independent processes. T_1 relaxation tilts the magnetic moments back to the longitudinal axis aligned to B_0. This results in an increase in M_z. On the other hand, T_2 relaxation causes the spins to precess out of phase leading to a decrease in M_T. Both processes have an exponential course with a certain time constant, T_1 and T_2 respectively. At T_1 63 % of M_z will be recovered and at T_2 M_T will have only 37 % of its initial value [84, 85].

In T_1 relaxation the spins loose their energy by interaction with the surrounding tissue (spin-lattice interaction). Therefore, the T_1 is tissue dependent. Also, the external magnetic field influences the T_1 and at higher field strengths the T_1 will be longer. T_2 relaxation is also tissue specific but is a bit faster than T_1, which implies that there is another process that speeds up the T_2 relaxation. Via interactions with each other (spin-spin interaction) dephasing of the spins is facilitated and this is independent from the field strength. Though, in reality the FID

will decrease faster than T_2, namely with a shorter time constant T_2* (Figure 3.4). This is the result of small imperfections in B_0 and the body of the patient [84, 85].

3.1.4 Measurement of signal and contrast

As mentioned before, the FID signal will decrease very fast due to the T_2* relaxation and therefore be difficult to measure by the MR system. To be able to measure the signal, mostly the spin echo sequence is used. This is also the basic sequence of MRI.

First, a 90° excitation RF pulse is administered which - as discussed previously - flips the spins and creates M_T (Figure 3.4). However, the T_2 and T_2* relaxation will *dephase* the spins and the net M_T is lost. Subsequently, a 180° refocusing RF pulse is given to *rephase* the spins and M_T is (partially) rebuilt. The resulting signal is called the spin echo and can be measured by the RF coil. The time between the 90° RF pulse and the echo is called the Echo Time (TE) and the time between two 90° pulses and to run through the whole sequence is called the Repetition Time (TR) [84].

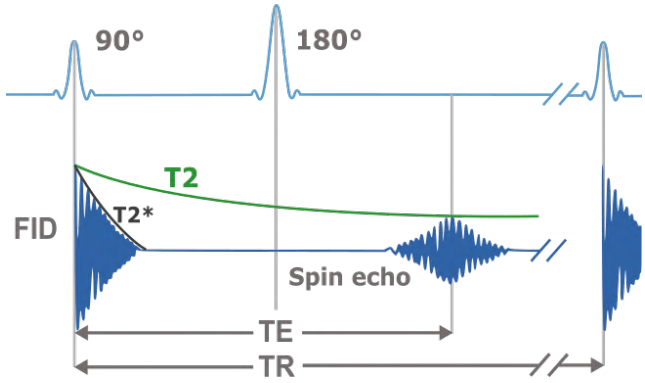

Figure 3.4: The basic Spin-Echo sequence. Following the 90° excitation pulse the FID signal is created and rapidly decays. However, the signal can be rebuild with a 180° refocusing pulse and results in the spin echo. The time between the excitation pulse and the creation of the echo is called the echo time (TE). The time to run through the whole imaging sequence is called the repetition time (TR). Figure adapted from [84]

MRI is a technique with excellent soft tissue contrast and in order to discriminate the different tissue types from each other, we want to make the contrast as high as possible. Since tissues with a high proton density will induce a higher signal, the contrast is partly influenced by the proton density of the tissue types. Additionally, the TE and TR will also have an influence on image contrast. The most basic types of contrast in anatomical MRI are T_1- and T_2-weighted images and proton density images. In order to obtain such images the TE and TR will have to be adjusted (Table 3.1). To obtain a T_1-weighted image a short TE and TR will be applied. Fatty tissues have many spin-lattice interactions which leads to a fast recovery of M_z and appear bright on the T_1-weighted image. Contrary, tissues with less spin-lattice interactions (e.g., CSF) appear black [84].

Table 3.1: Relation of TE and TR duration and the obtained contrast.

	short TR	long TR
short TE	T1	PD
long TE	not useful	T2

The T_2-weighted image is created using a long TE and TR. Fatty tissues will have many spin-spin interactions which lead to a quick decrease in M_T and loss of signal. Spins in watery tissues on the other hand will dephase less quick and yield a high signal on T_2 weighted images [84].

In a Proton Density (PD) image there is no T_1 or T_2 contrast because the TR and TE are too long and too short respectively. Thus, the signal will only depend on the local proton density. Tissues with a high amount of protons will generate a high signal and tissues with a low amount of protons will produce a low signal [84].

3.1.5 From signal to image

To know where exactly in the body the signal came from, gradient coils are used. The three coil pairs each have their function: slice selection (z-axis), frequency encoding (x-axis) and phase encoding (y -

axis). This way all the voxels in the three orthogonal directions can be analysed.

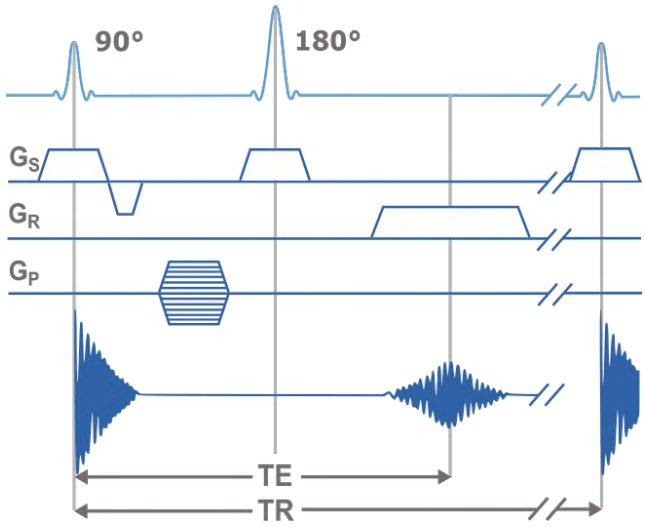

Figure 3.5: Application of the slice selection, frequency encoding and phase encoding gradients in a basic spin echo sequence. Figure adapted from [84]

First, a slice selective gradient G_S is applied in the z-direction during administration of the RF pulses (Figure 3.5). This has as effect that the magnetic field surrounding the patient is no longer homogeneous but varies linearly. Since the Larmor frequency is dependent on the local magnetic field, the spins will no longer precess with the same frequency. So, only spins that precess with the same frequency as the RF pulses will be affected. In the x-direction a frequency encoding gradient G_R is administered during the read out of the echo. As a result, the measured signal will contain multiple frequencies that depend on the position of the spins along the x-axis. Lastly, a phase encoding gradient G_P is applied along the y-direction between the 90° and 180° RF pulse. The spins will dephase at a different rate and a phase difference is built up between spins depending on their position along the y-axis. This phase encoding has to be repeated as many times as there are voxels in the y-direction and with each G_P differing in strength[84].

This is because the individual phase shifts contributed by each voxel in phase encoding direction cannot be uniquely decoded from a single echo. Or, in other words, the individual contributions of each voxel that make a summed phase cannot be sorted out from one single observation where you measure a signal of certain frequency and summed phase. However, by making as many observations as there are voxels in the phase encoding direction it is possible to determine their individual contributions [86].

The measured signal obtained from all previous encoding steps is stored in the so called k-space matrix or frequency domain. This contains all the frequencies and their corresponding amplitudes. To create the image we need to go from the frequency domain to the spatial domain by applying an inverse Fourier transform [84].

3.1.6 Small animal MRI

Imaging of small animals requires specialised hardware including higher field strenght, stronger gradients and small RF coils. Most preclinical MRI systems use field strengths between 4.7 - 11.7 T. By using higher field strengths, a higher net magnetisation can be obtained that will result in higher MR signals, and thus in a higher Signal-to-Noise Ratio (SNR). A higher SNR implies that the voxel size in the images can be decreased, and thus that the spatial resolution can be increased, which is necessary to provide sufficient details when imaging the small organs of rats and mice. Stronger gradients are required because voxel size is also determined by the strength or steepness of the gradients. A smaller voxel size can be obtained by using gradient systems with rapid rise time and high amplitudes. To further improve the SNR, RF coils of the appropriate size are used [87]. Since many preclinical systems do not yet have the ability to perform parallel imaging, the scan time can become quite long - especially in comparison with human MRI - and can become a limiting factor to perform advanced imaging sequences. Several other attributes are needed to image small animals. During scanning, the animals are commonly anaesthetised using a mixture of isoflurane and O_2. In the magnet, an animal that is asleep will lose body heat rapidly so the animal is covered with a circulating warm water blanket to maintain its body temperature. Also, the respiration

Figure 3.6: A small animal 7 T MRI system set up. The blue wire is part of the pressure pad that will send the respiration signal to the respiration monitor whereas the thick black cord contains tubes that deliver warm water to the warming blanket (blue pad on top of rat). The white nose cone delivers the anaesthesia (A). In this dissertation a quadrature volume coil was used to perform diffusion scanning and slides over the head of the rat (B).

rate of the animal needs to be monitored with a pressure pad to make sure that the animal is not sleeping too deep nor waking up too soon.

3.2 Diffusion Weighted Imaging

Because mTBI is commonly undetected using conventional T1-, T2- or PD-weighted MRI, newer techniques are being developed to better identify the DAI. In this dissertation we will make use of diffusion weighted imaging (DWI) to investigate the microstructural changes that occur after an mTBI and cognitive training. In the sections that follow we will briefly explain the principles of diffusion weighted imaging and the diffusion models used in this dissertation.

3.2.1 The diffusion motion

Molecular diffusion, or Brownian motion, refers to the notion that any type of molecule in an environment without borders will displace at random and with equal distances in all directions due to thermal

energy. This is also termed *isotropic* diffusion and the displacement distribution of the molecules will have a Gaussian profile. However, when the molecules encounter obstacles with a certain direction, e.g., axons, the diffusion will be hindered and no longer be equal in each direction. This is called *anisotropic* diffusion [88].

In Diffusion Weighted Magnetic Resonance Imaging (dMRI) the displacement of water molecules in a certain direction is measured over a few milliseconds. By measuring the degree and direction of the diffusion, information about the structure of the brain can be obtained. At body temperature (37 °C) and during a small diffusion time interval (Δ), the molecules will only travel a distance of several micrometers. In a non-obstructed environment, e.g., CSF, the diffusion will be more or less the same in each direction and thus induce the same MRI signal in each direction. However, in an environment with a lot of boundaries, e.g., cell membranes and axons, the diffusion and MRI signal will differ depending on the direction [88].

3.2.2 The diffusion gradient and signal

DWI data are collected by applying diffusion gradients. Currently, the Pulsed Gradient Spin Echo (PGSE) sequence is most commonly used to sensitise the MRI signal to molecular diffusion (Figure 3.7). First, a reference image needs to be obtained without the two diffusion gradients, the so called b_0 image [88]. Subsequently, the sequence will be run again, now with the diffusion gradients. The diffusion gradient before the refocusing pulse will dephase the spins, the diffusion gradient immediately after the refocusing pulse will rephase the spins. If the spins are stationary, they sense both diffusion gradients and they will fully rephase. The signal will be the same as in the reference image. However, spins that diffused during the application of the diffusion gradients will experience a different field and a phase difference will be induced, resulting in signal attenuation. The extent at which the signal attenuates can be described with the following expression:

$$S = S_0 e^{-bD} \text{ with } b = \gamma^2 G^2 \delta^2 (\Delta - \frac{\delta}{3}) \tag{3.2}$$

In this formula S_0 is the signal of the reference image without diffusion gradients, γ the gyromagnetic ratio, G the strength of the diffusion gradients, δ the duration of the diffusion gradients, Δ the time between two diffusion gradients and D the (apparent) diffusion coefficient [88]. The b-value is an important factor describing the relation of G, δ and Δ and a raw measure that describes the influence of diffusion on signal intensity. At high b-values the signal will be attenuated more which makes the difference in diffusion between voxels more clear. However, the total amount of signal in the image will be decreased and thus the SNR will be a limiting factor for high b-values. In practice, a b-value of 1000 s/mm^2 is mostly used for brain imaging.

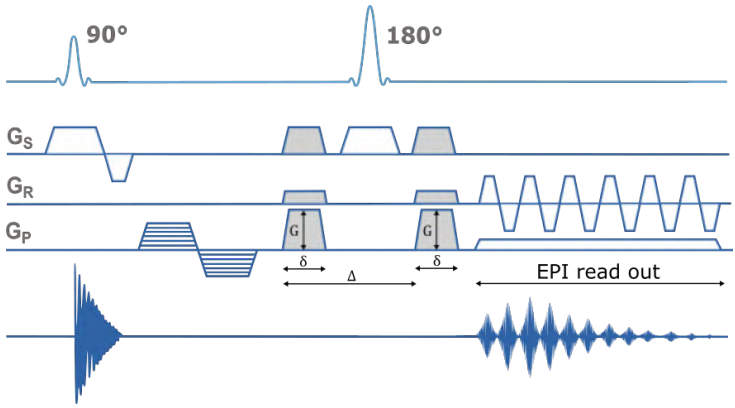

Figure 3.7: The Pulsed Gradient Spin Echo sequence with diffusion gradients (grey) and an EPI read out. The diffusion gradients are characterised with G the strength of the diffusion gradients, δ the duration of the diffusion gradients and Δ the time between two diffusion gradients. Figure adapted from [84]

In dMRI the diffusion of the water molecules is typically investigated along multiple directions to obtain directional information [88]. However, repeating the image sequence several times will make diffusion scanning sessions very long. To speed up the acquisition multiple k-space lines can be acquired at the same time during the read out of the echo using Echo Planar Imaging (EPI). However, this can cause the image to have more artefacts which will have to be corrected during image processing steps [88].

3.3 Diffusion Tensor Imaging and beyond

In the brain there are a lot of 'obstacles' (cell membranes, macromolecules, organelles,...) that will hinder/restrict the diffusion of water molecules in certain directions. Therefore, the previously described DWI model (equation 3.2) is a too simple representation of the brain tissue and can be further refined with a tensor and more advanced models [88]. In the next sections we will discuss the models selected for analysing the diffusion data in this dissertation.

3.3.1 Diffusion Tensor Imaging

Diffusion Tensor Imaging (DTI) uses the tensor model to analytically describe the diffusion shape and can be represented as an ellipsoid [88]. Equation 3.2 will now become:

$$S_{\mathrm{k}} = S_0 e^{-b\overline{\overline{D}}} \text{ with } \overline{\overline{D}} = \mathbf{g}^{\mathbf{T}} \begin{bmatrix} D_{xx} & D_{xy} & D_{xz} \\ D_{xy} & D_{yy} & D_{yz} \\ D_{xz} & D_{yz} & D_{zz} \end{bmatrix} \mathbf{g} \tag{3.3}$$

S_{k} is the signal measured after application of the k^{th} diffusion gradient in direction $\mathbf{g}$. The so called diffusion tensor $\overline{\overline{D}}$ is a matrix symmetrical along the diagonal. To calculate the six unique values (D_{xx}, D_{yy}, D_{zz}, D_{xy}, D_{xz} and D_{yz}), at least six Diffusion Weighted Images (DWIs) are needed in addition to the b_0 image. These six DWIs are measured along six diffusion directions and generate six values for S_{k}. Nowadays, diffusion schemes of 30 diffusion gradients or more are used to calculate the tensor more precisely [88, 89].

To describe the orientation of the diffusion ellipsoid the tensor is decomposed into its three eigenvectors (ε_1, ε_2 and ε_3) with their eigenvalue (λ_1, λ_2 and λ_3) (Figure 3.8). The three vectors now define a local coordinate system for the microstructure in that voxel. The largest eigenvector (ε_1) describes the direction of principle diffusion. Its corresponding eigenvalue is a measure of diffusivity along that direction. This is also called Axial Diffusivity (AD). The Radial Diffusivity (RD) is the mean of the two smaller eigenvalues (RD = $(\lambda_2 + \lambda_3)/2$). For

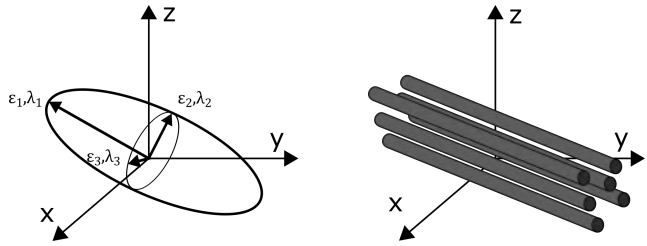

Figure 3.8: The three-dimensional diffusivity is modelled as an ellipsoid whose orientation is characterised by three eigenvectors (ϵ_1, ϵ_2, ϵ_3) and whose shape is characterised three eigenvalues (λ_1, λ_2, λ_3). The eigenvectors represent the major, medium, and minor principle axes of the ellipsoid, and the eigenvalues represent the diffusivities in these three directions, respectively. Fiber tracts have an arbitrary orientation with respect to scanner geometry (x, y, z axes).

example, in white matter the water molecules will primarily diffuse along the axons since the myelin and cell membranes of the axons are an obstacle. The radial diffusion across the axons will thus be much lower than the axial diffusion. To have an overall measure of the diffusivity in the voxel, the Mean Diffusivity (MD) is calculated (MD = $(\lambda_1 + \lambda_2 + \lambda_3)/3$). A last important measure in DTI is Fractional Anisotropy (FA). This measure describes the degree of anisotropy in the voxel and indicates how much the ellipsoid is different from a perfect sphere:

$$FA = \sqrt{\frac{(\lambda_1 - \lambda_2)^2 + (\lambda_2 - \lambda_3)^2 + (\lambda_1 - \lambda_3)^2}{2(\lambda_1^2 + \lambda_2^2 + \lambda_3^2)}} \tag{3.4}$$

The more the ellipsoid is elongated, the higher the FA will be, a perfect sphere will have an FA value equal to 0. When FA is represented on an image (FA map), the image will be black and white scaled. The FA map is often coloured as well to indicate the diffusion directions: red represents left-right diffusion, green front-back and blue inferior-superior (Figure 3.9) [88].

A drawback of the tensor model is the assumption that the probability distribution function of the diffusion process follows an anisotropic Gaussian distribution [90]. Due to barriers and compartments in biological tissue, this assumption is most of the times invalid (except for CSF in the ventricles). Therefore, newer models have emerged that extent the tensor model by also estimating the degree of non-Gaussian diffusion

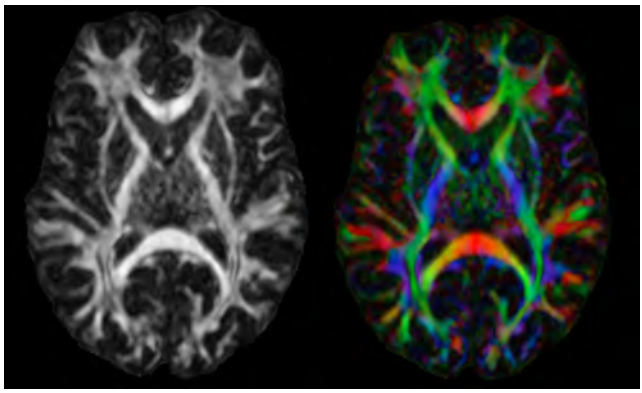

Figure 3.9: FA map (left) and a colour encoded FA image (right) where red represents left-right diffusion, green front-back diffusion and blue inferior-superior diffusion.

(Diffusion Kurtosis Imaging (DKI)) or incorporating a priori biological information (e.g., White Matter Tract Integrity (WMTI) model) [91, 92].

3.3.2 Diffusion Kurtosis Imaging and the white matter model

Diffusion Kurtosis Imaging

The DKI model attempts to accommodate better for non-mono-exponential (non-Gaussian) decay of the diffusion signal as a result of the presence of compartments with different diffusion constants or restricted diffusion within the axons [91] (Figure 3.10). The DKI model includes an additional kurtosis term (K) to capture this deviation from the Gaussian distribution:

$$S(b) = S_0 e^{-bD + \frac{1}{6}b^2 D^2 K} \tag{3.5}$$

Since the model has 15 degrees of freedom (in contrast to the 6 degrees of freedom in DTI), the acquisition scheme will need to be adjusted. In a DKI acquisition at least 3 distinct b-values and at least 15 distinct diffusion gradient directions are required. As in DTI, diffusion schemes with more than 30 directions are used more generally [91, 93].

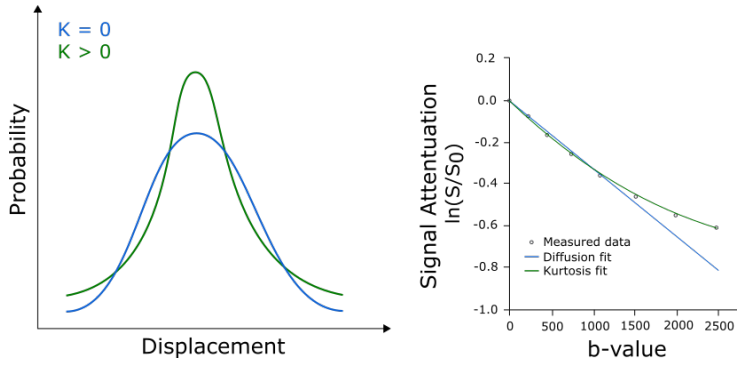

Figure 3.10: Graph on the left shows the diffusion displacement probability distribution with different degrees of kurtosis. The DTI model (K = 0) will assume a Gaussian distribution. The DKI model will assume a positive kurtosis (K > 0). On the right the diffusion weighted signal attenuation is presented in function of the b-value. The DKI model (green line) clearly deviates from the linear fit of the DTI model (blue line) by making use of the information obtained from multiple higher b-values. Figure adapted from [93]

Similar to the DTI metrics AD, RD and MD, the DKI model can provide kurtosis metrics to describe the deviation from Gaussian diffusion: Axial Kurtosis (AK), Radial Kurtosis (RK) and Mean Kurtosis (MK). In white matter, AK is typically low because the diffusion along the direction of the axon is relatively unrestricted. Contrary, RK will be higher as membranes and myelin sheets hinder the diffusion and cause a heterogeneous diffusion pattern that leads to a non-Gaussian displacement distribution [91, 93]. While physical, signal driven diffusion models (DTI and DKI) present metrics that are related to the extent and preferred orientation of water diffusion, specificity to microstructure or pathology is lacking [90, 94].

Biophysical model of white matter

In response to the signal driven models, biophysical or microstructure driven models have been developed, which incorporate a-priori biological information (assumptions) into the model, to assess tissue compartments and its biological attributes more directly [94]. Here, we describe the model defined by Fieremans et al. [92] which provides specific information of the intra- and extra-axonal compartments.

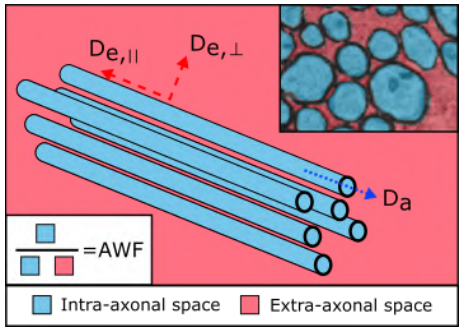

Figure 3.11: Correspondence between the WMTI model and the tissue components (inset right upper corner). The schematic representation shows the axial and radial extra-axonal diffusivity ($D_{e,||}$ and $D_{e,\perp}$) which are metrics of the extra-axonal space. On the other hand the axonal water fraction (AWF) and axonal diffusivity (D_a) are measures of the intra-axonal space. Figure adapted from [39, 95]

Based on D and K derived from the DKI model two tissue compartments can be modelled and together with a set of relationships, several compartment-specific metrics can be derived in addition to the usual DTI/DKI metrics in highly aligned fibre bundles. Exchange of water molecules between the two compartments is neglected and the intra-axonal diffusivity is assumed to be lower than the extra-axonal diffusivity. It should also be noted that water trapped between the myelin sheets is not detectable with typical diffusion scanning parameters and therefore the compartment fractions correspond to measurable water fractions. The WMTI model thus provides the axonal water fraction (AWF), axonal diffusivity (D_a), the axial and radial extra-axonal diffusivity ($D_{e,||}$ and $D_{e,\perp}$) and tortuosity (α). The AWF of the intra-axonal space is estimated based on the maximal kurtosis in the voxel and the axonal diffusivity is the trace of the intra-axonal tensor. Analogous to AD and RD, the Axial Extra Axonal Diffusivity (AxEAD) and Radial Extra Axonal Diffusivity (RadEAD) are calculated by the primary, and second and third eigenvalue respectively, of the extra-axonal tensor (AxEAD $= \lambda_{e,1}$, RadEAD $= \frac{\lambda_{e,2}+\lambda_{e,3}}{2}$). Lastly, the Tortuosity (TORT) of the extra-axonal space is calculated based on the AxEAD and RadEAD($\alpha = \frac{AxEAD}{RadEAD}$) [92].

3.3.3 Fibre specific analysis: introduction to the fixel

Fixel-based analysis (FBA) is a recently developed whole brain analysis technique that allows the examination of white matter organisation of multiple fibre populations within one voxel (i.e., fixels) based on constrained spherical deconvolution [96, 97]. In contrast to the previously described techniques (the DTI, DKI or WMTI models) the spherical deconvolution technique is not dependent on any assumed model of diffusion and does not need to impose any a priori information about the likely number of fibre populations present [98]. It does estimate a Fibre Orientation Distribution (FOD) function. This way, in theory an infinite number of crossing fibres can be distinguished from one another which shows an advantage in crossing fibre regions (Figure 3.12).

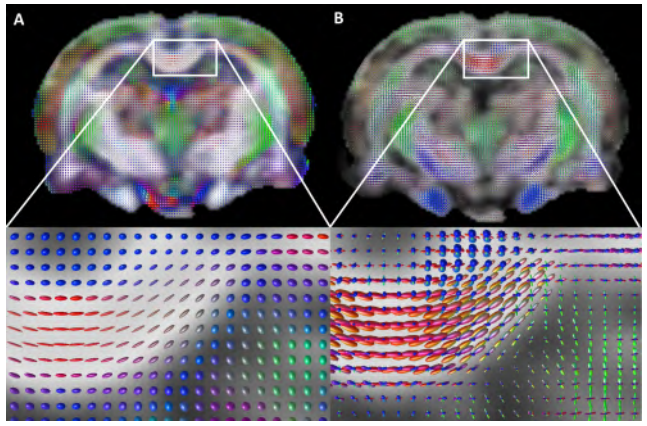

Figure 3.12: An axial section of the rat brain showing diffusion tensor (A) and FOD (B) estimations. In contrast to diffusion tensor imaging, which fits an ellipsoid representing only a single fibre orientation, constrained spherical deconvolution estimates a FOD and is able to resolve multiple fibre bundles in single voxels (see zoomed sections below). Tensor ellipsoids and FODs are colour encoded according to direction: left-right is mapped to red, front-back to blue and inferior-superior to green.

The FBA method provides information derived from morphology differences in fibre bundle cross-section which allows for the inference of group differences [97]. The Fibre Density (FD) and Fibre Cross-Section (FC) are related to the intra-axonal compartment and try to give an interpretation of the compactness and thickness of the fibre-bundle

(Figure 3.13). By combining the two measures into one Fibre Density and Cross-Section (FDC) a more comprehensive measure related to the total intra-axonal volume within a pathway can be obtained.

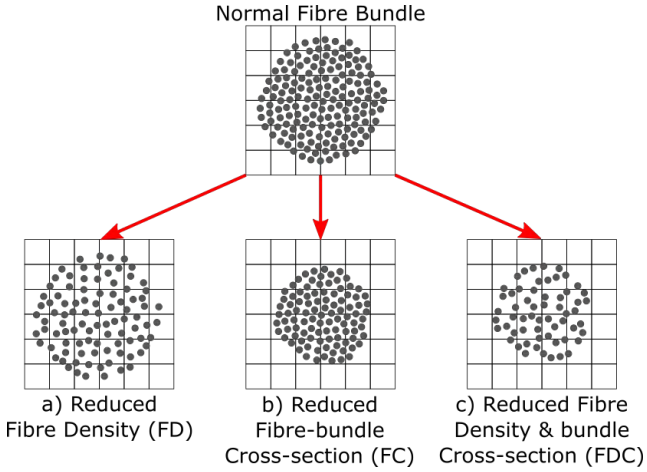

Figure 3.13: A schematic representing a fibre bundle cross-section (grey circles represent axons, while the grid represents imaging voxels). A change to the intra-axonal volume may manifest as: (a) changes in tissue microstructure that result in a change in within-voxel fibre density (b) a macroscopic difference in a fibre bundle's cross-section, or (c) a combination of both fibre density and bundle cross-sectional area. Figure adapted from [97]

3.4 Diffusion weighted imaging in mTBI

Mild TBI is commonly undetected using conventional MRI scans. Therefore, diffusion MRI has gained more interest to investigate microstructural changes following mTBI. However, because mTBI patients are often a very heterogeneous population (differences in age, impact severity, impact location, cause,...) and given the fact that mTBI is an evolving and degenerative process, there is not yet a clear consensus in the results of dMRI research in mTBI. Also, in preclinical studies the multitude of TBI models and different imaging time points does not increase insight in the disease process. Despite the heterogeneity, some recurring findings have emerged. Recent dMRI reviews in mTBI patients described predominantly increased FA and reduced MD at acute time points (up to two weeks post injury) [99–101] and reduced FA

and increased MD values in the chronic phase of mTBI (several months after injury) [102, 103]. To date, there have been only a few longitudinal animal studies using a closed head impact model of mTBI, to investigate brain structure alterations over time with DTI [47, 104–106]. These studies provided evidence of alterations in FA and MD already detectable within a week after mTBI, however, both increases and decreases in MD or FA were reported. Furthermore, imaging is often not performed beyond 30 days after trauma.

In this dissertation, we will combine longitudinal animal experiments (from acute to chronic phase) and different diffusion models (DTI, DKI, WMTI and FBA) with the goal to get a better insight into the disease process of mTBI.

3.5 Macro-, meso- and microscopic imaging of brain tissue

Since mTBI has such a complex pathophysiology, visualisation of the full extent of the damage is not easy. One hallmark of complex processes is that they exhibit structural changes at many spatial scales. In mTBI for example, microscopic axonal damage at the sub-micrometre level might result in changes of the diffusion signal at the sub-millimetre (mesoscale) level observed using dMRI. However, it is possible that these changes do not result in abnormalities at the macroscale level (conventional CT and MRI).

Because of its unique sensitivity to cellular architecture, diffusion MRI is a key modality for microstructural imaging and bridges the gap between macroscopic and microscopic imaging. This mesoscale imaging can be regarded as a way to perform *virtual* histology since it can estimate and map histological features of tissue using non-invasive techniques. This virtual histology has several advantages over classical histology [107]: it is non-invasive, avoiding the need for tissue sampling; it views intact *in-situ* tissue, avoiding disruptions that arise from tissue extraction and preparation; it is non-destructive so it enables longitudinal measurements; it provides a wide field of view, typically showing a whole brain rather than the small samples often used in classical

histology. However, it will not provide the same level of anatomical detail as obtained from classical histology since microstructure imaging provides only statistical descriptions of the tissue over the extent of sub-millimetre sized imaging voxels.

Classical histology has thus been vital (and still is) for the development of modern neuroscience. The major advantage is that it can provide vivid insight into the cellular architecture of tissue because of the high level of anatomical detail. To obtain such high resolution images, sliced post-mortem tissue samples and a standard bright-field microscope are used (Figure 3.14). The lenses are the most important components and a minimum of three lenses are required [108]: the condenser lens forms a cone of light that illuminates the specimen and through the objective lens an image will be formed in the focus of the projector lens. The objectives are instrumental in determining the magnification of a particular specimen and in standard microscopy magnification typically ranges from 4× to 100×. Together with the 10× magnification of the projector lens, the specimen can thus maximally be 1000× magnified allowing a resolution between 1 - 10 μm. Though, this high resolution comes at the cost of a limited field of view. Automated microscopy can overcome this limitation by acquiring a grid of partially overlapping images that are stitched together allowing to obtain a whole brain microscopic image. By stitching several microscopic images together into a larger image, the gap between microscopic imaging and macroscopic imaging (e.g., MRI) can be reduced.

In this work, we will combine classical histology with microstructural MR imaging to investigate structural changes in mTBI at different spatial scales. Histology can help pinpoint the underlying microstructural structures and processes that induce the diffusion signal. Validation of the biological correlates of the diffusion metrics is therefore crucial to better understand the fundamental pathological processes in mTBI.

Another interesting microscopic imaging technique that will be applied in this dissertation is Raman microspectroscopy which can provide a 'structural fingerprint' of brain tissue samples. Raman spectroscopy is a technique that is used to probe the internal structure of molecules

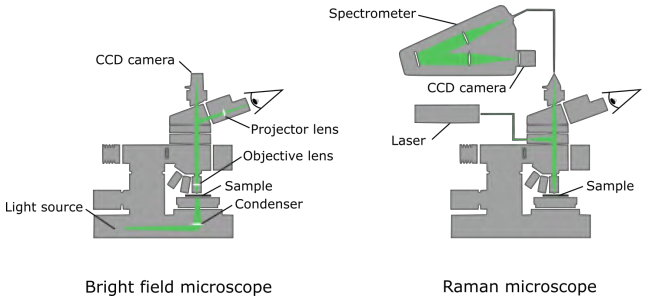

Figure 3.14: Schematic representation of the standard bright field microscope (left) and the Raman microscope (right). Figure adapted from [109]

and has been used as an analytical chemistry tool for studying alterations in chemical bonding [110]. When a beam of monochromatic light from a laser source is used to excite a molecule, most photons are scattered elastically (Rayleigh scattering) which has as a consequence that the wavelength of the scattered light is the same as the excitation wavelength. However, one in every ten million incident photons are scattered inelastically (Raman scattering) which causes the scattered light to display a shift in wavelength compared to the wavelength of the excitation light. When the molecules with which the photons interact absorbs energy from the incident photons, the scattered light will present with a longer wavelength compared to that of the laser source (Stokes scattering). On the other hand, when the molecules loose energy to the photons, the scattered light will have a shorter wavelength. The size of the observed wavelength shift is called the Raman shift and every molecule has its own unique signature shift or spectral fingerprint [111]. This way Raman spectroscopy can be used to detect numerous different molecules within the same tissue sample simultaneously, demonstrating its high multiplexing capabilities [110]. The ability to visualise different biochemical targets simultaneously will yield a more complete picture of biological systems and shows a promising new area of research within the context of imaging. For example, the aromatic ring of phenylalanine will result in a peak at 1002 cm^{-1} and the CH_2-chains of fatty acids will present peaks at 1064, 1297 and 1439 cm^{-1} (Figure 3.15) [112, 113]. Based on differences in peak heights, the difference in protein or fat content can be detected and the grey and white matter spectra can be distinguished from each other. Raman microspectrometry combines

a standard optical microscope with a Raman spectrometer that uses a laser as light source and filters to obtain the correct emitting wave length (Figure 3.14). Photons from the laser are focussed in a spot on the specimen (0.5 - 10 μm) and the Raman scattering is analysed in the spectrometer. By scanning the whole specimen step by step in small spots, a map can be obtained containing the spectrum of all the scanned pixels (spectrogram) [109]. A more detailed description of Raman spectroscopy can be found in [111].

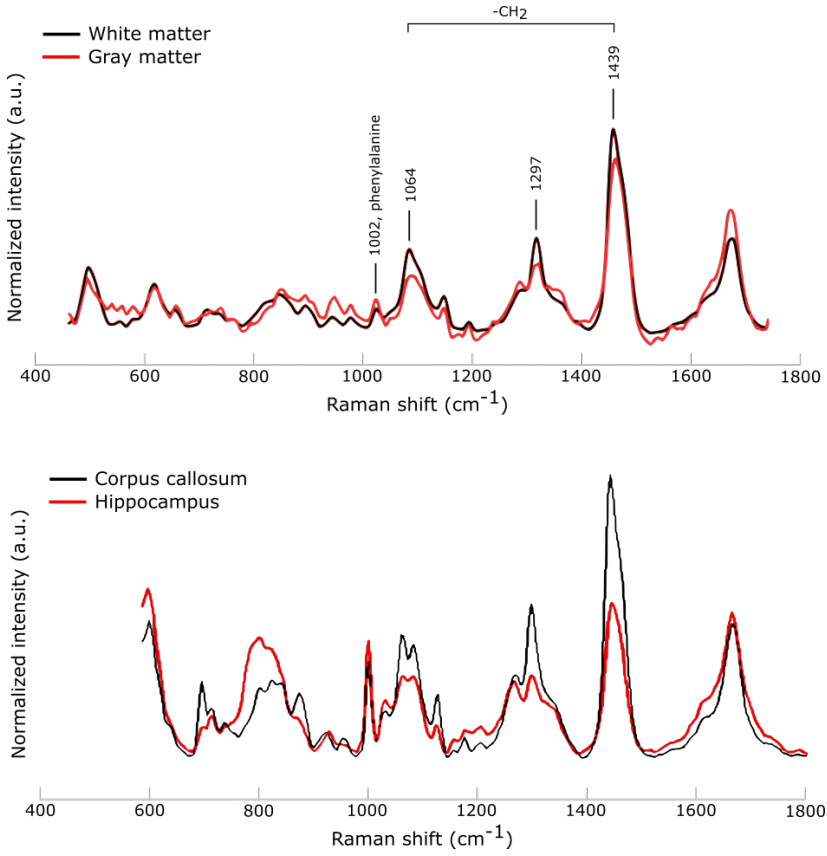

Figure 3.15: Example Raman spectrum of grey and white matter (upper panel). Grey matter has a higher protein content (higher peak of phenylalanine) and white matter has a higher lipid content (higher peaks representing the carbon tail in fatty acids). In the lower pannel an example Raman spectrum obtained from the corpus callosum (white matter) and hippocampus (grey matter) of a rat brain showing the same characteristic peaks. Figure adapted from [113, 114].

4 | Aims of the dissertation

The overall aim of the research outlined in this dissertation was to provide a deeper understanding of the microstructural changes and its biological correlates in the brain following a mild traumatic brain injury (mTBI). Furthermore, we wanted to evaluate whether two cognitive training tasks could specifically improve the induced alterations in two brain regions affected by the mTBI as witnessed by alterations in diffusion MRI metrics.

Currently, the most used diffusion imaging technique in TBI research is diffusion tensor imaging (DTI) and alterations in fractional anisotropy (FA) and mean diffusivity (MD) - the two most commonly used metrics - are widely established. Though, both increases and decreases have been reported in both metrics and thus no consistent outcome can be demonstrated. Additionally, these metrics can be influenced by several underlying biological processes. For example, an increase in FA can be mediated by axonal swelling as well as an increase in myelination. Also, the exact time-course of diffusion changes after sustaining brain injury are not entirely clear. Another drawback of the commonly used DTI model is the assumption of fitting only a single fibre population in a voxel. However, in reality a single voxel can contain several fibre populations that cross or intermingle, also leading to lower FA values. Interpreting these changes in FA as a loss of fibre integrity can thus be a misinterpretation of the underlying processes at play. Therefore, in **Chapter 5, 6 and 7** we will address the following questions:

- *Can advanced diffusion models, i.e., Diffusion Kurtosis Imaging (DKI) and the White Matter Tract Integrity (WMTI) model, provide complementary information to the metrics derived by the DTI model?*

- *How do the diffusion metrics change following an mTBI in both the acute time point (within the first week) and chronic time point (after three months)?*

- *Can we provide morphological fibre information using a model that is able to resolve crossing fibres and performs statistical analysis for the individual fibre populations in a mildly injured rat brain and disentangle the changes to the white matter tracts?*

- *What are the underlying biological correlates that induce the microstructural alterations following mTBI?*

Several recent studies have developed computerised cognitive training in TBI patients and the results have been modestly positive about the beneficial effects on cognitive outcome. However, more research is needed to increase the understanding of the underlying biological mechanisms of cognitive training in TBI. Characterisation of the effects of training on cognition in humans remains a difficult challenge and animal models provide several advantages. Preclinical studies allow for a tighter control over the subjects' health history and are less of a practical challenge when longitudinal MRI scans are combined with an intensive cognitive training program. Currently, only six neuroimaging reports on training-induced alterations using diffusion imaging have been published in healthy rodents and to the best of our knowledge no preclinical studies have investigated these neuroplastic changes in a TBI model. This leads us to the following questions which will be addressed in **Chapter 8**:

- *Can a computerised (touchscreen) training system induce neuroplastic changes following mTBI in rats as witnessed by changes in diffusion metrics?*

- *Do the neuroplastic changes coincide with behavioural improvements?*

- *Can the two training tasks used in this dissertation, i.e., the Paired Associate Learning and 5-Choice Continuous Performance tasks,*

selectively alter the microstructure of the hippocampus and cingulum, respectively?

5 | Longitudinal dMRI in rat model mTBI

This chapter includes data from:

Braeckman K, Descamps B, Pieters L, Vral A, Caeyenberghs K, Vanhove C. **Dynamic changes in hippocampal diffusion and kurtosis metrics following experimental mTBI correlate with glial reactivity**, 2019. NeuroImage: Clinical, 21, 101669.

5.1 Introduction

Traumatic brain injury (TBI) yearly affects more than 10 million people worldwide and is the leading cause of acquired disability in young adults, often caused by traffic accidents or sport injuries [115, 116]. Mild TBI (mTBI) is the most prevalent type of severity of TBI (about 80 % of all TBI cases) and is often termed 'silent epidemic' since many patients suffer from symptoms that are not overtly visible [15]. In mTBI, the brain is subjected to shear-strain forces leading to diffuse axonal injuries with most lesions emerging at the interface between brain regions with different tissue densities, such as the grey-white matter junctions [117]. Furthermore, conventional scans, such as computed tomography (CT) scans or anatomical magnetic resonance imaging (MRI) scans, often show no evidence of injury due to the diffuse and subtle nature of mTBI. Despite the lack of radiological evidence, mTBI patients suffer from cognitive deficits, such as memory problems and executive control deficits, even years after their injury [13]. This lack of radiological evidence of brain injury has led to the application of more advanced MR

imaging methods such as Diffusion MRI (dMRI), that is more sensitive to assess microstructural changes following mTBI.

Diffusion MRI is an MRI technique which is being used more often the past decades due to its greater sensitivity to detect white matter changes following TBI [118, 119]. Fractional anisotropy (FA) and mean diffusivity (MD) are measures most commonly used to follow up changes in diffusion properties related to TBI [100]. Recent dMRI reviews in mTBI described predominantly increased FA and reduced MD at acute time points (up to two weeks post injury) [99–101]. These changes in diffusion metrics have been interpreted as axonal swelling [120, 121]. Contrary, reduced FA and increased MD values could be observed in the chronic phase of mTBI (several months after injury), possibly due to a disruption in parenchymal structure following oedema formation, axonal degeneration or fiber misalignment/disruption [102, 103]. However, the exact time-course and cellular processes underlying alterations in diffusion metrics after sustaining brain injury are not entirely clear in human TBI and pre-injury information is often not available.

Recently, animal TBI models have been developed to overcome these issues and enable to obtain baseline scans pre-injury. To date, there have been only a few longitudinal animal studies using a closed head impact model of mTBI, investigating brain structure alterations over time with diffusion tensor imaging (DTI) [47, 104, 105]. These studies provide evidence of alterations in FA and MD already detectable within a week after mTBI. However, it has been stated that these parameters lack specificity for histological features, despite being sensitive in detecting subtle tissue changes following brain trauma [90].

Diffusion kurtosis imaging (DKI) is an expansion of the tensor model and measures the degree of non-Gaussian diffusion which could provide additional information about tissue heterogeneity or complexity [91]. Using DKI, Grossman et al. [122, 123] and Zhang et al. [124] found reductions in mean kurtosis (MK) in mTBI patients that were associated with cognitive impairments. However, DTI and DKI are only representations of the diffusion signal and aim to characterise the probabilistic water displacement profile without microstructural specificity.

Microstructural mapping techniques based on biophysical models could overcome this non-specificity issue and may offer new information for describing abnormalities after mTBI [94, 125]. These models incorporate a-priori biological information (assumptions) into the model, to assess tissue compartments and its biological attributes more directly. For example, Fieremans et al. [92] recently introduced a novel white matter model (White Matter Tract Integrity model (WMTI)), which provides specific information of the intra- and extra-axonal compartments in highly aligned fibre bundles. The WMTI model estimates the axonal water fraction (AWF), axonal diffusivity (IAD) and the axial and radial extra-axonal diffusivity (AxEAD and RadEAD). This model has already been applied on human data in many pathologies, including TBI [126, 127], multiple sclerosis [128], autism [129] and Alzheimer's disease [130]. In mTBI patients, a reduction in intra-axonal diffusivity in the splenium of the corpus callosum was observed compared to controls and was interpreted as axonal stretch injury [126]. Only a few studies have applied the WMTI model in animal models. In hypomyelinated [131] and demyelinated mouse models [132, 133] was found that the AWF and intra-axonal diffusivity could be informative about acute inflammatory de-myelination and later spontaneous re-myelination.

To the best of our knowledge this is the first study that applies the WMTI model in a rat model of mTBI. Also, by making use of the Marmarou weight drop model [45], producing a diffuse trauma, we believe we model the patients with no clearly visible symptoms after a mTBI much better in comparison to TBI models that produce a more focal injury (for example the controlled cortical impact model) and thus induce more moderate to severe TBI. Furthermore, the changes in diffusion metrics were obtained across time from pre-injury into the acute (one day and one week post injury) and chronic stage (three months post injury) of mTBI.

5.2 Materials & Methods

5.2.1 Animal studies

The study was approved by the Animal Ethics Committee at Ghent University (ECD 15/44Aanv) and all experiments were conducted in accordance with the guidelines of the European Commission (Directive 2010/63/EU). The animals were group-housed and kept under controlled laboratory conditions (12 h light/dark cycle, 20 – 23 °C and 40 – 60 % humidity).

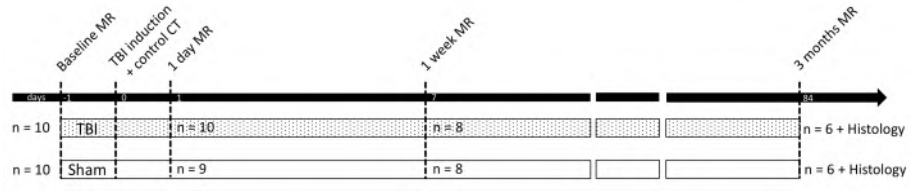

Figure 5.1: Outline of the longitudinal scanning design.

5.2.2 Induction of mild traumatic brain injury

Adult female Wistar rats (n = 20, 262 ± 14 g) purchased from Janvier Labs (Le Genest-Saint-Isle, France) were divided in two groups: 10 rats that received a mild traumatic brain injury and 10 rats that did not receive the impact (sham injury)(Figure 5.1). Female rats were chosen for this longitudinal study as they are more gentile towards cage companions than males when group-housed, and are expected to grow less over the time period of three months.

Mild traumatic brain injury was induced using the Marmarou weight drop model [45], using a multistep procedure (Figure 5.2). First, rats were anaesthetised with a mixture of isoflurane and O_2 (5 % induction, 2 % maintenance) and injected with 0.05 mg/kg buprenorphine (Temgesic, Indivior) subcutaneously. After 30 min, the rat's head was shaved, 100 μl of 2 % lidocaine (Xylocaine, AstraZeneca) was locally injected in the scalp and an incision was made along the centre line to expose the skull. Body temperature was maintained during surgery with a heating pad. A metallic disc with a diameter of 10 mm and

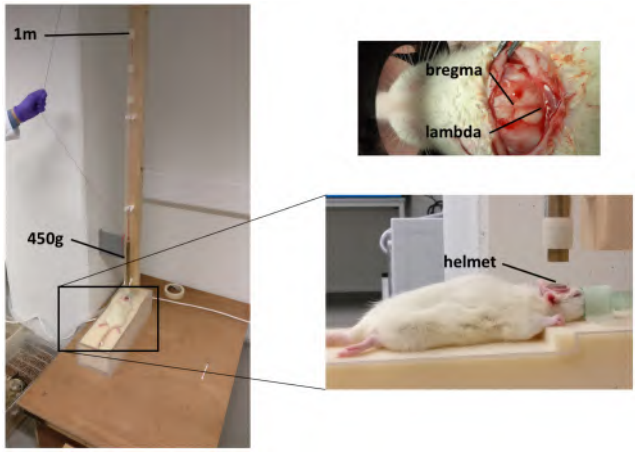

Figure 5.2: The Marmarou weight drop model as modelled in our lab. The brass weight (450g) is released from a height of 1m onto the steel helmet which is fixated onto the skull 1/3 before and 2/3 behind bregma.

3 mm thickness, which acted as a helmet, was glued onto the skull 1/3 before and 2/3 behind bregma. Next, the rat was placed on the custom-made foam bed with a matrass of certain spring constant (Type E, Foam to Size, Ashland, Virginia, USA) and positioned directly under a Plexiglas tube with a 450 g brass weight. The rat was briefly detached from anaesthesia and the weight was dropped from a height of 1 m. Immediately after impact, the rat with the bed was moved away from the tube to prevent a second impact and the rat was reattached to the anaesthesia. To reduce the haemodynamic shock, 1 ml of physiological solution (0.9 % NaCl) was injected through a catheter that was placed in the lateral tail vein. Subsequently, the helmet was removed and the incision was stitched. Then, a CT scan (X-Cube, Molecubes, Ghent, Belgium) was administered to rule out any skull fractures since this is a criterion for euthanasia. To minimize the dose, a general purpose low dose one bed position scan was performed. One day post impact the rats received an extra dose of 0.05 mg/kg buprenorphine after the MR scan.

5.2.3 In vivo longitudinal multi-shell diffusion weighted imaging

MRI data were acquired on a 7 T MRI scanner (BioSpin PharmaScan 70/16, Bruker, Ettlingen, Germany) using a volume rat brain/mouse whole body RF coil. Rats were scanned at baseline, one day, one week and three months post impact (Figure 5.1). During the scanning sessions, the animals were under 2 % isoflurane anaesthesia (5 % for induction), body temperature was kept constant with a circulating warm water heated blanket and bubble wrap, and respiration rate was monitored with a pressure pad.

At each time point, a whole brain anatomical T2-weighted scan was acquired first using a Rapid Acquisition with Refocused Echoes (RARE) sequence: TR = 5.5 s, TE = 37 ms, RARE factor = 8, FOV = 2.5 × 2.5 cm, in plane resolution = 109 × 109 μm, 600 μm slice thickness, 45 slices, 12 min acquisition time. Diffusion images were acquired with a spin echo, echo-planar imaging (EPI) sequence between the olfactory bulb and the cerebellum. Multi-shell diffusion weighted acquisitions were recorded using an encoding scheme of 32, 46 and 64 gradient directions with b-values of 800, 1500 and 2000 s/mm^2 and with 5, 5 and 7 b0 images (scanned at the beginning of each shell), respectively. Other diffusion scanning parameters were as follows: TR = 6.250 s, TE = 24 ms, number of segments = 4, number of averages = 1, FOV = 3 × 3 cm, in plane resolution = 333 × 333 μm, 600 μm slice thickness, 600 μm interslice distance, 25 slices, 65 min acquisition time.

5.2.4 MRI data analysis

Diffusion weighted images (DWIs) were first corrected for noise using the `dwidenoise` function in MRtrix3 [134, 135]. An overview of the image processing pipeline can be found in Figure 5.3. Next, the images were corrected for signal drift and Gibbs ringing artefact for each shell using the ExploreDTI toolbox version 4.8.6. [136]. After concatenation of the three shells, the images were also corrected for EPI, eddy current and motion-induced geometric distortions in ExploreDTI. From the corrected DWIs, the diffusion kurtosis tensor was estimated using the weighted linear least squares method [137]. For

the diffusion tensor model we obtained axial diffusivity (AD), fractional anisotropy (FA), mean diffusivity (MD), radial diffusivity (RD). The kurtosis metrics included axial kurtosis (AK), mean kurtosis (MK) and radial kurtosis (RK) and were calculated based on the diffusion kurtosis imaging model [138]. Based on a white matter diffusion model axonal water fraction (AWF), axial extra-axonal diffusivity (AxEAD), radial extra- axonal diffusivity (RadEAD), intra-axonal diffusivity (IAD) and tortuosity (TORT) were calculated [92]. A total of 12 parametric maps were obtained for each animal at each time point.

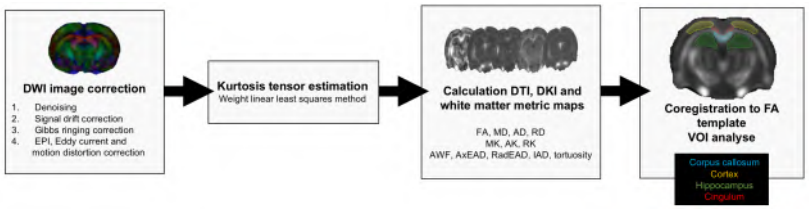

Figure 5.3: Overview of the processing pipeline. First, DWIs were preprocessed to correct for image artefacts. Next, the kurtosis tensor was estimated and the different parametric maps were calculated. Lastly, the maps were coregistered to the FA template and a VOI analysis was performed.

An FA template was made in SPM 12 based on the local population at one week post injury. Since it is the middle time point, this will ensure a good coregistration with scans of other time points (even three months post injury) before performing the Volume-of-Interest (VOI) analysis. To create this FA template first, all subjects were realigned to the first subject using rigid transformation and after this step co-registered to the mean image of the realignment step using affine and non-linear registration. All previously obtained parametric maps were then co-registered in SPM 12 on the FA template using the FA images and a 12 parameters affine non-linear transformation with trilinear interpolation. Next a VOI analysis was performed for the DTI and DKI parameters in the corpus callosum, hippocampus, cingulum and cortex using the Amide toolbox [139] since these regions are closest to the impact site. Because the corpus callosum is a heterogeneous structure, this region is also subdivided in genu, body and splenium.

Metrics of the white matter model were only calculated in the white matter tracts of the corpus callosum and cingulum.

5.2.5 Statistical analysis

Linear mixed model analyses were performed in SPSS Statistics 24 for each diffusion metric in each VOI [140]. We opted mixed models because these enable us to include data of subjects with missing values. The 'group' factor (TBI or sham) was included as a between-subjects variable and the factor 'time' (4 levels, baseline, one day, one week and three months post injury) as within-subject variable. Also, we used an unstructured covariance structure with no assumptions regarding the variances to allow for variable variances across time points. We corrected for multiple comparisons using Bonferroni correction, for the number of metrics within each used diffusion model. Therefore, a p-value ≤ 0.01 was considered significant. Subsequently, post-hoc tests with Bonferroni correction were carried out to test for differences between time points or between groups.

5.3 Results

5.3.1 Animals

With the exception of one animal (from the sham group), all animals survived the entire experimental period. This sole non-survivor did not wake up from anaesthesia after the baseline MRI scan. Therefore, the cause of death was not related to the induction of mTBI. This led to a survival rate of 100 % after impact which is to be expected for the height and weight that we used in the Marmarou model [45]. After mTBI, all rats regained consciousness within 15 min and there was no evidence of skull fractures on the CT images. Moreover, the anatomical T2 scans acquired after impact did not reveal any major abnormalities such as enlarged ventricles, bleedings or contusions (Figure 5.4). In short, we could not identify focal lesions, supporting validity for the diffuse nature of the Marmarou model.

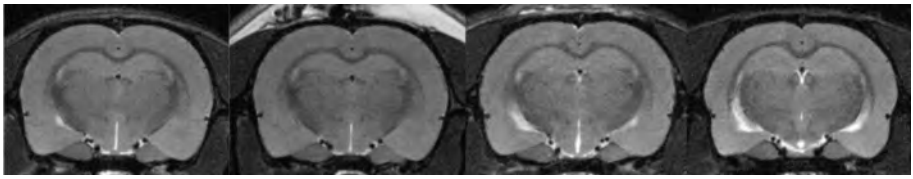

Figure 5.4: Anatomical T2 weighted images from left to right (before), 1 day, 1 week and 3 months post injury from a respective mTBI animal.

5.3.2 In vivo longitudinal MRI changes following mTBI

Figure 5.5 shows the diffusion maps of a representative mTBI rat one day after injury (FA, MD, MK, AWF, AxEAD, RadEAD and TORT). In the following paragraphs, the findings will be presented according to the diffusion model.

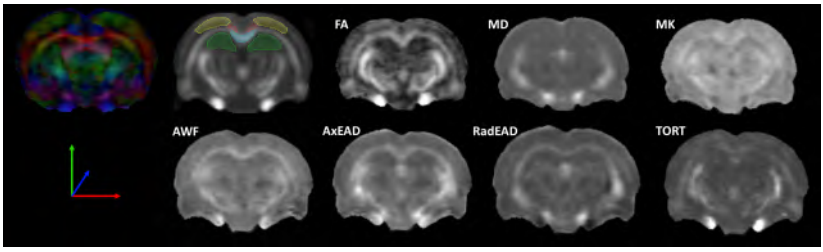

Figure 5.5: Top row: representative coloured FA map on the left (left-right orientation: red, front-back: blue and up-down: green), the FA template with the VOIs and the FA, MD and MK map one day post impact. On the bottom row are representative images for the metrics of the white matter model. From left to right: AWF, AxEAD, RadEAD and TORT.

Diffusion tensor imaging

As can be seen in Table 5.1, linear mixed model analysis revealed a significant group by time interaction effect for MD in the hippocampus and corpus callosum. Also, AD in the hippocampus and RD in the cingulum showed a significant group by time interaction effect. In the corpus callosum and hippocampus interaction effect in RD was near significant ($p = 0.013$ and $p = 0.011$, respectively). Subdividing the corpus callosum in genu, body and splenium did not reveal additional info and therefore we will discuss the corpus callosum as a total volume

only and the results for genu, body and splenium can be found in Table A.1 of the Appendix. Post hoc tests revealed a significant decrease in MD in the hippocampus ($p = 0.008$) (Figure 5.6.C) and in RD in the cingulum ($p = 0.010$) (Figure 5.7.C) of the mTBI group one week post injury compared to baseline. Furthermore, RD in the cingulum stayed decreased three months post impact and was significantly lower than RD in the sham group ($p = 0.003$). Also, in the corpus callosum MD was significantly lower in the mTBI group compared to sham three months post impact ($p = 0.007$), in the hippocampus this was near significant ($p = 0.013$). In the sham group post hoc time differences could be observed only three months post injury (Figure 5.6.A and C) (Table A.2).

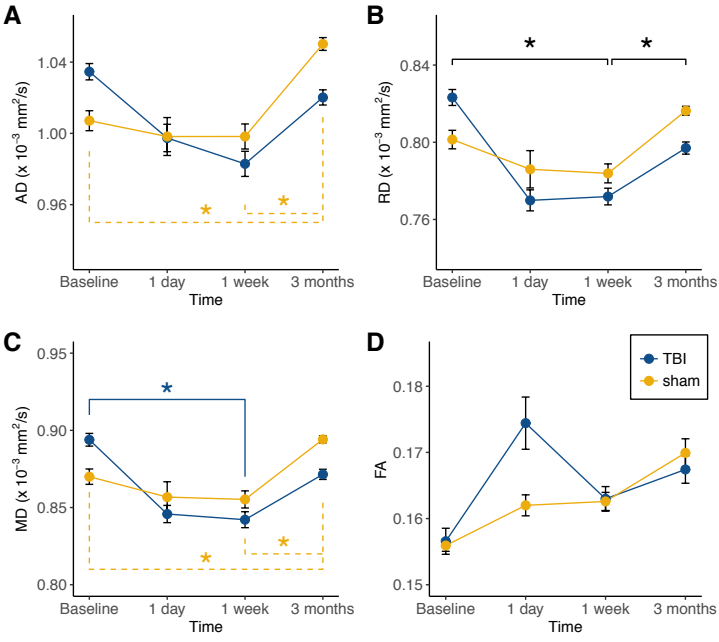

Figure 5.6: Temporal changes in AD, RD, MD and FA in the hippocampus. Error bars indicate standard of the mean. Post hoc results for the TBI and sham group are indicated with a blue solid line and yellow dashed line, respectively, as statistical markers. A solid black line represents significant main time effects. * $p < 0.01$

A significant main effect of time could be found for all diffusion

Table 5.1: F-values and p-values of univariate F-test for group by time interaction effect and main time effect in the corpus callosum, hippocampus, cingulum and cortex.

GROUP BY TIME	Corpus callosum		Hippocampus		Cingulum		Cortex	
	F-value	p-value	F-value	p-value	F-value	p-value	F-value	p-value
MD	**5.961**	**0.006**	**7.185**	**0.002**	7.485	0.091	1.024	0.403
AD	1.202	0.333	**6.140**	**0.005**	1.669	0.204	1.643	0.206
RD	5.759	0.013	4.970	0.011	**7.439**	**0.010**	1.007	0.041
FA	2.086	0.103	1.378	0.286	1.952	0.176	2.873	0.079
MK	0.327	0.806	0.658	0.595	0.459	0.715	0.603	0.326
AK	0.123	0.945	1.344	0.312	1.083	0.393	1.447	0.268
RK	0.299	0.926	0.690	0.573	0.526	0.671	0.268	0.848
AWF	0.203	0.893	na		0.443	0.726	na	
IAD	0.353	0.787	na		1.046	0.405	na	
AxEAD	0.694	0.569	na		1.695	0.192	na	
RadEAD	3.622	0.036	na		**5.139**	**0.008**	na	
TORT	3.539	0.054	na		2.271	0.131	na	
TIME	Corpus callosum		Hippocampus		Cingulum		Cortex	
	F-value	p-value	F-value	p-value	F-value	p-value	F-value	p-value
AD	**39.868**	**< 0.001**	**13.392**	**< 0.001**	13.342	**< 0.001**	7.599	**0.001**
RD	**7.105**	**0.006**	**7.711**	**0.002**	**7.724**	**0.009**	**6.512**	**0.003**
MD	**13.862**	**< 0.001**	**12.015**	**< 0.001**	15.106	0.042	**6.534**	**0.003**
FA	3.036	0.045	**17.113**	**< 0.001**	4.063	0.034	4.342	0.026
AK	3.430	0.055	4.672	0.025	**16.176**	**< 0.001**	**8.077**	**0.002**
RK	**7.906**	**0.002**	**7.116**	**0.004**	**14.750**	**< 0.001**	**5.427**	**0.010**
MK	**7.104**	**0.004**	**6.258**	**0.010**	**11.500**	**< 0.001**	**5.747**	**0.008**
AWF	**13.478**	**< 0.001**	na		**18.533**	**< 0.001**	na	
IAD	1.706	0.186	na		3.467	0.048	na	
AxEAD	**41.377**	**< 0.001**	na		**20.608**	**< 0.001**	na	
RadEAD	**5.809**	**0.007**	na		**10.040**	**< 0.001**	na	
TORT	2.619	0.106	na		5.667	0.011	na	

na = not applicable.

Bold indicates the p-values that survived Bonferroni correction for multiple comparisons.

tensor parameters across all four VOIs, with the exception of MD in the cingulum and FA in the corpus callosum, cingulum and cortex (see Table 5.1). This significant time effect was mostly driven by changes at the three months post injury timepoint, which represents natural developmental/aging processes and are not of particular interest in this study. Therefore, we will focus on differences at acute timepoints for the further analysis. Other significant post hoc results can be found in Table A.2. In the cingulum and cortex, pairwise comparisons between baseline and one day post injury showed significant decreases in AD ($p = 0.001$ and $p = 0.001$, respectively) (Figure 5.7.B). For MD in the cortex we also obtained a decrease one day ($p = 0.001$) post injury compared to baseline and in the cingulum AD was decreased one week post injury compared to baseline as well ($p = 0.009$) (Figure 5.7.B). One week post injury, RD was significantly decreased in the hippocampus ($p = 0.008$) (Figure 5.6.B). All values returned towards baseline levels after three months. In the hippocampus FA showed an increase between baseline and one day post injury – especially in the mTBI group after visual inspection – and remained elevated after three months, however this effect did not survive multiple comparisons correction ($p = 0.023$) (Figure 5.6.D). In the corpus callosum we found a significant increase in AD three months post injury compared to baseline ($p < 0.001$). The main group effect was not significant across all DTI parameters and VOIs.

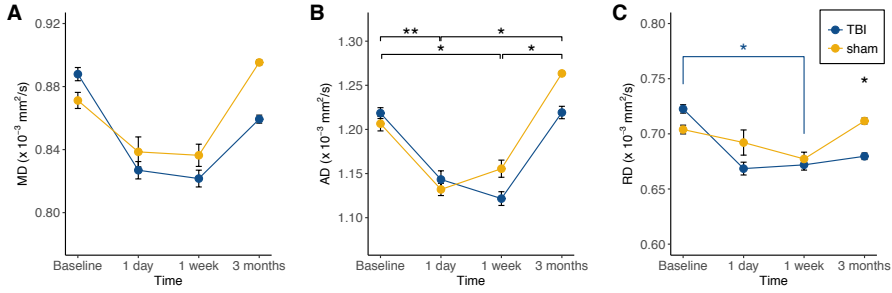

Figure 5.7: Temporal changes in MD, AD and RD in the cingulum. Error bars indicate standard of the mean. The post hoc result for the TBI group is indicated with a blue solid line. A solid black line represents significant main time effects. * $p < 0.01$, ** $p \leq 0.001$

Diffusion kurtosis imaging

No significant group by time interactions effects or significant main effects of group could be demonstrated for any of the DKI parameters in any of the four VOIs. Although, AK, RK and MK values showed a significant main effect of time for the majority of the VOIs (Table 5.1). Post hoc tests revealed that AK of the cortex ($p = 0.009$) was significantly decreased after one week compared to baseline. In the hippocampus ($p = 0.005$) and cingulum ($p = 0.006$) RK was significantly decreased after one week compared to baseline which coincided with a decrease in MK in the hippocampus ($p = 0.007$) (Figure A.1). Similar as with the DTI parameters, the DKI parameters returned to baseline levels after three months. In the corpus callosum significant time effects were found only after three months (Table A.2).

White matter model in corpus callosum and cingulum

Mixed model analysis revealed a significant interaction effect for RadEAD of the cingulum (Table 5.1). Post hoc tests showed that RadEAD of the cingulum was significantly decreased ($p < 0.001$) in the mTBI group one week post injury (Figure 5.8). In the sham group this change in RadEAD could not be observed and only a significant increase between one week and three months was present ($p = 0.006$).

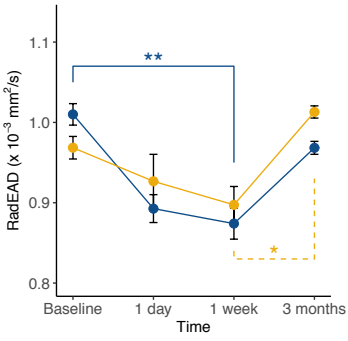

Figure 5.8: Temporal changes in RadEAD in the cingulum. Error bars indicate standard of the mean. Post hoc results for the TBI and sham group are indicated with a blue solid line and yellow dashed line, respectively, as statistical markers. * $p < 0.01$, ** $p \leq 0.001$

In addition, we found a significant main effect of time for AxEAD, RadEAD and AWF in the white matter bundles, IAD did not show a main effect of time except in the body of the corpus callosum ($p = 0.004$) (Table A.1). Pairwise comparisons revealed a significant decrease in RadEAD in the corpus callosum ($p = 0.009$) after one week compared to baseline and these values returned to baseline levels after three months. IAD in the body of the corpus callosum did not survive multiple comparisons. Additionally, in the cingulum AxEAD was significantly decreased after one day ($p = 0.001$) and one week ($p = 0.001$) and in the corpus callosum increased ($p = 0.002$) after three months compared to baseline. AWF showed a significant increase in the corpus callosum ($p < 0.001$) and cingulum ($p = 0.008$) after three months compared to baseline. Main effects of group were absent.

5.4 Discussion

In this chapter, we investigated whether two advanced diffusion models (i.e., diffusion kurtosis imaging and the white matter tract integrity model) could provide additional information to the metrics derived by the widely used diffusion tensor model in a closed head rat model of mild TBI. We were able to demonstrate changes in the diffusion metrics of the three models, both at the acute timepoints (within the week after sustaining a mTBI) and chronic time point at three months post injury by linking back to pre injury scans.

Several studies have used dMRI to follow up the complex and heterogeneous microstructural changes following mTBI, whereby DTI metrics have been used most often. In support of our findings, previous studies found decreases in diffusivity in both single and repetitive impact models throughout the brain in the first week after injury [39, 47, 104, 105, 141, 142]. In the hippocampus and cingulum of the mTBI group, we demonstrated significant decreases in respectively MD and RD one week post injury which was already visible one day post injury (Figures 5.6 and 5.7). Cytotoxic oedema in the acute stage can reduce the extracellular space and highly restrict water diffusion leading to decreases in diffusivity [141]. Additionally, we were able to demonstrate a significant decrease in RadEAD in the cingulum one week

post injury for the first time. The study by Guglielmetti et al. [132] could also demonstrate a decrease in RadEAD along with a decrease in IAD and AxEAD in the corpus callosum following three weeks of cuprizone ingestion which induces demyelination. They hypothesised that an inflammatory response could induce infiltration of microglia and myelin debris and this way reduce the extracellular space. Inflammation could also explain the reduction in RadEAD we found in the cingulum, however we do not believe myelin debris is present in our model given the mild impact. From the present findings, it seems thus that mTBI has predominantly an influence in the cingulum and hippocampus. Furthermore, the decrease in diffusivity was mainly driven by a strong decrease in the radial components and to a lesser extent the axial components. Though, a decrease in AD has previously been described in the hippocampus, cortex, external capsule and corpus callosum 10 days post injury, the decrease in AD in the hippocampus we noticed one week post injury was not significant from baseline and we could not attribute it to the mTBI group (Table 5.1 and Figure 5.6 A) [106, 141]. Therefore, we suggest, as stated before, that the axonal integrity in our injury model is more or less preserved (i.e., probably there were no disrupted axons or cell debris) since diffusion along the axons changed minor. Notwithstanding, diffusion in perpendicular (radial) directions will be more restricted due to the reduced extracellular space possibly filled with inflammatory cells.

It is clear from the present study that moving beyond the diffusion tensor model can bring more insights into the underlying brain changes following mTBI. Nonetheless, a good preclinical model should also be able to mirror the diffusion changes observed in human populations. In the last few years there have been a handful of human studies investigating not only DTI but also DKI or WMTI brain changes following mTBI [126, 143–146]. For example, we were able to reproduce the decrease in MD and RD in the cingulum found in concussed athletes at 24 hours and 8 days post impact [145]. Also, this study did not find any significant changes in FA or any of the DKI parameters. In the follow up study at 6 months post injury they could also show an increase in MD compared to the acute time points in the injured athletes, though still lower than the control group [146]. Again, DKI failed to detect any changes. This

agreement and strong resemblance of diffusion alterations with human concussed patients strengthens the idea that the mTBI rat model we show here, is a good model to study concussion without lesions visible on anatomical scans.

Interestingly to note is that a couple of our findings in a mTBI rat model are not always in line with the results from human mTBI studies. As already mentioned, we observed a decrease in RadEAD that is inconsistent with the human study of Grossman et al. [127]. The study by Chung et al. [126] demonstrated significantly lower IAD in the splenium of the corpus callosum of mTBI patients, compared with controls, but did not reveal significant changes in the radial metrics. These discrepancies in findings show that rodent models do not always translate into human studies. Also, researchers put forward that the classification of mild, moderate and severe in experimental models is not always equal to the classification of severity in human patients [147, 148]. Therefore, we suggest that future rodent models of mTBI should take into account the different mechanical forces of sustaining a TBI (coup versus rotational forces) or site of impact (frontal, temporal).

A limitation of this study is that we observed a significant main effect of time in several DTI and DKI metrics, proving diffusion changes in both the sham and mTBI group. This time effect was mostly driven by changes at the three-month timepoint and could be explained by early aging processes. Specifically, we observed increased MD and increased DKI-related metrics, in both mTBI and sham groups, between the one-week and three-month time points. These increases were also seen in the study of Lancaster et al. [146], however since their controls were non concussed athletes they explained these longitudinal increases to be an effect of physical exertion. Because it is unlikely that our rats had more physical activity during the three months awaiting follow up, we interpret this alterations in MD and DKI-related metrics as early aging processes, which is consistent with previous diffusion MRI studies over the lifespan [149–151]. Lastly, we noted a large intersubject variability, especially in the kurtosis and white matter metrics – which is common for the technique – and makes it difficult to detect group differences [152, 153]. In our study, we found this especially challenging

since the mTBI induces an effect size that cannot always overcome the intersubject variability and possible scanner fluctuations in this relatively small sample size. It is therefore possible that we missed small but relevant effects and we are now limited to finding only the large effects. Furthermore, we noticed a non-significant difference between the sham and mTBI group at baseline which was not associated to weight or timing differences. Therefore, a suggestion could be to semi-randomise the animals after the baseline scans so that the two groups have the same average values in diffusion metrics and innate differences are removed.

Despite the aforementioned limitations, we were able to demonstrate that both DTI and more advanced diffusion models are sensitive in detecting longitudinal changes after mTBI. Our results revealed significant decreases in radial metrics in the cingulum and MD in the hippocampus one week after impact only in the mTBI group, which can be connected to cellular swelling, without major changes in axial metrics, which suggests that the axon integrity is preserved. Therefore, we think that radial diffusion metrics might be promising predictive biomarkers, which could be sensitive to identify specific microstructural changes in the early phase after a mild impact.

6 | Fixel based analysis of the rat brain after mild TBI

6.1 Introduction

It has long been assumed that following the recovery of the acute primary and secondary events of a traumatic brain injury (TBI), the brain remains rather stable. However, more and more researchers are starting to explore TBI as a neurodegenerative disease as well, since pathological outcomes are similar to those seen in several white matter neurodegenerative conditions, suggesting common linking pathways [154, 155]. The elevated risk of developing a neurodegenerative pathology has increased awareness on the importance of TBI. Although a history of mild TBI is less consistently associated with an increased risk of neurodegenerative outcomes (e.g., Alzheimer's disease and dementia) in comparison with more moderate to severe TBI, specific populations with complicated medical histories and comorbidities may be more susceptible [155]. Additionally, sustaining multiple milder injuries, e.g., during playing certain sports (football, rugby, ice hockey and others) can lead to Chronic Traumatic Encephalopathy (CTE), also increasing the risk for a neurodegenerative outcome.

Diffusion weighted imaging is a technique widely used in TBI research and although many studies have focussed on imaging white matter alterations within a more recent period of sustaining an injury (< 1

year), a current study has shown that persons who sustained a TBI had higher MD and lower FA values in several white matter regions even more than a decade after injury which could reflect reduced tract integrity [156]. Furthermore, the decreased values of FA were associated with poorer cognitive status. Using tractography the study of Haberg et al. [157] was able to show that the volume of the corpus callosum in TBI patients who sustained injury more than 2 years before imaging, was significantly smaller compared to controls. Together, these studies show the degenerative character of TBI.

The majority of the studies investigating white matter changes following TBI have used the diffusion tensor imaging (DTI) model despite its limitation of modelling only a single fibre population within one voxel. This can lead to misinterpretation of the underlying integrity of the tract especially in regions with crossing fibres (e.g., crossing of the corpus callosum and cortico-spinal tract) or when other biological processes are at play (e.g., myelination vs. axonal loss) which can result in lower FA values [90]. Fixel-based analysis (FBA) is a recently introduced technique that allows analysis of multiple fibre populations within a voxel (fixel)[96, 97]. Using probabilistic tractography structurally connected fixels can be identified and with this information it is possible to estimate diffusion measures for individual white matter fibre populations. More specifically, the fibre density (FD, reflection of axonal count or density of axonal packing), fibre cross-section (FC, reflection of volumetric size of a fibre bundle) and the combined effect of FD and FC, a measure called fibre density and cross-section (FDC), can be estimated.

To date, FBA has been applied in a limited number of studies investigating white matter pathologies such as multiple sclerosis (MS) [158], Alzheimer's disease and mild cognitive impairment [159] and motor neuron disease [96]. FBA was able to detect a decrease in FD and to a lesser extent in FC in the cingulum bundles and inferior longitudinal fasciculi in addition to the affected visual pathways of MS patients showing a degeneration of these tracts. On the other hand, in Alzheimer's disease there was a more pronounced reduction in FD as well as FC suggesting that substantial axonal loss occurs at a microstructural level in the presence of morphological alterations to white matter bundles.

Two recent studies in human TBI patients and a severe TBI rat model have also demonstrated changes in fixel metrics showing a decrease in FD indicative of tract degeneration and an increase in FC which can be explained by axonal swelling [160, 161].

These studies show that FBA could provide early markers of both axonal loss or fibre morphology in neurodegenerative diseases as well as TBI. To our knowledge, no study has examined white matter alterations following mild and diffuse TBI in rats using FBA. Therefore, the aim of this study was to investigate whether FBA can detect white matter alterations in rats within the first weeks of sustaining a mild diffuse trauma which could be the onset of degenerative processes. If FBA would be able to detect white matter alterations already in the acute phase, these metrics could be helpful to follow up fibre specific changes and possible degeneration later in life.

6.2 Materials & Methods

6.2.1 Animal studies

The study was approved by the Animal Ethics Committee at the University of Ghent (ECD 17/96) and all experiments were conducted in accordance with the guidelines of the European Commission (Directive 2010/63/EU). The animals were group housed and kept under controlled laboratory conditions (12 h light/dark cycle, 20 – 23 °C and 40 – 60 % humidity).

6.2.2 Induction of mild traumatic brain injury

Adult female Wistar rats (n = 15, 265 ± 14 g) purchased from Janvier Labs (Le Genest-Saint-Isle, France) were divided in two groups: 12 rats received a mild TBI and 3 rats did not receive a trauma and were used as healthy control (HC)(Figure 6.1). The surgical procedures to induce TBI in this experiment were performed as described in Chapter 5 (see section 5.2.2), with the only difference being the increase in height of the weight drop from 1 m to 1.3 m. This was done hoping to create more microbleeds (for a separate analysis not shown in this thesis) though still inducing a mild injury.

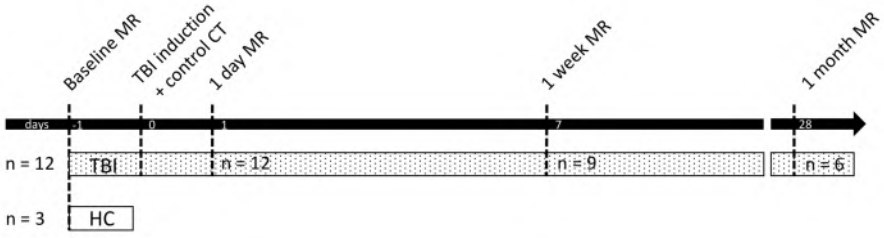

Figure 6.1: Outline of the study design. At each time point 3 TBI animals were sacrificed for a separate analysis (data not shown).

6.2.3 In vivo longitudinal multi-shell diffusion weighted imaging

MRI data were acquired on a 7 T MRI scanner (BioSpin PharmaScan 70/16, Bruker, Ettlingen, Germany) using a volume rat brain/mouse whole body RF coil. Rats were scanned before impact, one day, one week and one month post impact (Figure 6.1). During the scanning sessions, the animals were under 2 % isoflurane anaesthesia (5 % for induction), body temperature was kept constant with a circulating warm water heated blanket and bubble wrap, and respiration rate was monitored with a pressure pad.

At each time point, a whole brain anatomical T2-weighted scan was acquired first using a RARE sequence with the same parameters described in section 5.2.3. Multi-shell diffusion images were acquired with a spin-echo, EPI sequence between the olfactory bulb and the cerebellum using the exact same sequence parameters described in section 5.2.3. This resulted in a total acquisition time of 80 min.

6.2.4 Diffusion imaging processing

The acquired diffusion weighted images (DWIs) of the TBI group at each time point and of the HC group were pre-processed using MRtrix3 (version 3.0_RC3-86-g4b523b41) using a multi-step procedure. An overview of the image processing pipeline can be found in Figure 6.2. DWIs from the three separate imaging shells were first concatenated and a mask file containing only the brain tissue was created using the `dwi2mask`

function for each subject and time point. This mask was individually checked and manually corrected if the mask did not contain all brain tissue. Following a correction for noise, using the `dwidenoise` function, a correction for gibbs ringing artefact was performed using the `mrdegibbs` function in MRtrix3 [134, 135].

Fixel based analysis

The tissue response functions were estimated for white matter, grey matter and CSF by applying the dhollander algorithm [162, 163] and after upsampling of the DWIs and mask images by a factor 2, the fibre orientation distribution (FOD) was estimated using multi-shell and multi-tissue constrained spherical convolution (MSMT-CSD) [164]. To correct for intensity inhomogeneities between subjects the `mtnormalise` function was performed. After construction of a population template in common space using the `population_template` script (for each time point seperately) and coregistration of the white matter FOD images and mask images to the common space, a fixel mask was computed using the `fod2fixel` command. Next, the fixel metrics were extracted: fibre density (FD), fibre cross-section (FC) and a combined measure of fibre density and cross-section (FDC). To identify structurally connected fixels we constructed a whole-brain tractogram with 10 million streamlines, a maximum angle of 22.5 degrees between successive steps, lengths between 0.5 mm minimally and 25 mm maximally and a cutoff value of 0.2. Using a higher cutoff value than the default 0.06 we searched for a trade off between a more rigid delineation of tracts, which reduces the generation of false positive streamlines in the rat brain and allows for more variation in tract reconstructions [165]. To reduce bias in tractography densities, the spherical deconvolution informed filtering of tractograms (SIFT) method was applied, terminating with a final count of 2 million streamlines [166, 167]. Finally, statistical analysis using connectivity-based fixel enhancement was performed separately for each metric (FD, FC and FDC) using the `fixelcfestats` command [96]. Group differences were assessed at each time point using non-parametric permutation testing with 5000 permutations, fully corrected for family-wise error (FWE). A FWE corrected p-value < 0.05 was considered significant.

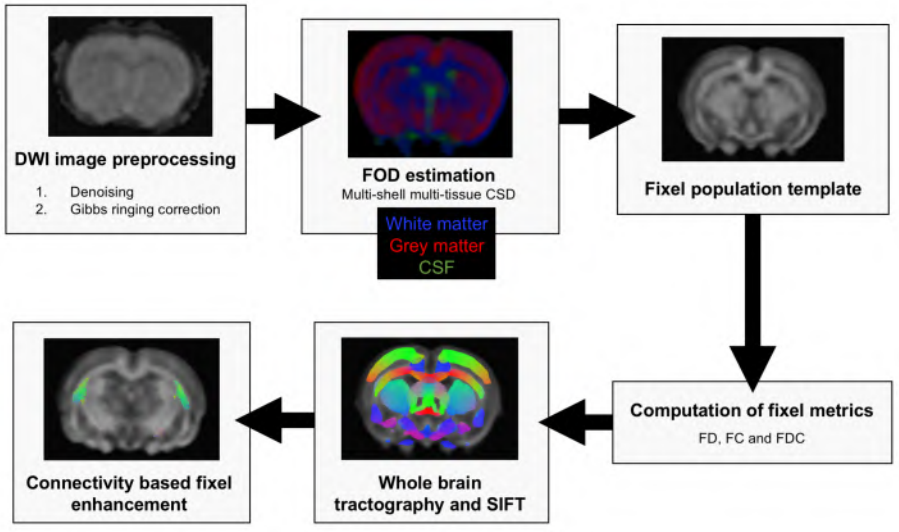

Figure 6.2: Outline of the diffusion image processing pipeline. After the preprocessing of the images (denoising and Gibbs ringing correction) the tissue response functions are estimated and the white matter fibre orientation distribution (FOD) is estimated using a multi-shell multi-tissue CSD. Next a FOD template is constructed of all animals at each time point and the fixel metrics are calculated. Following whole brain tractography and filtering of the tractogram (SIFT), the connectivity based fixel enhancement analysis is performed.

Voxel based DTI analysis

To relate the fixel analysis more easily to results obtained from the DTI ROI based analysis used in Chapter 5, we also performed a voxel analysis using DTI metrics (axial (AD), radial (RD) and mean diffusivity (MD) and fractional anisotropy (FA)) within the MRtrix framework. From the preprocessed and upsampled DWIs the tensor was estimated and DTI metrics calculated. These parametric maps were transformed into template space using the registration parameters obtained from the FOD registration process and smoothed at FWHM = 0.3 mm. Using the `mrclusterstats` command voxel-wise statistical analysis was performed with 5000 permutations and threshold-free cluster enhancement to test for differences between groups at each imaging time point [168]. An FWE corrected p-value < 0.05 was considered significant.

6.3 Results

6.3.1 Fixel based analysis in white matter

White matter fixel analysis revealed a significant increase ($p < 0.05$) in FC in the splenium and right side of the forceps major of the corpus callosum of the TBI group compared to the sham group one week after impact (Figure 6.3). This increase was already visible one day after impact and FC continued to be increased one months after impact, however never reaching significance.

6.3.2 Whole brain voxel analysis

Voxel-wise analysis did not reveal any changes at baseline or one day post impact but showed several decreases in diffusivity metrics at one week and one month post injury, though not overlapping with the significant region in the fixel analysis. One week following impact there was a significant decrease in AD in the prefrontal cingulate cortex, whereas this decrease in AD was present in the external capsule on the border between white and grey matter one month post impact (Figure 6.4). RD showed a significant decrease in the TBI group compared to sham animals in the posterior left hippocampus and right cingulum one month post injury (Figure 6.5). The decreases in AD and RD led to a combined

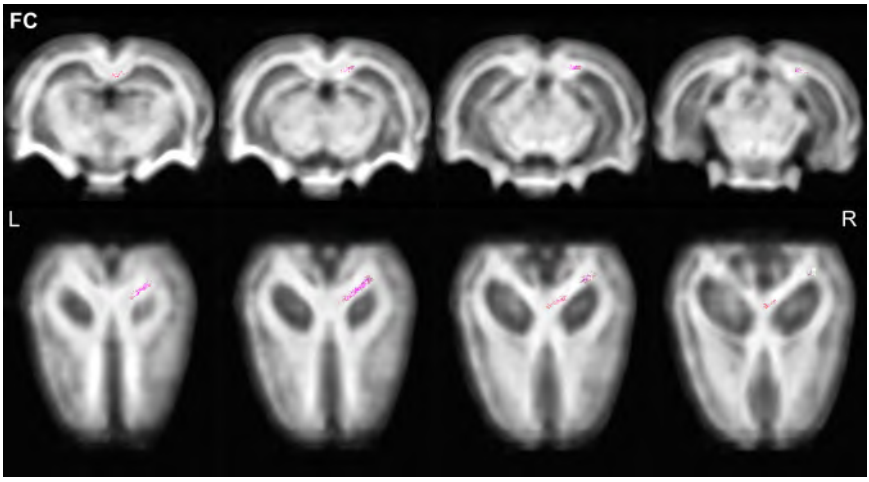

Figure 6.3: Significant fixels (FWE corrected $p < 0.05$) mapped to colour encoded tracts that indicate an increase in fibre cross-section in the right splenium and forceps major of the corpus callosum of the TBI group compared to the sham group. The purple colour indicates an oblique orientation from front to back combining red from left-right direction and blue from front-back direction.

effect of decreased MD in the TBI group compared to the sham group in posterior hippocampus, cingulum and internal capsule one month after injury (Figure 6.5). In contrast to the diffusivity measures, FA showed significant increases in FA in the TBI group in the prefrontal cortex after one month and again this region was situated at the border of white and grey matter (Figure 6.6).

6.4 Discussion

To the best of our knowledge this study describes the first longitudinal animal experiment using fixel-based analysis in a mild and diffuse TBI rat model. We were able to demonstrate an increase in fibre cross-section one week post injury in the TBI group. Moreover, we investigated differences in DTI metrics between TBI and healthy rats, using voxel-by-voxel analysis implemented within the MRtrix framework, to compare with fixel-based analysis and ROI analysis described in Chapter 5.

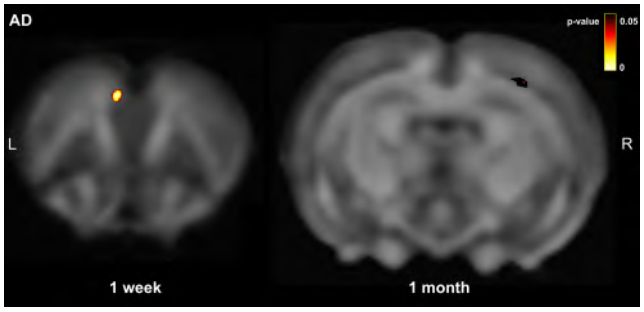

Figure 6.4: Significant decrease in AD in the prefrontal cortex at one week and at the border the external capsule at one month post injury for the TBI group. For illustrative purposes the brain map depicted at one month post injury shows voxels significant with a FWE corrected $p < 0.10$. Black voxels represent voxels with a p-value between 0.05 and 0.10 and the bright voxels in the centre represent voxels with a p-value < 0.05.

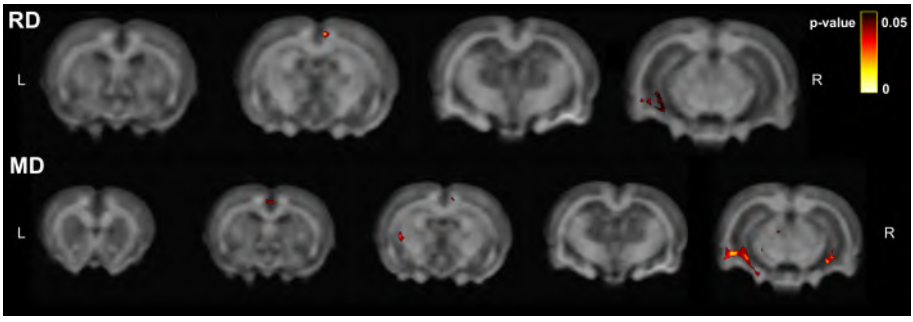

Figure 6.5: Significant decreases in RD and MD throughout the brain one month post impact.

Fixel-based analysis in white matter tracts of the injured rat brain revealed a significant increase in fibre cross-section in the splenium and forceps major of the corpus callosum compared to the healthy controls one week post injury which could be the result of axonal swelling. Because there was no change in fibre density or the combined fibre density and cross-section we believe that there is no axonal loss but only a temporary change in morphology. First of all, this result is in concordance with the results of Chapter 5 which also demonstrated major changes one week post injury and where we hypothesised that the decreases in diffusivity could be the result of cytotoxic oedema

and inflammation. These processes could also be the driver for the increase in fibre cross-section. Furthermore, this result is supported by a fixel-based analysis study in human TBI patients demonstrating significant increases in FC in the body of the corpus callosum and left superior longitudinal fasciculus without any changes in the other metrics [160]. They also attributed this change to axonal swelling. There has been only one study using fixel-based analysis in a severe TBI rat model investigating microstructural changes 12 weeks after inducing a fluid percussion injury [161]. This study did not investigate FC but could demonstrate widespread decreases in FD in the corticospinal tract, external capsule, fimbriae and corpus callosum predominantly on the ipsilesional site which could be indicative of axonal loss and is in line with considering TBI as a neurodegenerative disease. Since we did not find this decrease in FD in our study, we believe that our injury model does not produce large enough damage to cause the axons to degenerate at the imaged time points but it is possible that multiple and repetitive mild injuries can lead to neurodegeneration. However, this was not within the scope of this study.

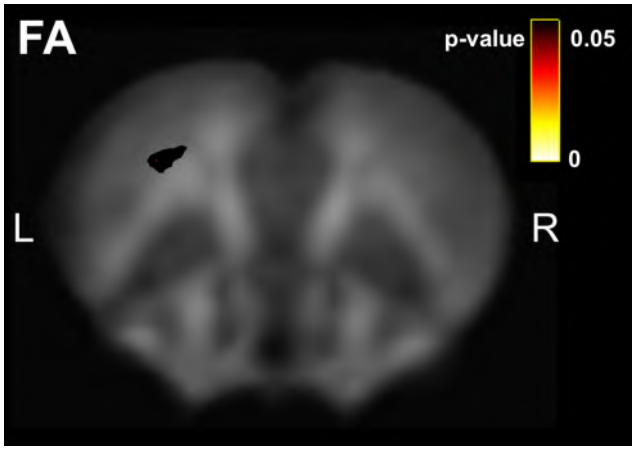

Figure 6.6: Significant increase in FA in the prefrontal cortex of TBI animals one month post injury. For illustrative purposes the brain map shows voxels significant with a FWE corrected $p < 0.10$. Black voxels represent voxels with a p-value between 0.05 and 0.10 and the small region in the centre represent voxels with a p-value < 0.05.

In contrast to what we would expect, none of the clusters found in the DTI voxel analysis overlapped with the significant region found in the fixel-based analysis. Voxel-based analysis demonstrated scattered, diffuse changes in brain microstructure in more frontal regions at the border between grey and white matter, cingulum associated cortical regions or hippocampal grey matter. This discrepancy could be explained by the occurrence of only small alterations in white matter and larger injuries to cells at the grey-white matter junction. It might be possible that the CSD method is more sensitive to changes in white matter since fixel-based analysis is more restricted to white matter regions. The study by Wright et al. [161] could demonstrate larger changes in fibre-derived metrics, compared to DTI metrics, which were also more robust. They concluded that the DTI metrics are probably more affected by the problem of crossing fibres but that the two methods can be considered complementary. By combining DTI and fixel-based analysis, the diffusion changes post-TBI can be explained more comprehensively. Although our changes found using voxel-based analysis of DTI metrics did not overlap with the fixel-based analysis, they did demonstrate similar results as the ROI-based analysis presented in Chapter 5. Voxel-based DTI changes showed significant decreases in diffusivity metrics in prefrontal cingulate and hippocampal regions, starting one week post injury, which also could be indicative for cytotoxic oedema and cellular swelling.

There have been a few studies investigating the discrepancies between whole brain voxel- (or fixel-) and ROI-based analysis. A recent meta-analysis study by Hunter et al. [169] investigating mild and moderate TBI patients found that ROI analysis detected larger changes in diffusion metrics than voxel analysis which indicates that ROI analysis has more power. Additionally, both methods were able to detect increases in MD but not all regions displaying significant changes overlapped between the ROI and voxel-wise analysis. As discussed before we also observed this non-overlap between regions in our data and this clearly demonstrates the difference between the two methods and the trade off that has to be made. If there is no clear hypothesis on the brain regions that will be affected, it is helpful to start exploring the brain using a whole brain voxel/fixel-wise analysis. However, because one needs to specify a

conservative threshold to obtain significant clusters (leading to smaller clusters) and has to correct for multiple comparisons between all voxels, this comes with a cost of sensitivity [169]. On the other hand, a ROI-based analysis is useful when there is already a hypothesis on the possible brain regions that are affected and will allow to increase statistical power to detect abnormalities since the effect is averaged over the entire region. For example, the study by Alruwaili et al. [170] which investigated changes in DTI metrics during follow up of amyotrophic lateral sclerosis (ALS) patients, was able to demonstrate a very small effect in FA in several white matter tracts using a ROI-based analysis but failed to detect these changes using a voxel-wise analysis.

There are some limitations to this study that should be noted. We only had 3 healthy control animals which were scanned only once. Ideally, this control group should be increased and scanned at the same time points as the TBI group. Furthermore, at each time point 3 TBI animals were sacrificed for separate analysis reducing the number of TBI animals along time. This further reduced the ability of the voxel/fixel analysis to find statistical differences between groups. Although we had longitudinal data, we did not test for differences between time points. This simply because this paired testing is not yet implemented in the fixel analysis framework. However, future studies with increased sample size should investigate these changes as well since we could clearly demonstrate longitudinal changes in brain microstructure in Chapter 5 which were larger than the differences between the mTBI and sham group. Lastly, we only imaged until one month post injury and could therefore not investigate the long term influence on white matter structure. Future studies should therefore image at even later time points as well to investigate possible neurodegeneration.

In conclusion, we were able to detect changes in FC using fixel-based analysis in a diffuse TBI rat model within the first week after impact possibly indicating neuronal swelling. This increase in FC was also found in human TBI study and was complementary to changes in diffusion metrics presented in Chapter 5 showing the potential of fixel-based analysis to be a translational method to investigate white matter changes following TBI already in the acute phase.

7 | Validation of neuroimaging findings with light and Raman microscopy

This chapter includes data from:

Braeckman K, Descamps B, Pieters L, Vral A, Caeyenberghs K, Vanhove C. **Dynamic changes in hippocampal diffusion and kurtosis metrics following experimental mTBI correlate with glial reactivity**, 2019. NeuroImage: Clinical, 21, 101669.

Khalenkow D, Donche S, Braeckman K, Vanhove C, Skirtach AG. **Added Value of Microscale Raman Chemical Analysis in Mild Traumatic Brain Injury (TBI): A Comparison with Macroscale MRI**, 2018. ASC Omega, 3, 16806-16811.

7.1 Introduction

In Chapter 5 we were able to identify possible imaging biomarkers to follow up the microstructural changes induced by a mTBI. However, it has been stated that parameters extracted from the DTI model are not specific for the underlying microstructure and although newer diffusion models that incorporate a-priori biological information may overcome this non-specificity, validation of the observed diffusion changes should be performed to establish the link between mesoscale diffusion scanning

and the microscale ground truth.

Immunohistological analysis has been the gold standard to investigate tissue microstructure for many years, and some animal studies have been able to pinpoint the underlying cellular mechanisms of mTBI by correlating diffusion metrics with histological markers. For example, Tu et al. [106] found a positive correlation between FA and Glial Fibrillary Acidic Protein (GFAP) in the cortex over time using a weight drop closed head injury model for TBI in rats, which was attributed to the formation of astrocytic processes resulting in more coherent pathways for diffusion. Utilising DKI, Zhuo et al. [105] observed a significant ipsilesional increase in MK in the hippocampus, cortex and external capsule using a controlled cortical impact model, which was associated with increases in GFAP staining. The authors suggested that MK might be a potential biomarker to detect reactive gliosis. However, other biophysical processes could also drive these changes in diffusion and kurtosis metrics, e.g., alterations in myelin can result in changes in FA/MD and the use of other histological markers will need to be further investigated.

A possible drawback of immunohistological analysis is the need for separate markers (and thus several tissue sections) for each cellular component of interest. In recent years, Raman spectroscopy has become more popular to examine pathological tissue alterations because it allows non-destructive analysis and imaging of numerous different molecules within the same tissue sample simultaneously with spatial resolutions in the micrometer range [171]. Therefore it can become a viable addition to neuroimaging tools. It is a label-free, optical method based on inelastic laser light scattering from molecular vibrations inherent to any material. It has been shown that Raman microscopy allows label-free detection of cancer cells in the brain [172]. Raman spectroscopy was also used for analysis of biochemical changes in peripheral nerves after an injury [173] and to track the molecular changes on the surface of the brain hemispheres after TBI [174] where temporal changes in tissue biochemistry were monitored.

In this chapter we will validate the diffusion changes demonstrated in Chapter 5 by performing correlation analysis between diffusion metrics and three selected immunohistochemical markers in four regions of interest in the rat brain (i.e., corpus callosum, hippocampus, cingulum and cortex). Using anti-neurofilament and anti-synaptophysin we want to visualise whether or not the structure (through staining of the neurofilaments) and synapse density (through staining of the synaptic vesicles), respectively, are affected by mTBI. Anti-GFAP staining will be used to evaluate astrocytic response, which is related to neuroinflammation and/or -plasticity and may play a role in mTBI. In addition, we will explore the potential of Raman spectroscopy to provide complementary molecular information on cellular compounds affected by the trauma in the corpus callosum.

7.2 Materials & Methods

7.2.1 Animal studies

All studies were approved by the Animal Ethics Committee at Ghent University (ECD 15/44Aanv and 17/96), and experiments were conducted in accordance with the guidelines of the European Commission (Directive 2010/63/EU). The animals were group-housed and kept under controlled laboratory conditions (12 h light/dark cycle, 20 - 23 °C, and 40 - 60 % humidity).

7.2.2 Induction of traumatic brain injury

The animals used for histological analysis were the same 20 animals described in Chapter 5 and included 10 rats that received a mTBI (mTBI group) and 10 that did not receive impact (sham group) (Figure 5.1). For Raman spectroscopy analysis female Wistar rats (n = 5, 265 ± 16 g) were purchased from Janvier Labs (Le Genest-Saint-Isle, France). Two rats received traumatic brain injury with a weight drop from 1.30 m (TBI-130), and three rats were used as the control group and did not receive any impact. The surgical procedures in this experiment were performed as described in Chapter 5 (see section 5.2.2), with the only difference being the alteration in height of the weight drop.

7.2.3 In vivo longitudinal MRI

For the Raman spectroscopy group (n = 5) MRI data were acquired on a 7 T MRI scanner (BioSpin Pharmascan 70/16, Bruker, Ettlingen, Germany) using a rat brain/mouse whole-body RF volume coil. All rats were imaged at baseline, 1 day and one week post injury. During imaging, the animals were under 2 % isoflurane anesthesia (5 % for induction), whereas their body temperature was kept constant with a circulating warm-water-heated blanket and bubble wrap; the respiration rate was monitored with a pressure pad. At each time point, a whole brain anatomical T2-weighted scan was acquired using a RARE sequence: TR = 5.5 s, TE = 37 ms, RARE factor = 8, FOV = 2.5 × 2.5 cm, and in-plane resolution of 109 × 109 μm^2 with 600 μm thick slices. A total of 45 slices were acquired and the total acquisition time was 12 min. No diffusion weighted images were acquired in this group of animals.

7.2.4 Histological analysis

At each time point after the induction of mTBI, animals were sacrificed for histological analysis (see Figure 5.1 for an overview of the timeline). Specifically, 2 rats in each group were sacrificed one day and one week post injury, and the remaining 12 rats were sacrificed three months post injury. Data collected from the rats sacrificed at the one day and one week time point were not used for further analysis and only results obtained from the rats euthanised three months post injury are presented here. In brief, rats were anaesthetised with 5 % isoflurane in O_2 and received an overdose of sodium pentobarbital intraperitoneally (> 100 mg/kg). After the breathing stopped, the animals were transcardially perfused with 4 % formaldehyde following an initial flush of phosphate buffered saline (PBS). The brains were extracted from the skull and left for 2 days in the 4 % formaldehyde solution. After this step, the brains were transferred to a PBS solution and embedded in paraffin.

Sections were made approximately 3.60 mm behind bregma and stained for the following cellular components: synapses (with anti-synaptophysin, SYN), glial cells (with anti-glial fibrillary acidic protein,

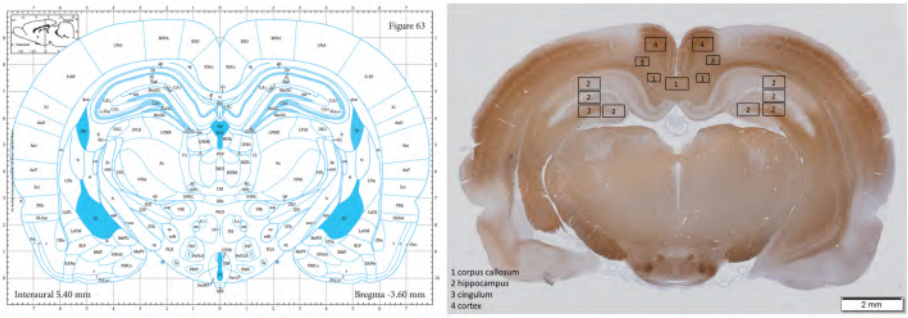

Figure 7.1: Paxinos atlas image of a brain slice at bregma -3.60 (left) [175] and the representative histological sections with regions-of-interest indicated with black rectangles.

GFAP) and neurofilaments (with anti-neurofilament, NF). Sections for SYN, GFAP or NF staining were immersed in citric acid (0.2 g/l, pH = 6), boiled in microwave for two cycles of 5 min, cooled to room temperature for 30 min and washed with PBS. Endogenous peroxidase activity was quenched with a 10 min H_2O_2 treatment (3 %). Sections were then incubated for 30 min with normal swine serum (SYN) or normal rabbit serum (GFAP and NF), followed by incubation with the primary antibodies: rabbit monoclonal (SYN, 1/1600, 2 h, Abcam ab32127) or mouse monoclonal (GFAP, 1/400, overnight, ThermoFisher, MA5-1203; NF, 1/750, 2 h, Sigma N2912 (staining the dephosphorylated medium and heavy neurofilament chains)). Next, sections were incubated with biotinylated secondary antibodies (1/200, 30 min), streptavidin-peroxidase complex (1/200, 30 min) and 3,3'- diaminobenzidine (DAB) peroxidase solution (10 min). Finally, sections were counterstained with haematoxylin (Mayer) and coverslipped using mounting medium (4111, Richard-Allan Scientific, Thermo Fisher Scientific) and glass coverslips (24 × 50 mm #1 (631-0146, VWR)).

All sections were digitally scanned at high resolution (40× magnification) with a virtual scanning microscope (Olympus BX51, Olympus Belgium SA/NV, Berchem, Belgium). Afterwards a different number of images was taken from sections made at the three months time point (Figure 7.1), to cover most of the four regions of interest (corpus callosum (n = 3), hippocampus (n = 8), cingulum (n = 2) and cortex

(n = 4)) at 10× magnification in OlyVIA 2.7 (Olympus Life Science) and further processed in ImageJ. For each image, first a background correction was applied with the rolling ball algorithm (radius = 50 pixels). Next, the images underwent colour deconvolution using the colour deconvolution plugin with the Haematoxyline DAB vector to obtain the image only with the DAB colour and the average pixel value was calculated. Lastly, the pixel values were calculated of a rectangular region of interest using the histogram tool. Mean and standard error values were calculated for all images and averaged within the region of interest.

7.2.5 Raman Spectrometry

After the MRI scan at one week post injury, rats were euthanised with 100 mg/kg sodium pentobarbital (20 %) (Kela NV, Hoogstraten, Belgium) via intravenous injection and brains were extracted from the skull. This was immediately followed by snap freezing of the brains in 2-methylbutane (Reagent-Plus 99 %, Sigma Aldrich), which was cooled with liquid nitrogen. Sections of 20 μm thickness were made with a cryomicrotome (CM3050 S, Leica Microsystems, Belgium). Tissue slices were put on quartz slides (Ted Pella, Inc.) and fixed for 10 min with 4 % formaldehyde (4078-9001, Klinipath). Tissue slices were submerged in the Hank's balanced salt solution (HBSS) (14025050, ThermoFisher) to avoid tissue detachment from the slides and scanned with a Raman microscope (Alpha300R+). Raman spectra were compared between TBI-130 and sham group on areas within the corpus callosum. In addition, blood samples were collected from the lateral tail vein either in a heparine coated tube or a non-coated tube (to allow for coagulation) to compare the Raman spectrum of blood with the signature from possible microbleeds in the brain sections.

The Raman microscope was equipped with a 785 nm laser (Toptica, Munich, Germany) and a CCD camera (ANDOR iDus 401 BR-DD, Belfast, Great Britain) cooled to -72 °C. The laser power was set to 225 mW and a water immersion 20×/0.6 NA objective (Nikon) was used for scanning. Tissue areas were mapped with a lateral resolution of 10 μm/pixel and an integration time of 1.5 s per data point. A total of 2500 spectra per slice were recorded. To investigate the blood samples

the power of the laser was decreased to 15 mW preventing saturation of the detector. Also, the heparinised blood sample was diluted 5 times with HBSS.

The resulting Raman spectral data sets were processed in R using the HyperSpec package [176]. Background subtraction and baseline correction were done by applying the asymmetric least squares function and normalisation by applying the area-under-curve method using the Baseline [177] and MALDIquant [178] packages, respectively. Hierarchical clustering analysis with the Bray-Curtis dissimilarity matrix was used to select the data points corresponding to the corpus callosum region and to detect the tissue structural and molecular abnormalities. After calculating the average mean spectrum in the corpus callosum of each animal, a peak ratio analysis was used to compare the data points between groups with the focus on the 2800 - 3000 cm^{-1} Raman spectral region whereby the peak around 2855 cm^{-1} is caused by the symmetric and asymmetric CH_2 stretching of lipids and the peak around 2940 cm^{-1} by the symmetric CH_3 stretching of proteins. The Wilcoxon Signed Rank test was used to test for differences between the two groups and a p-value < 0.05 was considered significant.

7.2.6 Statistical analysis

Group comparisons of the histological markers were performed using the Mann Whitney U test in SPSS Statistics 24 and a p-value < 0.05 was considered statistically significant. Correlation analyses were conducted between changes in diffusion MRI metrics obtained in Chapter 5 (i.e. 4 DTI metrics, 3 DKI metrics and 5 WMTI metrics of each time point within each VOI) and alterations in GFAP, SYN and NF reactivity of the histological sections (performed at three months post impact) using Pearson correlation coefficients. The correlations were corrected for multiple comparisons using the Benjamini-Hochberg procedure and an FDR correction of 0.10 [179].

7.3 Results

7.3.1 Histological analysis

Figure 7.2 shows sections stained with GFAP, SYN and NF of representative mTBI and sham rats. Groupwise comparisons did not show any statistically significant difference between the mTBI and sham group. In the mTBI group, only correlation coefficients from the GFAP and NF staining in the hippocampus survived following multiple comparison correction. One day after mTBI, a strong positive correlation coefficient was observed between average pixel value of the GFAP staining and FA in the hippocampus ($r = 0.908$ – $p = 0.012$) (Figure 7.3.A). This correlation indicates that high values of FA, correspond to a higher degree of glial staining. Three months post injury, we also found a positive and strong correlation between GFAP reactivity and MK values (Table 7.1) (Figure 7.3.B). Other significant correlations surviving multiple comparisons correction for GFAP can be found in Table 7.1.

With regards to the neurofilament marker, we observed strong negative correlations between NF and AK, MD, RD and MK three months after impact(see Table 7.1) denoting more dephosphorylated neurofilaments at lower values of the diffusion metrics (Figure 7.3.C-D). In the mTBI group, no other VOIs showed significant associations surviving the multiple comparisons correction. We could only demonstrate a significant positive correlation between SYN staining and MD ($r = 0.957$ – $p = 0.003$) in the cingulum of the sham group 3 months post impact that survived the correction for multiple comparison.

7.3.2 Raman spectroscopy

All animals from the TBI-130 group survived the impact from TBI induction and were able to regain consciousness within 30 minutes after anaesthesia detachment. There was no evidence of abnormalities visible on the T2-weighted anatomical images one day and one week post injury (such as bleedings, contusions or oedema formation) supporting the validity of the diffuse nature of the Marmarou model even from higher impacts (1.30 m).

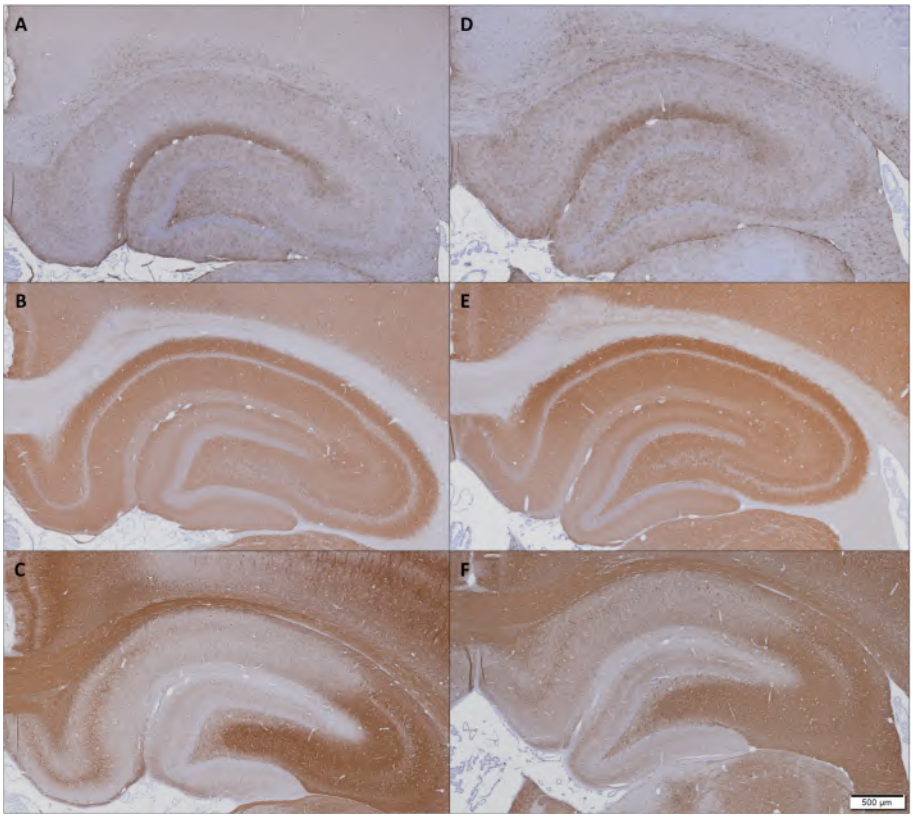

Figure 7.2: Representative sections for Sham (left) and TBI (right) animals three months post injury. Upper row sections stained for GFAP, middle row SYN and bottom row NF.

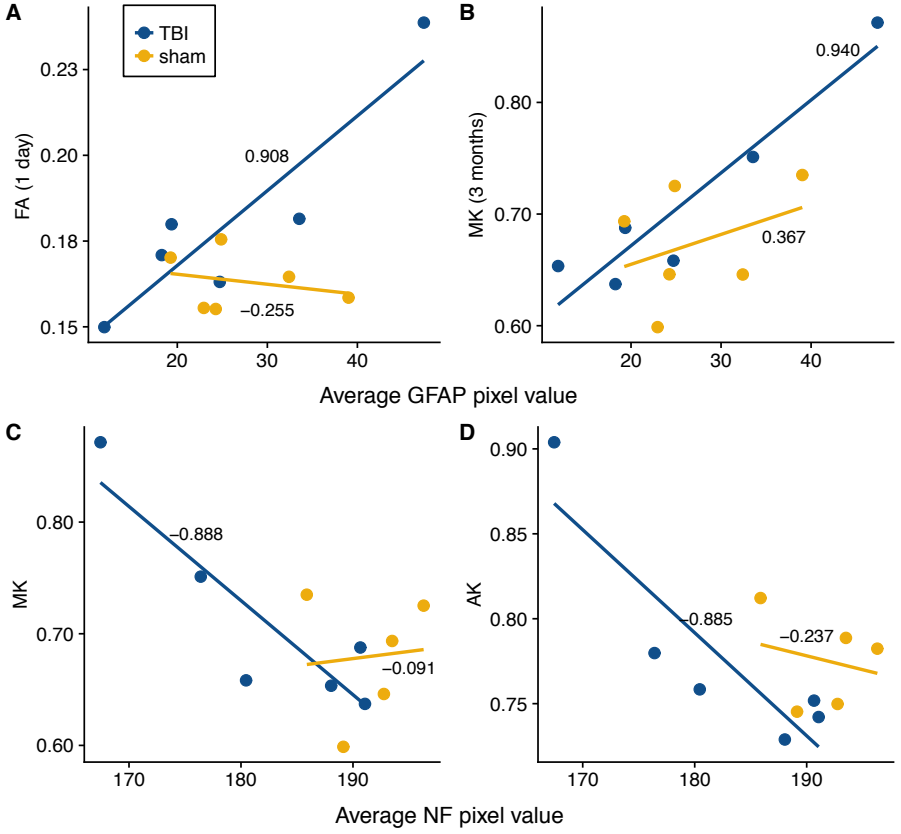

Figure 7.3: Correlations of GFAP with FA in the hippocampus one day post impact (A) and with MK 3 months post injury (B). Correlation of NF with MK and AK in the hippocampus 3 months post injury (C-D).

Table 7.1: Significant correlations between the diffusion metrics and GFAP and NF staining in the hippocampus three months post injury.

3 months post injury	GFAP		NF	
	r	p-value	r	p-value
AK	**0.943**	**0.005**	**-0.885**	**0.019**
RK	**0.900**	**0.014**	-0.856	0.030
MD	0.854	0.030	**-0.902**	**0.014**
RD	**0.873**	**0.023**	**-0.888**	**0.018**
MK	**0.940**	**0.005**	**-0.888**	**0.018**

Bold indicates the r- and p-values that survived Bonferroni correction for multiple comparisons.

The hierarchical clustering analysis allowed to visualize and assign the data points to different tissues present in the scanned areas (Figure 7.4.A). The hierarchical clustering analysis of a section containing the corpus callosum from a rat 1 week after TBI (1.30 m), revealed a histologically abnormal area (15 - 20 μm in size) (Figure 7.4.B). This area had two times higher Raman signal intensity compared to that of the signal from the surrounding tissues and contained no molecular peaks. A similar signal pattern was observed in the molecular fingerprint from dried/coagulated rat blood suggesting that the abnormal region can be the result of a microhaemorrhage (Figure A.2). Only non-coagulated blood was able to show distinct haemoglobin peaks (Figure A.2).

By performing the peak ratio analysis, a significant decrease of the 2940/2855 peak ratio was found in the TBI-130 group ($p < 0.001$) compared to the control rats indicating a decrease in protein content (Figure 7.5).

7.4 Discussion

In this chapter we investigated the underlying biological correlates that can be linked to diffusion MRI alterations induced by a mTBI and studied in Chapter 5. We revealed strong correlations of the advanced diffusion MRI metrics and the histopathological markers, and have identified the underlying specific microstructural processes following a mild closed head injury. More specifically, the diffusion metrics correlated

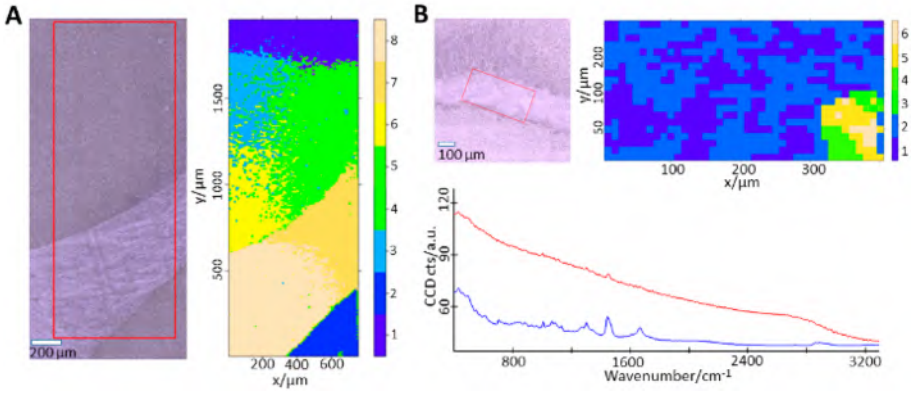

Figure 7.4: Light and Raman microscopy of the corpus callosum. (A) Light microscope image (left panel) and the corresponding Raman microscope image of the cortex and corpus callosum of a representative animal produced by hierarchical clustering analysis (right panel). The area scanned with a Raman microscope is marked with a red rectangle. (B) Light microscope image (top-left panel) and the corresponding Raman microscope image (top-right panel) of the corpus callosum with an abnormal region (bottom right). The mean Raman spectra of the corpus callosum (blue color) and the high intensity spectrum of the abnormal region (red color) are shown below (bottom panel).

with histological markers indicative of a compromise in neuronal structure and glial response. Additionally, we presented the potential of Raman spectroscopy to investigate the molecular profile of damaged brain tissue.

In the hippocampus we found several significant correlations between the histological markers and diffusion metrics. We observed a negative correlation between NF and MD, MK and AK three months post injury, indicating a higher dephosphorylation status (the antibody stained only de **de**phosphorylated side chains of the neurofilaments) at lower values of diffusion or kurtosis. Neurofilaments are a major part of the neuronal cytoskeleton and provide structural support for axons to ensure optimal transport. TBI can influence the structure of the neurofilaments by altering the phosphorylation status [180]. After mTBI a secondary chemical cascade starts – even within hours of the injury – and this can activate Ca^{2+} dependent proteases. These proteases can cause in turn serious damage to the cytoskeleton and ion channels of the cells. One pathway that can mediate side chain phosphorylation of the neurofila-

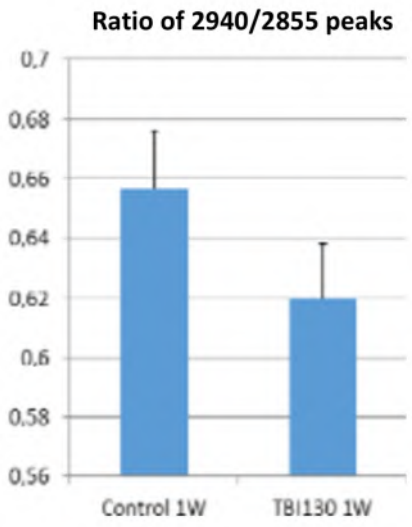

Figure 7.5: Change in the Raman scattering intensity peak ratio at 2940 cm^{-1} to that at 2855 cm^{-1} in the corpus callosum after TBI (TBI-130) compared to sham animals (control).

ment is led by the Ca^{2+}-dependent calpain and calcineurin [181]. These activated proteins can dephosphorylate the neurofilament side chains and this leads to compaction of the neurofilaments, misalignment of the cytoskeletal network and axonal functioning [180]. This result is in concordance with the human mTBI study by Grossman et al. [127], whereby reduced N-acteyl aspartate (NAA) levels coincided with decreased AWF values, which supports the hypothesis of shrinkage of the axonal space and impairments in the axonal transport. The group of Grossman et al. also revealed that NAA was negatively correlated with RadEAD and is opposite to our findings of reduced RadEAD after mTBI. We suggest that reduced RadEAD could be explained by increased activity or hypertrophy of glial cells surrounding the axons. Unfortunately, correlation analysis of the cingulum did not survive multiple comparisons and we cannot confirm this hypothesis.

Apart from neurons, glial cells also suffer from the mechanical forces that could lead to a secondary chemical cascade. Normally, these cells help to maintain homeostasis but the chemical cascade can activate the

astrocytes (most prevalent type of glia cell and sometimes referred to as astrogliosis) to start an inflammatory response that releases stress factors [182]. At the acute stage, Zhuo et al. [105] found that MK was sensitive to changes associated with reactive gliosis as indicated with an increase in GFAP reactivity. This increased cellularity could be explained by the presence of more and hypertrophic astrocytes responding to the severe injury with a widespread inflammatory response. In our study, we also found that MK – and by extension also AK and RK – was highly sensitive to changes in GFAP – though at the more subacute time point (three months post injury). Thus, increased values of the kurtosis three months post injury could related to a prolonged inflammatory response and the increase in cellularity it governs. However, in response to injury astrocytes can also react with a more neuroprotective neuroplastic response promoting the formation of new synapses and development of neuronal circuits. Therefore, it is likely that - considering the later time point, mild injury and the lack of statistical difference in GFAP staining between the sham and mTBI group - the astrocytes not only respond with a neuroinflammatory response but also a neuroplastic response. Interestingly, one day post injury FA was (near) significantly increased in the hippocampus, and these elevated values were strongly positively correlated with GFAP in the mTBI group. This could suggest that FA can be a predictive marker for higher tissue organization from astrocyte processes that form more coherent pathways for the neuronal circuit later on. By combining increased values of FA at the acute timepoint and increased kurtosis values at later timepoints as biomarkers, we could detect astrocytic activity in the hippocampus early on and monitor its progression.

In this study histological sections were stained using three markers (GFAP, NF and SYN) to investigate cellular changes. Although we demonstrated clear associations of GFAP and NF with FA and kurtosis metrics in the hippocampus, we should keep in mind that also other biophysical processes may alter the diffusion metrics after TBI. For example, demyelination could also drive the decrease in RD. However, the study by Sullivan et al. [39] concluded that the role of demyelination after mTBI is limited and is more likely to be associated with more severe TBI. Additionally, it is becoming clearer that – apart from the

way of sustaining the injury – also subtle differences in reaction of the tissue to trauma can act upon diffusion measures in complete opposite ways. For example, Lipton et al. [183] found bidirectional changes in FA throughout the white matter of the human brain. A similar pattern was identified in white and grey matter in the animal study of Harris et al. [184]. Another interesting discovery is the presence of an atypical astrocyte response which is characterised by the lack of GFAP expression, rapid and sustained downregulation of homeostatic proteins and impaired astrocyte coupling following repetitive mild TBI [185]. This indicates that astrocytes can have both an activated state (with upregulation of GFAP linked to both an inflammatory or neuroplastic response) or deactivated state which rapidly shuts down expression of astrocytic proteins (both structural e.g. GFAP or functional e.g. glutamate transporter). Therefore, in future studies, the association between the cellular processes and the diffusion metrics should be explored further, in order to fully understand their relation throughout the brain. This will enable us to identify a biomarker that can classify a patient with mTBI and also identify the underlying cellular damage of the affected brain regions.

In line with the significant correlation of decreased diffusivity with dephosphorylated neurofilaments one week post injury, Raman spectroscopy was able to show reduced protein content in the corpus callosum of the rat brain one week post injury. This reduction in protein content supports our hypothesis that the secondary injury process can lead to dephosphorylation of the neurofilament proteins and cause them to collapse and be non-functional. This could cause them to be broken down (hence the reduction in protein content). Using a controlled cortical impact model, Surmacki et al. [174] could also demonstrate this reduction in protein content two days following injury, though using the 1440/1660 cm^{-1} peak ratio describing the CH-bonds/mixed amide I and C=C stretching of lipids. In contrast, in tumour tissue the opposite is true. The very metabolically active cancer cells will show an increased protein profile as witnessed by an increase in the 2940/2855 cm^{-1} peak ratio [186]. This peak ratio can thus be an important feature to monitor the health status of tissues. In addition to the reduced protein profile a possible microhaemorrhage was detected in one section of a TBI animal after hierarchical clustering analysis. The spectrum at this region

showed a striking resemblance with that of coagulated blood and none of the characteristic haemoglobin peaks could be detected. This suggests that the observed abnormal area may be the result of coagulated blood leaked from ruptured capillaries. However, this was the only abnormal area detected in the scanned regions and the absence of such areas in other samples might indicate that microhaemorrhages are present only in a limited number and scattered throughout the brain. More samples should be analysed to confirm this finding.

In conclusion, we were able to demonstrate that decreases in diffusivity correlated with a higher dephosphorylation status of the neurofilaments suggesting a change in axonal morphology. Furthermore, higher glial activity in the hippocampus was associated to a higher FA one day post injury and kurtosis metrics three months post injury which could indicate later astrocytic activity. This shows that diffusion metrics can be related to cellular markers that play a role in the microstructural alterations following mTBI. Additionally, the Raman spectroscopy analysis has shown that it is feasible to investigate the molecular profile of damaged tissue in a label free manner and can have added value in future studies.

8 | Cognitive training therapy in mTBI

This chapter includes data from:

Braeckman K, Descamps B, Vanhove C, Caeyenberghs K. **Exploratory relationships between cognitive improvements and training induced plasticity in hippocampus and cingulum in a rat model of mild traumatic brain injury: a diffusion MRI study**, 2019. Brain Imaging and Behaviour.

8.1 Introduction

Traumatic brain injury (TBI) affects millions of people worldwide every year and is mostly caused by road traffic accidents and falls [187, 188]. Although the majority of TBI patients (between 70 - 90 % of all cases) can be classified as mild TBI (mTBI) , this mild injury can result in post-concussion syndrome (PCS) characterised by physical complaints (e.g., headaches), cognitive deficits (such as deficits in processing speed, attention or memory) or behavioural changes (e.g., irritability) [14]. These symptoms may become chronic in 10-15 % of the cases and last for several months to years after their injury [21]. Long-lasting cognitive deficits are one of the most debilitating consequences of TBI and can lead to reduced work productivity when patients return to work. They often report "getting less work done" or "making more mistakes" [24]. Diffusion magnetic resonance imaging (MRI) studies have revealed a relationship between cognitive deficits and alterations in white matter microstructure. Reduced fractional anisotropy (FA), possibly indicating

white matter damage, in the first weeks following trauma could be related to poorer cognitive status [122, 189, 190] and reduced structural brain connectivity was associated with worse cognitive performance in TBI patients [191–193].

It has been shown that cognitive rehabilitation can help alleviate complaints and improve cognitive functioning of TBI patients and, in recent years, computerized cognitive training programs have become more popular to train the affected cognitive functions [54, 194]. Several recent studies have developed training paradigms to target deficits in memory or executive functioning [55–58] and reviews are modestly positive about the added value of these training programs [59, 60]. However, more research is needed to increase the understanding underlying the biological mechanisms of cognitive training in TBI.

Characterisation of the effects of training on cognition in humans remains a difficult challenge. Preclinical studies allow tighter control over the subjects' health history, thereby reducing the potential confounding of comorbid disorders and/or co-existing psychological deficits. In addition, longitudinal MRI studies with intensive cognitive training paradigms prove to be a practical challenge. Furthermore, there is already a lot known about the neural systems that underlie learning and memory in rodents, allowing us to make valuable predictions about the potential locus of action for therapies to remedy cognitive impairments in TBI. Despite these advantages, very few studies have utilised rodent TBI models to investigate the effect of training on cognitive function [67, 195]. These studies revealed that training (memory training program) and environmental enrichment resulted in improved performance on a spatial memory task compared with non-trained TBI animals. For example, in the study of Brayer et al. [67], moderate to severely injured TBI rats were able to apply previously learned knowledge/skills during novel testing conditions in the Morris water maze which led to shorter platform searching latencies compared to non-trained rats. However, these studies only investigated the behavioural changes following training.

To date, only six neuroimaging reports on training-induced changes using diffusion tensor imaging (DTI) have been published, albeit in

healthy rodents. These studies revealed reductions in mean diffusivity (MD) and increases in FA with training, which were related with better performance [196–201]. However, the cognitive training tasks in these previous studies (e.g., Morris Water Maze for spatial memory training) cannot be easily translated to human training tasks. In response to the computerised testing and training in humans, a novel touchscreen training system has been developed for rodents, which is directly modelled from the Cambridge Neuropsychological Test Automated Battery (CANTAB) touchscreen tests for humans [202]. This cognitive training system closely mimics cognitive assessments used in clinical practice and may offer enhanced translational impact to the training paradigms used in preclinical TBI models. Also, the majority of previous animal studies did not include an active control group, making it impossible to assess the specificity to training. Therefore, in the present study we compared two TBI groups who trained on different tasks to show that the training-induced changes are specific to a given task and not a general effect of any training. This step also allows us to determine what aspects of any given task are critical for inducing structural changes.

To the best of our knowledge this is the first training study in a rat model of mTBI, to evaluate neuroplastic changes induced by a touchscreen training system. To overcome limitations of previous studies, we administered two different training tasks, i.e., the Paired Associate Learning (PAL) and the 5-Choice Continuous Performance (5-CCP) task, which are hypothesised to depend on different brain regions, i.e., the hippocampus and cingulum, respectively. We selected the PAL task because previous evidence has shown a relationship between learning difficulties and hippocampal dysfunction [203]. Also, hippocampal lesions have been associated with impaired visual memory and learning [72, 204]. In addition, we included the 5-CCP task as a second training protocol to enhance visual attention and impulsivity control [78], because previous studies have revealed that TBI animals have deficits in attention and processing speed [205, 206], which have been related to deficits in the limbic system [4]. Using diffusion MRI, we want to examine whether the PAL and 5-CCP task are beneficial for spatial memory and attention and inhibition control, and whether they can selectively alter the microstructure of the hippocampus and cingulum, respectively.

We hypothesise to find training-induced changes resulting in lower MD and higher FA values for the trained TBI animals compared to the non-trained TBI animals. Furthermore, by correlating the diffusion metrics with the outcome measures we hope to show the potential benefit of diffusion MRI to evaluate cognitive training in TBI and further improve the evidence based cognitive rehabilitation.

8.2 Materials & Methods

8.2.1 Animal study

Forty female Wistar rats (Janvier Labs, Le Genest-Saint-Isle, France) weighed 256.4 ± 8.7 g at arrival in our facility and were randomised in four groups (Figure 8.1): a first cohort of 10 rats received no impact and served as healthy controls (HC group), a second group of 10 rats received mTBI and were delivered a memory training program (TBI-PAL group), a third cohort of 10 rats sustained mTBI and were included in an attention training program (TBI-5CCP group), and a fourth cohort of 10 rats received only a mild traumatic brain injury (TBI group). In this study a Sham group was not included because we wanted to mimic the clinical situation as close as possible (the healthy control group will not get a sham injury either). The study was approved by the Animal Ethics Committee at Ghent University (ECD 15/44Aanv) and all experiments were conducted in accordance with the guidelines of the European Commission (Directive 2010/63/EU). All animals were group-housed and kept under controlled laboratory conditions (12h light/dark cycle, 20 - 23 °C and 40 - 60 % humidity).

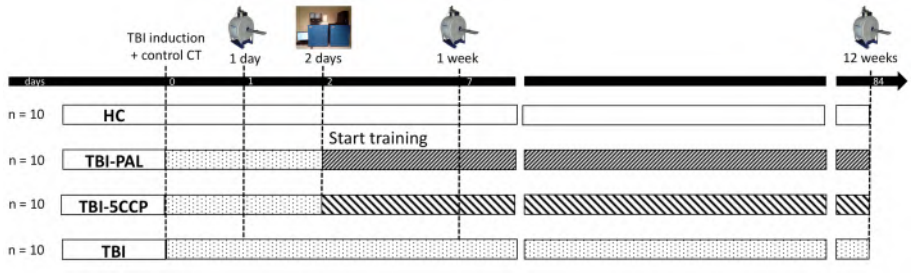

Figure 8.1: Outline of the experimental design with the healthy control (HC) group, two training groups (TBI-PAL and TBI-5CCP) and the negative control (TBI group).

The animals acclimatised to their new environment one week prior experimentation with free access to food and water and were daily weighed to obtain their baseline weight. The food restriction of the TBI-PAL and TBI-5CCP groups started after completion of the first habituation trial (see below). It is recommended in literature to maintain the body weights of the rats at 80 - 85 % of the baseline weight to ensure motivation to perform the training tasks. However, the rats in this study were not fully grown at the start of the experiments and we decided to monitor the weights daily and gradually increase the body weights over the weeks up to a maximum body weight between 270 - 300 g at the end of the training period. A daily food allowance of about 10 - 12 g rat chow per rat was sufficient to maintain motivation for training.

8.2.2 Induction of mild traumatic brain injury

The Marmarou weight drop model was used to induce a mild traumatic brain injury [45]. Briefly, rats were anaesthetised with a 5 % isoflurane induction and 2 % maintenance and injected with 0.05 mg/kg buprenorphin (Temgesic, Indivior) subcutaneously before further surgical procedure. For injury induction, the rat was placed on a foam matrass and positioned under a 450 g brass weight. The weight was dropped from 1 m guided through a plexiglass tube onto a metallic disc which served as a helmet and was fixated to the skull with tissue glue (Vetbond Tissue Adhesive, 3M). Immediately after impact, the rat was moved away from the tube and the helmet was removed. To

rule out any skull fractures, a low dose CT scan was performed (X-Cube, Molecubes, Ghent, Belgium). The rats received an extra dose of 0.05 mg/kg buprenorphin directly after the MRI scan acquired one day post-impact.

8.2.3 Touchscreen cognitive training program

Rats in the TBI-PAL and TBI-5CCP groups were trained using the Bussey-Saksida Rat Touchscreen System with Animal Behaviour Environment Test (ABET) II software (Campden Instruments Ltd., Loughborough, UK) (Figure 8.2.A). This computerised training system has previously been used in various rodent models of cognitive impairment including schizophrenia [207], Alzheimer's disease [208] and TBI [71]. The training chambers are equipped with a touch-sensitive monitor and a food magazine, which delivers the sucrose reward pellets (Purified Rodent Precision Tablet (45 mg), TestDiet, St. Louis, Missouri, USA) (Figure 8.2.B). Different masks for the presentation of the visual stimuli were used according to the type of training task. Specifically, a 5×1 mask - consisting of 1 bottom row of five windows (as shown in Figure 8.2.C) – was used for the 5-CCP task. A 3×1 mask together with a spring-hinched 'shelf' at a 90-degree angle 16 cm above the floor was used in the PAL training task (Figure 8.2.D). Of note, one animal in the PAL group was not able to train with the shelf present and therefore the shelf was removed when this particular animal was trained. At the start of the training, each rat in the two training groups was again randomised in one of the two training chambers that were available in our lab and was placed in this respective chamber each training session.

The cognitive training program started two days after the impact and followed the methods described in the instruction manuals provided by Campden Instruments [209, 210] and previously described protocols [72, 211, 212] with a few modifications (as described below). The animals were trained 5x/week (Monday-Friday) for 12 weeks and the body weights were monitored daily (including weekends). To remove odour cues, the training chambers were cleaned with 70 % ethanol between animals and the boxes were dismantled as much as possible at the end of each training week and cleaned with a damp cloth and Dettol disinfectant.

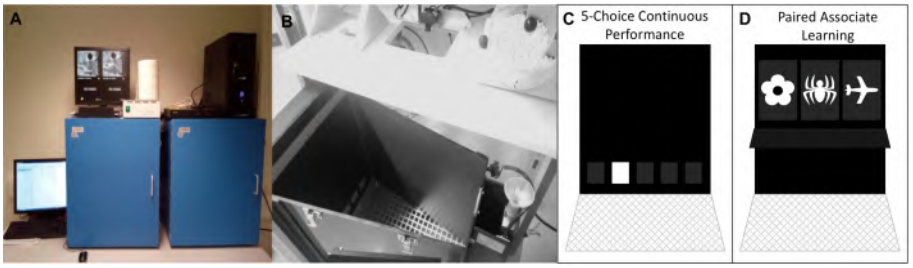

Figure 8.2: Touchscreen system setup (A), training box on the inside (B) and schematic representation of the 5-CCP (C) and PAL (D) training tasks.

Pre-training

Figure 8.3 provides a short overview of the pre-training program that includes 5 stages for the PAL task and 3 stages for the 5-CCP task. The first 3 stages are identical for both tasks.

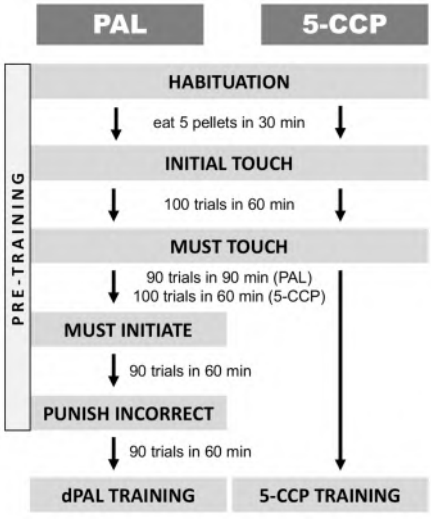

Figure 8.3: Schematic overview of the pre-training protocol before the actual training program using the PAL and 5-CCP task.

Stage 1 – Habituation. After return to the cage on the day of impact (day 0), the rats were introduced to the sucrose reward pellets. The rats

were also provided with the pellets on day 1. On day 2 the rats were placed in the training chambers of the touchscreen apparatus to allow for habitation with 5 reward pellets placed in the food tray. The rat could advance to stage 2 if they ate the pellets within 30 minutes.

Stage 2 - Initial Touch. In this step, rats were trained to associate a reward with a stimulus on the screen. A white square was shown in one of the windows in the mask. The image/stimulus disappeared after 30 seconds and one reward pellet was delivered in the illuminated food tray, which was accompanied by an auditory tone of 1 second. A new trial started after the rat successfully collected the reward. Two pellets were rewarded if the rat nose poked the correct window during stimulus presentation. Of note, we only gave two pellets instead of three (the default task parameters), because three was too much for our sample (i.e., the rats did not eat all the pellets and became unmotivated to perform the task). The rat had to complete 100 trials within 60 minutes to reach the criterion to advance to the next training step.

Stage 3 - Must Touch. Rats were trained to touch the screen in order to elicit a reward. A white square was randomly presented in one of the windows. In this stage, a pellet was only rewarded if the rat touched the correct window. The rewarded pellet was delivered in the illuminated food tray and was accompanied by an auditory tone. A new trial started immediately after the collection of the reward. The animal could advance to the next training stage, after the rat had successfully completed 100 trials (5-CCP task) or 90 trials (PAL task) within 60 minutes.

Stage 4 - Must Initiate (PAL task). This step was similar to the previous stage apart from the initiation of the training stage. Here the rat had to collect the reward, which was delivered in the illuminated food tray at the start of the training stage, to begin the session. The remaining time of the session was identical to the Must Touch training stage. After completion of 90 trials within 60 minutes the rats could advance to the next stage.

Stage 5 - Punish Incorrect (PAL task). In this stage, the rats in

the PAL training group did not receive a reward if they failed to touch the stimulus. Also, the stimulus disappeared, and the house light was illuminated for a time out period of 5 seconds. Additionally, a correction trial (the same stimulus as the previous trial) was presented and the rat had to repeat the same trial until a correct response to the stimulus was made, at which point it will receive a tone and reward. After completion of 90 trials within 60 minutes the rat could advance to the next training stage.

PAL training

In the different PAL task (dPAL), the rat is trained on associative memory and has to recall which graphic stimulus corresponds to a certain spatial location. There were three stimuli (spider, flower or airplane), with each stimulus corresponding to a specific spatial location in one of the three windows (flower: left, spider: middle and airplane: right) (Figure 8.2.D). Two stimuli were presented during each trial: one stimulus was presented in the correct position and the other stimulus was shown in the incorrect position. The rat had to touch the image that was presented in the correct position. If the rat successfully responded, the animal received a reward pellet accompanied by a tone in the illuminated food tray. Similar to pre-training stage 5, touching the incorrect window or a blank window resulted in a time out and no delivery of a reward. Once the time out period ended, the rats were represented with the same stimuli, which acted as a correction trial. This correction trial had to be successfully completed before the next trial with a new stimulus was presented. Each session was concluded either after 60 minutes or after completion of 90 trials. Not all rats were able to finish the 90 trials within one hour but were not excluded for further analysis.

5-CCP training

The 5-CCP task is an extension of the 5-Choice Serial Reaction Time (5-CSRT) task, which is widely used for assessment of attentional processes [78, 212]. Training on the 5-CCP task began with acquiring the 5-CSRT task (referred to here as the 5-Choice Touch Basic training stage) to exercise on visual attention. The session started with the delivery of the reward. After the rat removed its head from the food

tray, a trial began with an inter trial interval (ITI) of 5 seconds. At the end of this ITI, a stimulus was presented in one of the five windows which the rat had to nose poke (Figure 8.2.C). A reward pellet was delivered in the illuminated food tray accompanied by a tone if the rat had indicated the correct window either within the period of stimulus presentation or the 'Limited Hold' period (a pause period following stimulus presentation). Touching a blank window with no stimulus or not responding resulted in a 5 second time out whereby the house light was turned on. Once the time out period ended, the food tray was illuminated, and the rat had to enter the food tray to start a new trial. Training on the 5-Choice Touch Basic stage started with 'easy' settings (30 seconds stimulus duration and 30 seconds limited hold) and increased in task difficulty (i.e., decreased stimulus duration and limited hold) (Table 8.1) when the animals met the training criteria for each level similar to human training therapies. The criteria for each stage were met when the rat had completed 100 trials within 60 minutes with an accuracy > 70 % and omission percentage < 40 %. Of note, these criteria were not as stringent as the manual (accuracy > 80 % and omission < 20 %) because our animals were not able to reach these criteria.

Table 8.1: Overview of different levels in the acquisition of the 5-CCP task.

Training level 5-CCP	**Stimulus duration (s)**	**Limited hold (s)**
Level 1	60	60
Level 2	30	30
Level 3	20	20
Level 4	10	10
Level 5	5	5
Level 6	2.5	5
Level 7	1.5	5
Level 8	1	5
Variable ITI	1	5
5-CCP	1	5

Once the animals successfully completed level 8 (stimulus duration 1 s and limited hold 5 s) the animals could advance to a stage with

variable ITI (either 3, 4, 5, 6 or 7 seconds) with the same criteria as described before. Finally, the rats were trained on the 5-Choice Continuous Performance task which was similar as the previous level with variable ITI. However, in this level, there were also no-go trials (40 of the 120 trials in total) whereby all 5 windows were illuminated, and the rat had to withhold from making a response (inhibitory control). If the rat responded during this no-go trial, a time out period started, and this response was recorded as a false alarm without delivery of a reward.

8.2.4 Touchscreen training measures

During each training session (excluding pre-training) the following parameters were computed using the ABET II software for further analysis: (i) mean correct latency (MCL) of both training tasks, which is defined as the average time between the presentation of the stimulus and making a correct response, can be regarded as a measure of cognitive processing speed. Increased latency times therefore denote worse performance; (ii) mean reward latency (MRL) of both training tasks is the average time between a correct response and the collection of the reward pellet, and was used to asses motivation/motor control of the animals; (iii) percentage premature trials (PT) of the 5-CCP task indicates the portion of trials whereby the rat made a response before stimulus presentation. Consequently, higher scores on this measure denotes decreased inhibitory control, hence worse performance; (iv) accuracy of the PAL task was defined as the portion of the trials that were correct upon first presentation (excluding correction trials) and reflects cognitive control. We did not include the accuracy and omissions in the 5-CCP task, because these measures were used as training criteria and therefore matched across the animals.

8.2.5 In vivo longitudinal magnetic resonance imaging

MRI data were acquired on a 7 T MRI scanner (BioSpin PharmaScan 70/16, Bruker Biospin, Ettlingen, Germany) using a volume rat brain/mouse whole body RF coil 1 day, 1 week and 12 weeks post injury which corresponds to the end of the training period. We choose not to include a baseline scan to mimic the clinical situation (usually no pre-injury scans are available) and focus only on the effect of training

after infliction of injury. During the scanning sessions the rats were anaesthetised with 2 % isoflurane (5 % for induction) and the respiration rate was monitored with a pressure pad. To maintain body temperature the animals were covered with a circulating warm water heated blanket and wrapped in bubble wrap.

The MRI protocol included a whole brain anatomical T2-weighted scan using a Rapid Acquisition with Refocused Echoes (RARE) sequence with the following parameters: TR = 5500 ms, TE = 37 ms, RARE factor = 8, FOV = 2.5 x 2.5 cm, in plane resolution = 109 x 109 μm, 600 μm slice thickness, 45 slices, 12 min acquisition time. The diffusion images were acquired with a spin echo, echo-planar imaging (EPI) sequence between the olfactory bulb and the cerebellum. Multi-shell diffusion weighted acquisitions were recorded using an encoding scheme of 32, 46 and 64 gradient directions with b-values of 800, 1500 and 2000 s/mm^2 and with 5, 5 and 7 b0 images (scanned at the start of each shell), respectively. Other diffusion scanning parameters were as follows: TR = 6250 ms, TE = 24 ms, number of segments = 4, number of averages = 1, FOV = 3 x 3 cm, in plane resolution = 333 x 333 μm, 600 μm slice thickness, 600 μm interslice distance, 25 slices, 65 min acquisition time.

The acquired diffusion weighted images were pre-processed using MRtrix3 (version 3.0_RC3-86-g4b523b41) and ExploreDTI (v4.8.6., [136]) using a multi-step procedure. After concatenation of the three diffusion shells, a denoise and correction for Gibbs ringing step was performed in MRtrix3 [134, 135, 213]. Next, the images were imported in ExploreDTI to perform correction for Eddy currents, EPI and motion distortions. Finally, the diffusion tensor images were obtained for axial diffusivity (AD), fractional anisotropy (FA), mean diffusivity (MD), radial diffusivity (RD), the diffusion kurtosis images for axial (AK), radial (RK) and mean kurtosis (MK), and the white matter tract integrity images for axonal water fraction (AWF), intra axonal diffusivity (IAD), axial and radial extra-axonal diffusivity (AxEAD and RadEAD) and tortuosity (TORT) using a weighted linear least squares method [137]. These parametric maps were coregistered to an FA template that was based on the local population using 27 rats [214]. Finally, a volume-of-interest (VOI) analysis was performed in the hippocampus and cingulum using

the Amide toolbox [139], since these regions are expected to show microstructural changes induced by the two training tasks (the PAL and 5-CCP tasks, respectively). Metrics for the WMTI model were obtained only in the cingulum since this is a white matter tract with tightly aligned fibres that holds the validity of the WMTI model.

8.2.6 Statistical analysis

Statistical analyses were performed in SPSS Statistics 24. The diffusion metrics one week and 12 weeks after induction of mTBI were normalised to the metrics observed one day after impact to examine changes in the diffusion metrics during the training period. We decided to run an exploratory approach using unpaired t-tests were used as planned contrasts to investigate differences between groups on both time points (one week and 12 weeks) for each of the diffusion metrics. Paired t-tests were conducted to investigate differences between both time points within each group and the diffusion metric. To correct for multiple comparisons a Bonferroni correction was applied resulting in a significant p-value < 0.0125, 0.0166 and 0.010 for metrics of the DTI, DKI and WMTI model, respectively. Correlation analysis was conducted between the behavioural measures from the training tasks (i.e., MCL, MRL, PT and PC) and changes in diffusion measures after completion of the 12 week training program, using Pearson correlation coefficients. Again Bonferroni corrected p-value were considered significant. Important to note, three rats were not able to reach the last training stage of the 5-CCP task and were excluded for the correlation analysis to ensure similar training levels across all animals at the 12 week imaging time point.

8.3 Results

8.3.1 Behavioural results

The body weights of the rats in both training groups first showed a decrease due to the food restriction, followed by a steady increase during the training period indicating a constant growth rate (Figure 8.4.A). Both groups showed qualitative increases in performance on the training tasks, as evidenced by an increase in accuracy on the memory task (PAL

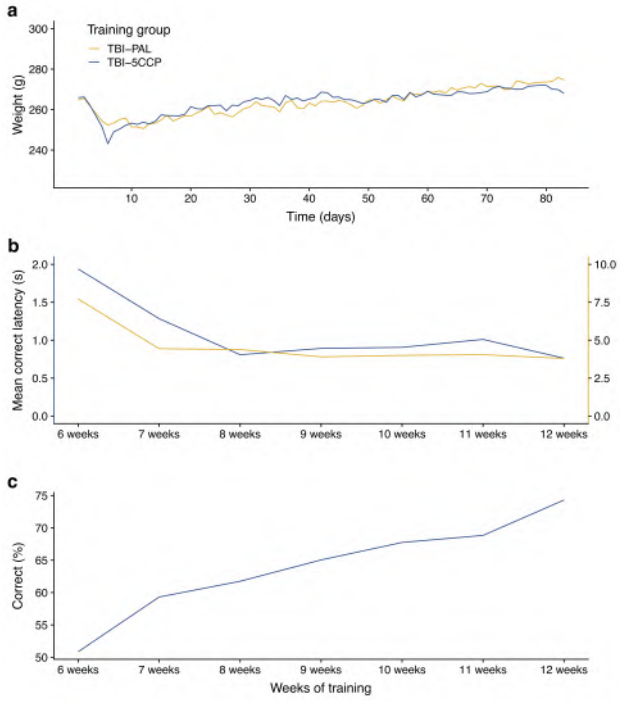

Figure 8.4: Evolution of the body weights of the rats over time (A). Increases in performance as witnessed by a decreasing latency in both tasks (B) and increase in correct percent for the PAL task (C).

group) and decreases in MCL (Figure 8.4.B-C). Of note, the MCL of the PAL group was about 3 - 4 times longer than the MCL of the CP group but showed the same decreasing trend, indicating that both groups had a comparable learning speed.

8.3.2 In vivo longitudinal MRI changes following training

At the one week imaging time point, none of the groups were significantly different from each other, except that the IAD of the TBI-5CCP group was significantly lower than the TBI ($p = 0.004$) and sham group ($p = 0.010$). In the next sections, we will describe the diffusion MRI changes following 12 weeks of training.

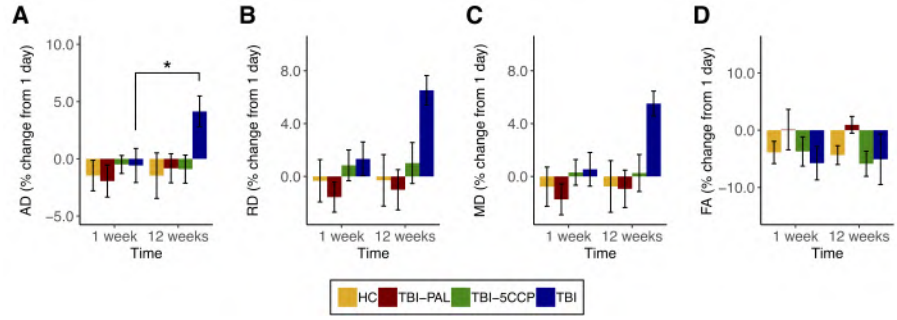

Figure 8.5: Changes in diffusion MRI metrics in hippocampus. Error bars indicate standard of the mean. * $p < 0.01$.

Diffusion tensor imaging

Paired samples t-tests revealed significant increases in FA in the cingulum of the TBI-PAL ($p = 0.003$) and TBI-5CCP group ($p = 0.010$) following 12 weeks training when compared to the one week time point (Figure 8.6.D)(Table 8.2). In the TBI group there were significant increases in AD of the hippocampus ($p = 0.011$) and in MD of the cingulum ($p = 0.011$) at 12 weeks when compared to the one week timepoint, which were not present in the training groups (Table 8.2).

A near significantly higher RD was found in the hippocampus of the TBI group compared to the TBI-PAL ($p = 0.016$) group using unpaired t-tests at the end of the 12 week training program. No other diffusion measures were significantly different between groups.

Diffusion kurtosis imaging

In the cingulum there were significant increases in both the TBI and TBI-5CCP group in AK at the 12 weeks imaging time point when compared to one week post injury which was accompanied by a near significant increase in RK for the TBI-5CCP group (Table 8.2). Though, kurtosis values of the TBI-5CCP tended to be higher at the one week time point as well indicating that these increases in kurtosis already occurred between one day and one week post injury. In the hippocampus there were no significant changes in any of the DKI metrics. Also,

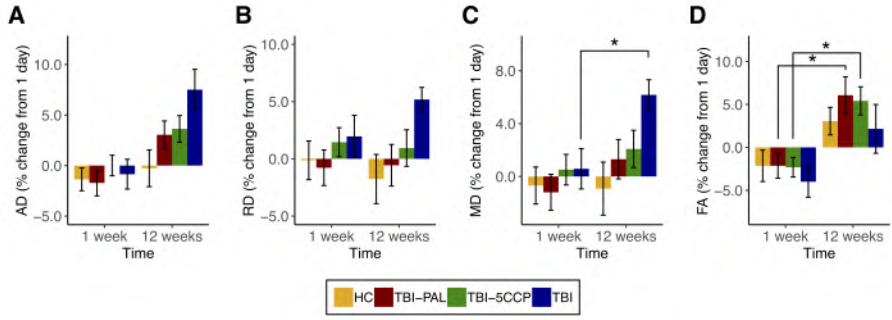

Figure 8.6: Changes in diffusion MRI metrics in the cingulum. Error bars indicate standard of the mean. * $p < 0.01$.

no group differences were found in either hippocampus or cingulum (Figure 8.7).

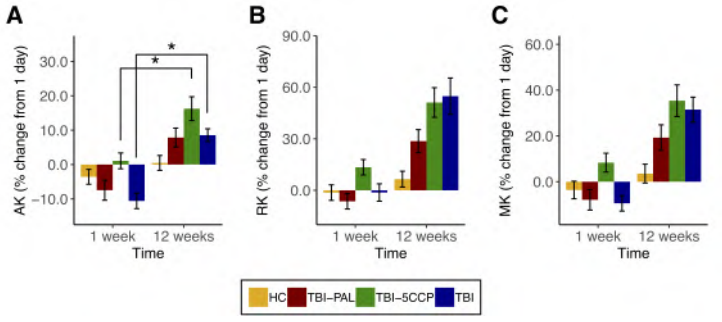

Figure 8.7: Changes in diffusion kurtosis metrics in the cingulum. Error bars indicate standard of the mean. * $p < 0.01$.

White matter model in cingulum

Pairwise comparisons revealed a near significant increase in AWF in both the TBI ($p = 0.015$) and TBI-5CCP group ($p = 0.016$) and coincided with an increase in AxEAD (Table 8.2), especially in the TBI group ($p = 0.003$). The TBI-5CCP group showed near significantly decreased values of IAD ($p = 0.022$) at the 12 weeks imaging time point which was significantly lower than the healthy control group ($p < 0.001$)(Figure 8.8).

Table 8.2: P-values of paired t-tests between the one week and 12 week time point in the healthy control, TBI-5CCP, TBI-PAL and TBI groups the cingulum.

Paired t-test	Cingulum			
DTI	Sham	TBI-5CCP	TBI-PAL	TBI
AD	ns	ns	ns	0.013
MD				0.011
FA		0.010	0.003	ns
DKI				
AK	ns	0.012	ns	0.006
RK		0.018		ns
MK		ns		
WMTI				
AWF	ns	0.016	ns	0.015
AxEAD		0.018		0.003
IAD		ns		ns

ns = not significant.

8.3.3 Relationship between diffusion metrics and behavioural changes

We observed a near significant correlation ($p = 0.018$, $r = -0.758$) between alterations in AK of the hippocampus in the PAL group and the accuracy on the PAL task. In other words, better performance on the PAL task coincided with decreases in AK values in the hippocampus. In both the hippocampus and cingulum, alterations in RD and MD were positively correlated with PT, indicating that smaller alterations in diffusivity following training were related to better inhibitory control (Figure 8.9). Furthermore, alterations in FA of the cingulum were negatively correlated with PT and thus increases in FA after the 12 weeks training program were associated with better performance on the 5-CCP task (Figure 8.9.D). Interestingly to note, we found a significant predictive correlation between MCL of the 5-CCP task and IAD in the cingulum ($p = 0.004$ and $r = 0.945$) one week after impact (Figure 8.10). This indicates that at the start of the training, lower values of IAD are indicative of better attention at the end of the training period.

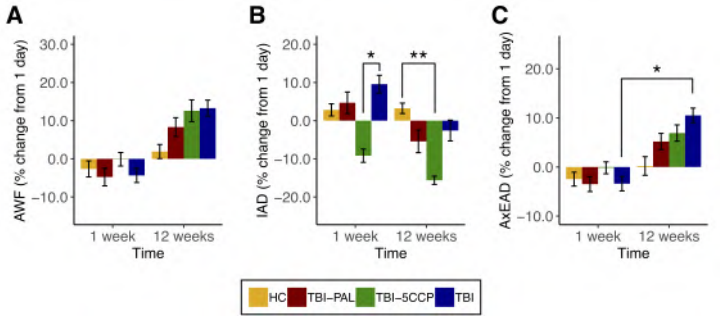

Figure 8.8: Changes in white matter model metrics in the cingulum. Error bars indicate standard of the mean. * $p < 0.01$, ** $p < 0.001$.

Table 8.3: Significant correlations between between behavioural measures from the PAL and 5-CCP training and diffusion metrics at the end of the 12 week training period.

	Hippocampus		Cingulum	
PAL	p-value	r-value	p-value	r-value
Accuracy - AK	0.018	-0.758	ns	
5-CCP	p-value	r-value	p-value	r-value
PT - RD	0.002	0.962	0.008	0.925
PT - MD	0.004	0.951	0.011	0.915
PT - FA	ns		0.005	-0.939

ns = not significant.

8.4 Discussion

The aim of this study was to evaluate a touchscreen cognitive training program, which is closely related to a human training program, in a rat model of mild TBI. Additionally, using diffusion MRI, we wanted to investigate whether memory vs attention training had a specific impact on the hippocampus and cingulum, respectively. This study showed for the first time that training delivered early after brain injury can slow further deterioration/secondary injuries in a rat model of mild TBI as evidenced by neuroimaging changes in both regions. Moreover, the neuroplastic changes coincided with behavioral improvements, showing

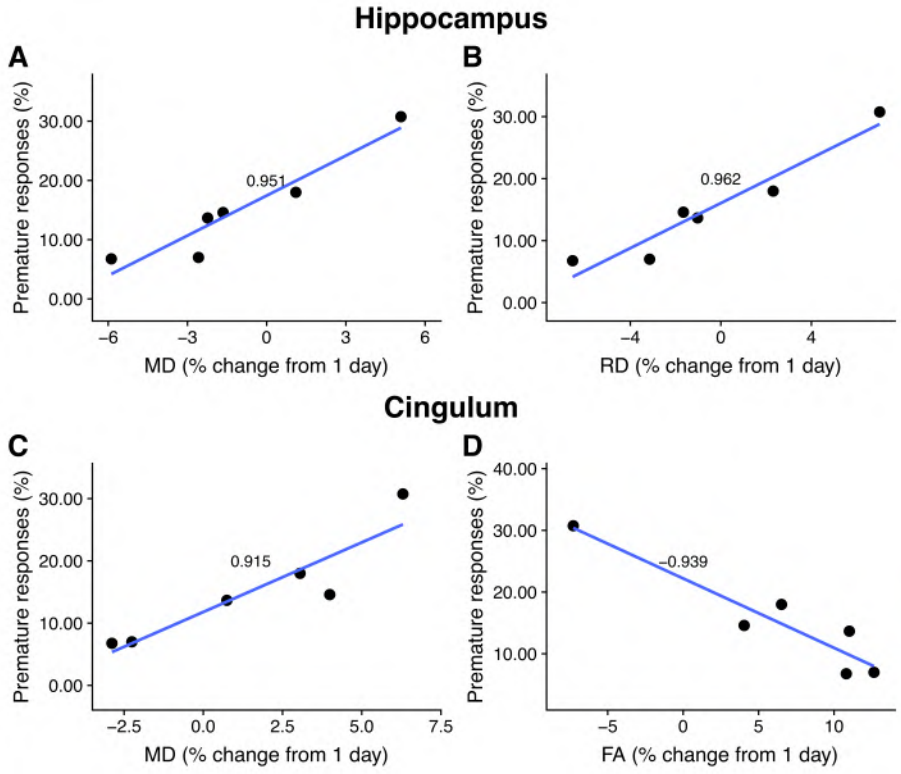

Figure 8.9: Correlation of premature responses on the 5-CCP task with MD and RD in the hippocampus (A, B) and with MD and FA in the cingulum (C-D) 12 weeks post training.

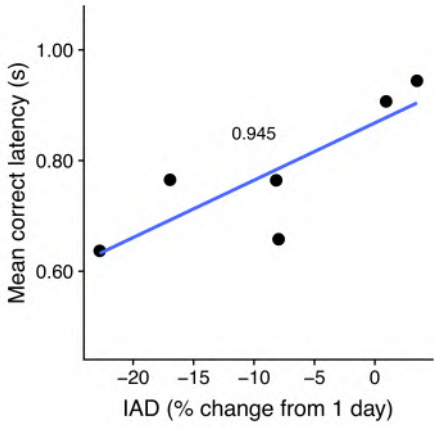

Figure 8.10: Correlation of mean correct latency on the 5-CCP task at 12 weeks post training with IAD in the cingulum one week post injury indicating a predictive outcome of decreased MCL with faster responses.

the clinical relevance of the induced changes.

8.4.1 Cognitive training interventions early after TBI may slow down the secondary disease progression

In the cingulum of both our training groups, we found significant increases in FA following training which is consistent with a previous study in healthy adults following 8 weeks of Cogmed training, suggesting a possible increase in myelination [215]. Furthermore, a cognitive training study in elderly adults showed the same increase in FA and decreases in diffusivity as in our study in areas containing the cingulum and corpus callosum following 10 weeks of memory training [216]. Moreover, these neuroplastic changes were correlated with improved memory performance showing the capacity of cognitive training to beneficially alter brain microstructure.

Compared with both training groups and the HC group, the mild TBI group without training showed higher diffusivity values at the end of the 12 week experimental period in the hippocampus and cingulum. Contrary, in the training groups, microstructural organization in the

hippocampus and cingulum was preserved at the end of the training and showed similar levels as the HC group, while a microstructural integrity worsening was found in the TBI group, showing damage progression likely due to axonal injuries and breakdown of brain microstructure. This result is consistent with previous neuroplasticity studies in other neurodegenerative disorders - TBI is considered more and more as a neurodegenerative disease - showing that training may halt otherwise accelerated shrinkage and atrophy. For example, in the study of Bonzano et al. [217] patients with multiple sclerosis who received training showed preserved white matter integrity in the corpus callosum and corticospinal tract, whilst microstructural integrity was worsening in the control group (as indexed by decreased values of fractional anisotropy together with increased radial diffusivity values in the corpus callosum and corticospinal tract).

In contrast to a recent study in healthy adults we did not find increases in AWF and MK to be correlated with better performance and suggesting higher axonal density, greater myelination and/or greater tissue complexity [218]. We did find the opposite and showed that decreased values of AK in the hippocampus were near significantly correlated with higher accuracy. This relation we could not demonstrate in the cingulum and furthermore, kurtosis values in the cingulum were increased at the end of the training period suggesting a lingering recovery process of the injured cells. In the study by Davenport et al. [144] investigating athletes pre- and post-season, increases in AWF and kurtosis metrics were widespread post season and were hypothesised to be the result of axonal swelling and increased cellularity. Thus, from these two measures we cannot make conclusive results about the health status of the underlying brain microstructure. In addition to these changes, we found that AxEAD and RadEAD were near significantly correlated with better performance in the cingulum ($p = 0.027$, $r = -0.726$ and $p = 0.036$, $r = 0.840$, respectively). Though, we also demonstrated a near significant increase in AxEAD in the TBI-5CCP group, this was not as high as the TBI group. Increases in EAD at the more subacute/chronic time point are said to be the result of vasogenic oedema [144] which makes it plausible that the training therapy could reduce this effect in the cingulum.

Together, our findings suggest that training interventions early after sustaining a TBI may have the potential to slow disease progression, which is of significant clinical interest also in other neurodegenerative disorders such as dementia, stroke and multiple sclerosis.

8.4.2 The type of training task does not have an impact on specific structures

Contrary to our hypotheses, the two training tasks induced similar neuroplastic changes in both brain regions. In other words, the type of training task did not influence specific structures. Specifically, both PAL training and 5-CCP training resulted in increased FA values in the cingulum and stable diffusivity values in hippocampus and cingulum. Increases in kurtosis values were demonstrated only in the TBI-5CCP group at the end of the training period and could be suggestive of a difference between training tasks but the TBI-5CCP group was not significantly higher than the TBI-PAL group and thus no statistical difference between training groups was found. Though, it has been demonstrated that more prefrontal cingulate areas are important regions for functioning on the 5-Choice Serial Reaction Time task (attentional processing) [219, 220], it is likely that sustained attention not only relies on the cingulum but on a distributed network of prefrontal, temporal and hippocampal structures as well [221]. Furthermore, two recent cognitive training studies in human TBI patients have found alterations in graph metrics across the whole brain network or connectome [222, 223] suggesting that investigating the brain as a whole network could provide more insight on how the brain adapts with cognitive training.

8.4.3 Neuroplastic changes coincide with behavioural improvements

We demonstrated that decreases in diffusivity were related to better performance on the PAL and 5-CCP task as evidenced by less premature responses, denoting better inhibitory control, and higher accuracy scores. These results are in accordance with previous studies in healthy rats showing associations between better performance on a memory task and reductions in MD [196, 199]. Furthermore, the

negative correlation between FA and premature responses suggests that the observed significant increases in FA in the cingulum are beneficial for attention and inhibition control. This result is in agreement with the study of Fan et al. [224] in stroke patients, showing that patients with higher increases in FA following training performed better. As discussed earlier, we found correlations of decreased kurtosis and EAD values with increases in accuracy and better inhibitory control which could indicate that training has the potential to slow down or decrease the secondary inflammatory process and promote the switch to a more homeostatic or even neuroplastic response. These results show thus the potential of DTI metrics combined with the more advanced DKI and WMTI metrics as a promising tool to improve TBI prognosis, including monitoring treatment effects in large-scale clinical trials.

8.4.4 Technical considerations and study limitations

This is the first study to use a touchscreen system for cognitive training therapy in a rat model of mild TBI. Because the training process was based on default settings of the trainings tasks it could be further optimised in future research to better suit a mild TBI population. One suggestion would be to reduce the number of trials the rats have to perform in each PAL training session. We noticed that the majority of the rats were not able to consistently perform all 90 trials within one hour (only 2 rats could finish 90 trials in 60 minutes 5 days in a row) and therefore we propose reducing the total number of trials to 60 - 70. Although the 5-CCP training rats had no trouble finishing the 100 or 120 trials per training session, not all animals reached the last training level at the end of the 12 week training program (Continuous Performance Test). Because this last training task is more closely related to the human task, we consider it important to reach this stage and suggest shortening the 5-Choice Touch Basic training stage. A stable performance of level 5 (stimulus duration of 5 seconds) with an accuracy > 80 % seems to be an achievable goal for mTBI rats since all rats in our sample were able to perform this level. Following this level, the actual 5-CCP with inhibition control training can commence with a stimulus duration of 5 seconds (other than the default 1 second stimulus duration) and variable ITI. During training at this stage, the task can again be made more difficult by shortening stimulus duration, and accuracy and

omissions can be used as criteria to advance the training. Another possibility would be to extent the training period until all rats have reached the last training stage. However, we believe this would induce more heterogeneity in the performance of the rats on the task, i.e., some would be overtrained whereas others would need the whole training period to reach the last training stage. Alternatively, Bhandari et al. [225] suggested to only include animals that reached a certain stage within a certain time limit because slow learners are more likely to be the result of less motivation to perform the task. However, within the mTBI population we cannot be sure that less motivation is either the result of the innate ability of the rat to perform the task or an effect of the mTBI. Therefore, we believe that making it more achievable for all rats to reach the target setting on the 5-CCP task is more favourable in this population.

During training, rats from the healthy control or TBI group without training remained in their home cage and did not have extra contact with the researchers (e.g. during the daily handling and weighing) or experienced a new environment (the training boxes). Although the duration of the daily weighing session of the trained rats was kept at a minimum, it is possible that the effects of the touchscreen training could be blended with the influence of this environmental factor and makes it difficult to isolate the effects of the touchscreen training alone. Furthermore, training took place in a new environment and can be considered (to a certain point) as environmental enrichment which has been shown to improve spatial learning or motor functioning following TBI [64, 65]. Therefore, future studies should include a daily weighing moment for the control and mTBI group as well and introduce the rat to the training boxes and reward pellets but without running a training paradigm.

Using two types of cognitive training, i.e., memory vs attention training, we wanted to evaluate whether the type of training has an influence on the recovery process. However, we failed to detect any differences between the two training groups. Both training groups showed a similar learning rate and comparable diffusion metrics. The limited number of animals in the training groups and the differences between the rats in

their ability to perform the task (due to a mixed effect of innate ability and mTBI) may be a reason why we could not detect the influence of the training type in our study cohort. On a side note, based on unpaired t-tests at baseline (data not in included) we could not detect any differences in diffusion metrics between groups indicating that possible baseline differences are not an issue here. Further, we found a difference in IAD between both training groups at the start of the training period (one week post injury) which could not be explained by a difference between training tasks since both training groups are in the pre-training phase at this time point and pre-training is performed the same way for both groups. Because this difference between training groups was only visible in this one metric, we hypothesise this is simply a result of innate variability and future studies should include a higher number of animals in each training paradigm to reduce this and aforementioned limitations.

8.5 Conclusion

With this study we were the first to demonstrate neuroplastic changes induced by a touchscreen cognitive training program in an mTBI rat model using DTI, DKI and white matter metrics. Although we were not able to link the two types of training to specific brain regions, we could demonstrate the positive effect of training in general based on neuroimaging findings. Additionally, the neuroplastic changes coincided with better behavioural outcome as witnessed by reduced impulsivity and increased performance. Based on these results we show the potential of diffusion MRI metrics to become a reliable measure to evaluate training therapy for TBI patients. This will facilitate future work investigating how training therapy can be further improved to enhance visuospatial memory and inhibition control.

9 | General Discussion and conclusion

The main objective of the present dissertation was to examine the added value and microstructural specificity of advanced diffusion MRI models to investigate changes in brain microstructure in rats with mild traumatic brain injury. In addition, we wanted to evaluate whether cognitive training can induce neuroplastic changes that improve the alterations in affected brain regions. In the next sections we will discuss the main findings of this research.

9.1 Microstructural changes in the rat brain following mTBI

Added value of advanced diffusion models

In our first study, **Chapter 5**, the goal was to evaluate three different diffusion models in their ability to detect and follow up the microstructural alterations following mTBI. More specifically, we investigated the ability of the DKI and WMTI model, which are more specific to the underlying brain microstructure, to provide complementary information to the more widely used and established DTI model. Because the exact time course of possible structural alterations is still not fully understood and no consistent outcomes can be demonstrated, we made use of a multi-sessions scanning design where imaging was performed at both the acute time point (one day and one week post injury) and the chronic time point (3 months post injury) in four predefined ROIs (i.e., corpus

callosum, hippocampus, cingulum and cortex).

In agreement with previous research in mTBI rat models, we found decreases in diffusivity throughout the brain within the first week of injury [39, 47, 104, 105, 141, 142]. In the mTBI group we demonstrated significant decreases in RD and MD of the DTI model in the cingulum and hippocampus, respectively, which could be the result of cytotoxic oedema and a reduction of extracellular space. We could not detect any significant changes in the DKI metrics, however, we were able to show a reduction in RadEAD of the WMTI model in the cingulum one week post injury. This reduction was also demonstrated in a hypomyelinated mouse model and could be explained by inflammatory processes [131]. This strengthens our hypothesis that cellular swelling and possibly neuroinflammation is involved in mTBI. A continued significant decrease in RD in the cingulum of the mTBI group at the later time points could indicate prolonged cellular swelling.

A good preclinical model should be able to mirror the diffusion changes observed in human populations. In the last few years there have been a few human studies using these more advanced diffusion models in mTBI research [126, 143–146]. In concussed athletes reduction in RD and MD could be demonstrated without any changes in the DKI metrics in the first week post concussion [145]. This study also demonstrated prolonged reductions in diffusivity 6 months post concussion [146]. This strong agreement between our preclinical results and human concussed athletes is highly encouraging and indicates that our rat model is a good model to study mTBI when no lesions are visible on conventional anatomical scans. Furthermore, the decreases in diffusivity were mainly driven by a decrease in radial (RD and RadEAD) and not the axial components, suggesting that axonal stability is more or less preserved. Therefore, we believe that radial metrics could be sensitive to identify an imbalance in neuronal and glial homeostasis and might be promising biomarkers to detect microstructural changes in the acute and chronic phase after mTBI.

In a follow up study, **Chapter 6**, we investigated the feasibility to provide fiber specific information on the morphology of injured tracts

using fixel-based analysis in mTBI rats. This recently developed technique has shown great potential in white matter affecting diseases but only limited research has been done in TBI [96, 158, 159]. This study could expand literature and provide further insights by exploring the morphology of tracts affected by TBI. We observed a significant increase in fibre cross-section (FC) in the splenium and forceps major of the corpus callosum of mTBI rats compared to a sham group one week after impact without any changes in the other fixel-based measures. This result is in agreement with a recent study in human TBI patients where an increase in FC was found in the splenium of the corpus callosum and the left superior longitudinal fasciculus when compared to controls [160]. Also this study did not find any changes in other fixel-based metrics and attributed the increase in FC to axonal swelling. Contrary to the study by Wright et al. [161], we could not demonstrate decreases in fibre density indicative of fibre atrophy. However, they investigated fibre changes at a later time point (12 weeks post impact) and made use of a severe TBI rat model which is more likely to induce large and widespread white matter damages.

Interestingly, the supporting voxel-based analysis could not detect the same affected regions as identified by fixel-based analysis. Voxel-based analysis revealed multiple and diffuse affected regions in frontal, hippocampal and cingulate regions but not in the splenium of the corpus callosum. This discrepancy could be explained by the occurrence of larger lesions to cells at the grey-white matter junction and smaller lesions in the white matter, where fixel-based analysis might have a better sensitivity because the method can only be applied in these white matter regions. However, alterations detected by the voxel-based analysis did resemble the changes observed in the ROI-based analysis of Chapter 5 showing decreases in MD and RD in the hippocampus and cingulum one week after impact which could be the result of cellular swelling.

The combined results of Chapter 5 and 6 show that the different diffusion models have great potential to detect microstructural changes induced by mTBI, but that each model (DTI, DKI, WMTI or fixel-based analysis) and each analysis method (region-of-interest vs voxel-/fixel-based) should be considered as complementary and supportive of

each other. Combining the different models and methods can provide a bigger and clearer picture of the underlying biological processes in mTBI and probably also in other neurological disorder (e.g., dementia, multiple sclerosis,...).

Underlying biological correlates

Imaging biomarkers are characteristics that are measured on medical images that can serve as an indicator of biological processes. They should be sensitive and specific to biological tissue properties such as microstructure, and can detect early disease progression that has not yet resulted in gross morphological abnormalities. Therefore, in order to develop possible biomarkers for mTBI, the specificity of the imaging metrics for underlying biological processes should be examined. In **Chapter 7** we investigated the link between the alterations in diffusion metrics presented in Chapter 5 and neuronal structure, synaptic functioning and glial response. Additionally, we explored the potential of Raman spectroscopy to provide molecular information on cellular compounds affected by the trauma in a label-free and multiplexed manner. In this way we try to provide a piece of the (imaging) puzzle to better understand the multitude of biological processes that play a role in mTBI.

At the end of our non-invasive in-vivo imaging experiments, three months after a mild impact, animals were sacrificed and brain sections were stained for three histological markers, i.e., neurofilament (NF), synaptophysin (SYN) and glial fibrillary acidic protein (GFAP). Correlation analysis between changes in the diffusion metrics and the histological markers revealed several significant associations in the hippocampus of mTBI rats. Decreased values in diffusivity were related to neurofilaments with a higher dephosphorylation status and could be indicative of compaction and misalignment in the cytoskeletal network [180]. This result was in agreement with a supporting Raman spectroscopy analysis showing a reduced protein content one week post injury and could indicate that the cytoskeleton of neurons has lost part of its structure. This shows that it is possible to investigate the molecular profile of damaged tissue in a label-free manner using Raman spectroscopy. We also found a positive correlation between GFAP reactivity

and kurtosis metrics three months post injury, and FA values one day post injury. This indicates that increased values in FA in the acute phase of mTBI are predictive for a higher glial activity later on in the chronic phase. Together with the increased kurtosis values, implying an increase in cellularity, this could suggest a prolonged neuroinflammatory response three months after impact or alternatively higher tissue organisation due reorganisation of the neuronal circuits (neuroplasticity).

To summarise our findings observed in Chapters 5 to 7: the decreases in radial diffusion measures in both the hippocampus and cingulum, and increase in FC in the corpus callosum one week post injury are indicative of cellular and axonal swelling and can be the result of a neuroinflammatory respons. Because the axial components of the diffusion measures did not significantly change we believe that our mild and diffuse trauma does not cause major structural damages but more an unbalance in the neuronal homeostasis. The prolonged decreases in diffusivity and a positive correlation between GFAP reactivity and kurtosis metrics could suggest ongoing neuroinflammation with infiltration of inflammatory cells (increase in kurtosis) and swelling of tissues (decreased diffusivity) or neuronal reorganisation where more and/or hypertrophic astrocytes modulate the synapses and form coherent pathways for neuronal circuits (increased kurtosis and decreased diffusivity).

9.2 Effect of cognitive training in a mTBI rat model

Our last goal was to evaluate whether diffusion metrics have the ability to detect training-induced plasticity and to detect specificity of the type of training. Therefore, we administered an intensive touchscreen training program of 12 weeks consisting of two types of training, memory (TBI-PAL group) or attention (TBI-5CCP group) training, to rats with a mTBI and diffusion MRI was acquired before and after training intervention.

Neuroplastic changes induced by touchscreen training

Both training groups showed significant increases of FA in the cingulum at the end of the 12 week training intervention, which was not present in the mTBI group that did not receive this cognitive training. Increases in FA after training intervention have been demonstrated in elderly humans and could be the result of an increase in myelination [215]. Furthermore, increases in diffusivity in the hippocampus and cingulum were observed in rats that received no training and were not present in the training groups, suggesting a microstructural worsening in the mTBI without training. We could not detect any changes in the DKI and WMTI metrics of the training groups except for an increase in AK in the cingulum of rats that received attention training. Increases in kurtosis values have also been reported in concussed athletes at the end of the training season [144]. However, since this increase was also present in the group without training, we believe that this can be the result of both lingering inflammation or neuroplasticity (either as natural recovery or training induced).

Contrary to our hypothesis, we did not find any difference between diffusion metrics after the two different types of training and we could not establish the specificity of the type of training to their hypothesised target, i.e., memory training is specific to the hippocampus and the attention training to the cingulum. It has been demonstrated that more prefrontal cingulate areas are important regions for attentional processing, and it is likely that sustained attention not only relies on the cingulum but on a distributed network of prefrontal, temporal and hippocampal structures [219–221]. Using graph theory metrics and structural connectome analysis it has been shown that cognitive training following TBI can induce neuroplastic changes and investigating the brain as a whole network could provide more insight on how the brain adapts with cognitive training [222, 223]. Nevertheless, to the best of our knowledge, our study was the first that observed neuroplastistic changes induced by a touchscreen cognitive training program in a mTBI rat model as witnessed by changes in diffusion metrics. This neuroplasticity demonstrates a positive effect of training in general and shows the potential of cognitive training to slow down the secondary disease progress.

Structural neuroplasticity is associated with behavioural improvements

The administration of an intensive cognitive training program is not very relevant if it does not have a positive effect on cognitive complaints. Therefore, we monitored behavioural outcome measures to evaluate the training progress. We could clearly see improvements in accuracy on the memory task and a reduction in reaction time on the attention task. More importantly, these behavioural improvements correlated with the neuroplastic imaging findings showing that reductions in diffusivity were associated with less premature responses (and thus better inhibitory control) and higher accuracy scores. These results are in accordance with a study in healthy rats showing a better performance at lower diffusivity values [196, 199]. Additionally, a negative correlation between FA and premature responses could indicate that the increases in FA in the cingulum are beneficial for attention and inhibitory control. DKI or WMTI metrics did not survive the multiple comparisons correction but showed near significant correlations between decreased kurtosis and increases in accuracy, and between decreased extra-axonal diffusivity values and better inhibitory control. Together, these results highlight that diffusion MRI metrics could become a reliable measure to evaluate training therapy for TBI patients and could be a promising tool to improve TBI prognosis, including monitoring treatment effects in large clinical trials.

9.3 Final conclusion

Longitudinal multi-shell diffusion MRI has great potential to provide a more complete view to better understand the underlying biological processes following a mild and diffuse traumatic brain injury in rats. In addition, diffusion MRI can be used to assess the treatment effects of a cognitive training program on injured brain regions. We recommend further validation of the diffusion models described in this work, not only in other preclinical TBI models to investigate the disease mechanisms in other types of trauma, but also in larger human prospective trials to test the method in a heterogeneous population. This can ultimately lead to an effective method to follow up the influence of cognitive training in

an objective way and allow for the development of biologically driven training interventions.

10 | Broader context and future perspectives

With an estimated 10 million people affected annually by TBI, it is clear that TBI is a pressing problem that leaves a significant mark on mortality, residual disability, health economic costs and reduced productivity in all societies [226]. Moreover, we have to be aware that the true incidence of TBI may be substantially underestimated because the milder forms of trauma remain mostly and often for long times unnoticed. Therefore, TBI has been termed as silent epidemic [9]. Although there have been improvements in clinical care and development of authoritative guidelines which have reduced mortality of severe TBI over the years, improvements in favourable outcomes have slowed and are less obvious [227]. In the next sections, we outline a few of the biggest remaining problems, discuss how this dissertation fits in this TBI puzzle and provide recommendations for future research.

Bottlenecks and priorities for action

TBI can be considered as "the most complex disease in our most complex organ" and is characterised by high heterogeneity in terms of causes, pathophysiological mechanisms, severity, treatments and outcomes. Because of this great variability, gaps in our knowledge about TBI remain [227]. For example, we do not fully understand why patients with similar injuries respond differently and we do not include pre- or co-morbid factors in the evaluation process.

Furthermore, the main approach of classification of initial severity (the Glasgow Coma Scale) has not been updated in over 40 years and CT lacks sensitivity for mild injuries.

During a workshop in Brussels on "Feasibility and benefits of international collaboration in the field of TBI research" in October 2011, the main priorities in future research on TBI have been identified and has led to the formation of the CENTER-TBI project, a focused European effort to advance the care of patients with TBI, within the broader international framework [228]. In relation to this thesis two aims are of most importance:

1. A better characterisation of TBI as a chronic process (and thus not an acute single event) in which the development of biomarkers (blood, imaging or genomics-based) and a better classification based on patho-anatomical and mechanical data are 2 key priorities.

2. Identification of the most effective interventions for managing TBI. Here it is important to provide a good outcome prediction in relation to the care that is given and to determine which therapies are effective.

In this doctoral research, our goal was to better characterise the TBI processes using a longitudinal and advanced diffusion MR imaging scheme. We were able to follow up the disease process from the acute phase (one day and one week post injury) until the chronic phase three months after injury and have identified a distinct profile of diffusion changes in mTBI rats that did not show any abnormalities visible on conventional CT or anatomical MRI scans. This shows that, especially in mTBI, newer and more sensitive methods are needed to describe the microstructural changes induced by the mTBI. Furthermore, the diffusion MRI metrics could be linked to certain underlying biological processes and thus provide further insight in the mechanisms of disease progression and recovery. With the training study, we investigated whether a translational touchscreen cognitive training intervention could alter the damages induced by the mTBI and be specific for certain brain targets. We have shown - for the first time - that a touchscreen training

system can be used to slow down secondary disease progress in mTBI rats as witnessed by the neuroplastic changes in diffusion measures. Correlation between the neuroplastic changes and behavioural improvements showed that the training intervention was effective as well.

Towards MRI biomarkers for TBI

Although our findings certainly seem promising, some methodological considerations must be covered. As already touched upon, TBI is characterised by a high heterogeneity in the way of sustaining the injury and the resulting injury severity. By making use of an animal model, we were able to standardise the injury to obtain a more uniform study population. This helps us to detect small alterations that would otherwise be missed in a patient population, but also means that the results we presented here can only be translated to a small subgroup of the TBI patients, namely the mild and diffuse injured patients without any lesion visible using conventional medical imaging. Today however, the classification of TBI patients is still quite rigid and only describes the mild, moderate and severe classes [11]. One of the priorities of action is to develop a better classification that takes into account additional variables that can influence outcomes because the GCS and CT imaging is just not good enough anymore. For example some patients have major cognitive problems without lesions visible on CT and on the contrary some patients will have several lesions detected by CT but no major cognitive difficulties, which makes us wonder what can be considered a mild injury? Options for better classification include a combination of imaging (SWI, diffusion MRI,...), blood biomarkers (e.g., GFAP or ubiquitin C-terminal hydrolase-L1 (UCH-L1)), genomics and other co-morbidities (e.g., cause of injury, intoxicants or mental health status) and could be able to discriminate other relevant TBI populations [227]. Preclinical models should mimic the different TBI subgroups as good as possible. For example, the model that was used in this work mimics the diffuse and subtle nature of a mild impact caused by an object hitting the head, and recently a model has been developed that induces acceleration/deceleration and rotational forces on the brain to mimic brain injury caused by a car accident [48]. Additionally, more attention is shifting to awake animal models since anaesthesia could

exert neuroprotective effects [229, 230].

Another important prerequisite in finding a good biomarker for TBI is that they should be helpful in stratifying the injury severity and/or identifying the prevailing mechanisms of injury. Most studies on detecting neuroimaging alterations after trauma have used the DTI model and although this model has great *sensitivity* and has gained us valuable insight, we have also learnt that this model is not very specific to explain underlying biological processes. By using more advanced diffusion models (DKI, WMTI and fixel-based analysis) in this dissertation, we were able to provide a more complete view on the underlying biological mechanisms involved in mTBI and increased *specificity*. In addition to TBI patients, these models could also be applied in many other brain disorders that have been acquired (such as stroke) or develop only later in life (e.g., dementia or Alzheimer's) and also here increase the knowledge of brain functioning in health and disease. Although this seems very promising, we should keep in mind that preclinical research and clinical practice are two different worlds. In this thesis we were able to perform diffusion scanning at high field strength (7 T) combined with a high performing gradient system which allowed us to keep the diffusion gradients relatively short. However, in clinic these high performing gradient systems are not standard available meaning that in order to get the same gradient strengths as in our preclinical imaging protocol the diffusion gradients will have to be applied longer, increasing the scan time. Furthermore, the resolution will have to be lowered (2-3 mm isotropic resolution) to obtain a high enough SNR per voxel. One can argue that using parallel imaging we could reduce the scan time (possibly to under one hour) and this certainly has merit to a certain point but keeping in mind that TBI patients can have behavioural difficulties it is not recommended to let the total imaging protocol (including other scans than DWIs, e.g. structural T2 weighted images or SWI) last for more than 30 minutes. Thus, the diffusion imaging protocol used in this study will have to be adapted to fit more to a clinical situation. This means that possibly not all diffusion shells would be included and we would have to limit the protocol to two diffusion shells (together with the b0 images this makes it still possible to perform DKI measurements or multi-tissue CSD) or even only one shell (limiting the choice of models to analyse

the data). Therefore, it is more realistic to propose that the advanced diffusion models can have an added value in further research finetuning the classification of TBI and investigating the efficacy of therapies (not only in TBI but also neurological diseases), but with limited use in the acute setting.

Another major difficulty in getting the diffusion models into clinical practice is the lack of reference values for the diffusion metrics, or in other words: what can be considered a normal value? As there are usually no pre-injury scans available we do not know what, for example, this patient's normal MD value is in the hippocampus. This is mainly due to intersubject and site variability (different scanner hardware or scanning protocols). Therefore, efforts have been made to optimize scanning protocols across 3T scanners from different MR imaging vendors in a large-scale neuroimaging research study and several studies have investigated intersubject and intersession variability [231–233]. This can be considered a step forward on improving the *precision* and *accuracy* of diffusion imaging. However, we have still a long way ahead enhancing reproducibility of the diffusion metrics in order to use them to detect mTBI on a single subject. For example, also development and aging, type of trauma and time since injury could have an effect on the diffusion metrics and therefore reference values per classification category should be available [149–151].

The future is BIG

It has become evident that the key to finding biomarkers for (m)TBI to better diagnose, follow up and predict prognosis of TBI, lies in a pragmatic research approach. By generating big data sets through broad international collaborations the International Initiative for Traumatic Brain Injury hopes to succeed where smaller studies have failed [227]. These studies will work together to gather a large volume of demographic, imaging, genetic and proteomic information from TBI patients into a federated TBI database system. This would make it possible to investigate newer image analysis techniques such as radiomics (i.e., high-throughput extraction of quantitative features from medical images). In a recent study, de la Rosa et al. [234] was able to detect lesions on CT

scans of TBI patients with an accuracy of 89.7 % and can be considered the first step forward in this new analysis field. However, big data comes with big statistical issues and because the number of characterising variables (demographics, multiple image sequences, genomics,...) increases enormously, all the possible combinations in statistical testing becomes an issue. To address this problem computer-aided diagnosis will be inevitable together with a good and intense collaboration between clinicians, scientists, bioinformatici and biostatisticians. This will ultimately lead to an improved classification scheme of the full TBI spectrum and a precision medicine approach with personalised management of TBI.

A | Appendices

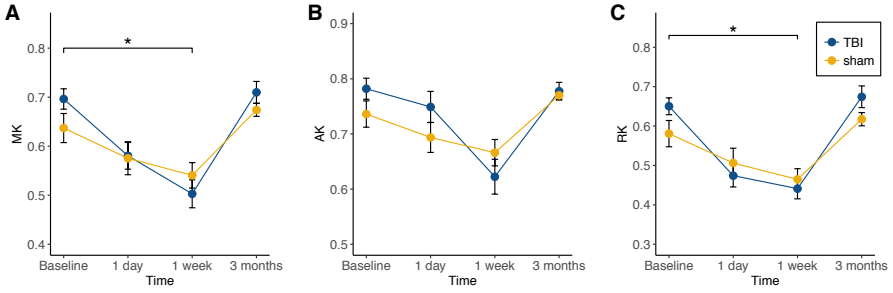

Figure A.1: Temporal changes in MK, AK and RK in the hippocampus. * p < 0.01

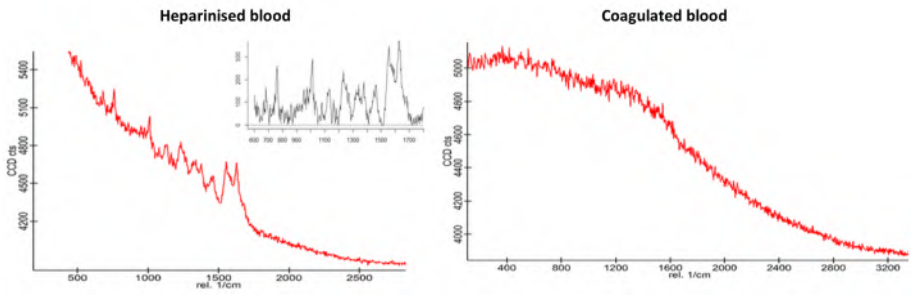

Figure A.2: Rat blood Raman spectrum. On the left is the spectrum obtained from the diluted heparinised blood sample with distinct haemoglobin peaks (see inset). On the right is the spectrum obtained from the coagulated blood sample.

Table A.1: F-values and p-values for group by time effect in the body, genu and splenium

GROUP BY TIME	Body		Genu		Splenium	
	F-value	p-value	F-value	p-value	F-value	p-value
MD	5.381	0.035	4.145	0.040	1.012	0.409
AD	1.936	0.169	0.566	0.648	0.662	0.585
RD	4.953	0.036	3.628	0.048	4.622	0.022
FA	1.957	0.208	0.911	0.465	2.528	0.107
MK	0.478	0.703	2.287	0.120	0.212	0.887
AK	0.335	0.801	0.342	0.795	1.099	0.388
RK	0.449	0.722	0.300	0.825	0.201	0.894
AWF	0.262	0.851	1.611	0.227	0.386	0.764
IAD	0.544	0.656	2.269	0.128	1.393	0.274
AxEAD	1.194	0.353	0.618	0.615	0.884	0.483
RadEAD	1.316	0.312	1.582	0.245	0.505	0.687
TORT	3.902	0.038	4.268	0.026	3.266	0.054
TIME	Body		Genu		Splenium	
	F-value	p-value	F-value	p-value	F-value	p-value
AD	**29.530**	**< 0.001**	**14.107**	**< 0.001**	1.076	0.380
RD	6.504	0.019	4.659	0.024	1.867	0.187
MD	**15.447**	**0.002**	**13.720**	**0.001**	0.630	0.604
FA	3.861	0.063	0.608	0.623	1.375	0.298
AK	5.161	0.019	3.091	0.060	2.551	0.106
RK	**8.601**	**0.002**	**6.084**	**0.006**	5.200	0.015
MK	**8.317**	**0.002**	**8.506**	**0.001**	**9.381**	**0.001**
AWF	**12.576**	**< 0.001**	**6.407**	**0.005**	**10.034**	**0.001**
IAD	**5.331**	**0.004**	0.482	0.700	2.249	0.114
AxEAD	**38.696**	**< 0.001**	**9.416**	**0.001**	3.533	0.059
RadEAD	**245.107**	**< 0.001**	**773.078**	**< 0.001**	**627.759**	**< 0.001**
TORT	1.410	0.289	3.138	0.061	3.143	0.060

Bold indicates the p-values that survived Bonferroni correction for multiple comparisons.

Table A.2: P-values for the post hoc comparisons for main effect of time for corpus callosum, hippocampus, cingulum, cortex and body, genu and splenium of the corpus callosum.

TIME	Post hoc test	Corpus callosum p-value	Hippocampus p-value	Cingulum p-value	Cortex p-value	Body p-value	Genu p-value	Splenium p-value
AD	1d - 3m	< 0.001	ns	< 0.001	ns	< 0.001	< 0.001	ns
	1w - 3m	< 0.001		< 0.001		< 0.001	ns	
MD	1d - 3m	0.002	ns	ns	ns	0.004	ns	ns
	1w - 3m	0.002	0.001			0.005		
RD	1w - 3m	ns	0.003	ns	ns	ns	ns	ns
AK	1d - 3m	ns	ns	< 0.001	ns	ns	ns	ns
	1w - 3m			< 0.001	0.003			
RK	1d - 3m	ns	ns	< 0.001	ns	ns	ns	ns
	1w - 3m	0.007		0.001		0.004	0.004	
MK	1d - 3m	ns	ns	0.001	ns	ns	ns	ns
	1w - 3m	0.007		0.002		0.003	0.010	
AxEAD	1d - 3m	< 0.001	na	< 0.001	na	< 0.001	0.009	ns
	1w - 3m	< 0.001		< 0.001		< 0.001	ns	
RadEAD	1w - 3m	0.003		< 0.001		0.006	ns	ns
AWF	1d - 3m	0.004		< 0.001		0.004	ns	ns
	1w - 3m	0.002		0.001		0.001		0.006

ns = not significant.

na = not applicable.

Note: FA and IAD did not show any significant post hoc results.

Bibliography

[1] Bear MF, Connors BW, and Paradiso MA. The structure of the nervous system. In *Neuroscience: Exploring the Brain*, volume 101, pages 167–204. Lippincott Williams And Wilkins, 3rd edition, 2007.

[2] Marieb EN, Wilhelm PB, and Mallatt J. *Human Anatomy Media Update*. Pearson Education, 5th edition, 2012.

[3] Patestas MA and Gartner LP. *A Textbook of Neuroanatomy*. Blackwell Publishing Ltd, 1st edition, 2006. ISBN 1-4051-0340-X.

[4] Catani M, Dell'Acqua F, and de Schotten TM. A revised limbic system model for memory, emotion and behaviour. *Neuroscience and Biobehavioral Reviews*, 37(8):1724–1737, 2013. doi:10.1016/j.neubiorev.2013.07.001.

[5] DAntonio F, Pagani G, Familiari A, Khalil A, Sagies TL, Malinger G, Leibovitz Z, Garel C, Moutard ML, Pilu G, Bhide A, Acharya G, Leombroni M, Manzoli L, Papageorghiou A, and Prefumo F. Outcomes Associated With Isolated Agenesis of the Corpus Callosum: A Meta-analysis. *PEDIATRICS*, 138(3):e20160445–e20160445, 2016. doi:10.1542/peds.2016-0445.

[6] Menon DK, Schwab K, Wright DW, and Maas AI. Position Statement: Definition of Traumatic Brain Injury. *Archives of Physical Medicine and Rehabilitation*, 91(11):1637–1640, 2010. doi:10.1016/j.apmr.2010.05.017.

[7] Majdan M, Plancikova D, Brazinovaa A, Rusnak M, Nieboer D, Feigin V, and Maas A. Epidemiology of traumatic brain injuries in Europe: a cross-sectional analysis. *The Lancet Public Health*, 1 (2):e76–e83, 2016. doi:10.1016/S2468-2667(16)30017-2.

[8] Tagliaferri F, Compagnone C, Korsic M, Servadei F, and Kraus J. A systematic review of brain injury epidemiology in Europe. *Acta Neurochirurgica*, 148(3):255–268, 2006. doi:10.1007/s00701-005-0651-y.

[9] Buck PW. Mild Traumatic Brain Injury: A Silent Epidemic in Our Practices. *Health & Social Work*, 36(4):299–302, 2011. doi:10.1093/hsw/36.4.299.

[10] Brazinova A, Rehorcikova V, Taylor MS, Buckova V, Majdan M, Psota M, Peeters W, Feigin V, Theadom A, Holkovic L, and Synnot A. Epidemiology of Traumatic Brain Injury in Europe: A Living Systematic Review. *Journal of Neurotrauma*, page neu.2015.4126, 2016. doi:10.1089/neu.2015.4126.

[11] Teasdale G, Maas A, Lecky F, Manley G, Stocchetti N, and Murray G. The Glasgow Coma Scale at 40 years: Standing the test of time. *The Lancet Neurology*, 13(8):844–854, 2014. doi:10.1016/S1474-4422(14)70120-6.

[12] Hall RCW and Chapman MJ. Definition, Diagnosis, and Forensic Implications of Postconcussional Syndrome. *Psychosomatics*, 46 (3):195–202, 2005. doi:10.1176/appi.psy.46.3.195.

[13] ArciniegasB DB, Held K, and Wagner P. Cognitive impairment following traumatic brain injury. *Current Treatment Options in Neurology*, 4(1):43–57, 2002. doi:10.1007/s11940-002-0004-6.

[14] The American Congress of Rehabilitation Medicine (ACRM). Definition of mild traumatic brain injury. *Journal of Head Trauma Rehabilitation*, 8(3):86–87, 1993. doi:10.1097/00001199-199309000-00010.

[15] Bruns J and Hauser WA. The Epidemiology of Traumatic Brain Injury: A Review. *Epilepsia*, 44(2):2–10, 2003. doi:10.1046/j.1528-1157.44.s10.3.x.

[16] Bodanapally UK, Sours C, Zhuo J, and Shanmuganathan K. Imaging of Traumatic Brain Injury. *Radiologic Clinics of North America*, 53(4):695–715, 2015. doi:10.1016/j.rcl.2015.02.011.

[17] Maas A, Stocchetti N, and Bullock R. Moderate and severe traumatic brain injury in adults. *The Lancet Neurology*, 7(8):728–741, 2008. doi:10.1016/S1474-4422(08)70164-9.

[18] Werner C and Engelhard K. Pathophysiology of traumatic brain injury. *British Journal of Anaesthesia*, 99(1):4–9, 2007. doi:10.1093/bja/aem131.

[19] Barkhoudarian G, Hovda DA, and Giza CC. The Molecular Pathophysiology of Concussive Brain Injury. *Clinics in Sports Medicine*, 30(1):33–48, 2011. doi:10.1016/j.csm.2010.09.001.

[20] Andriessen TMJC, Jacobs B, and Vos PE. Clinical characteristics and pathophysiological mechanisms of focal and diffuse traumatic brain injury. *Journal of Cellular and Molecular Medicine*, 14(10): 2381–2392, 2010. doi:10.1111/j.1582-4934.2010.01164.x.

[21] McInnes K, Friesen CL, MacKenzie DE, Westwood DA, and Boe SG. Mild Traumatic Brain Injury (mTBI) and chronic cognitive impairment: A scoping review. *PLOS ONE*, 12(4):e0174847, 2017. doi:10.1371/journal.pone.0174847.

[22] Neumann D and Lequerica A. Cognitive Problems After Traumatic Brain Injury. *Archives of Physical Medicine and Rehabilitation*, 96(1):179–180, 2015. doi:10.1016/j.apmr.2013.06.003.

[23] Keeler JF and Robbins TW. Translating cognition from animals to humans. *Biochemical Pharmacology*, 81(12):1356–1366, 2011. doi:10.1016/j.bcp.2010.12.028.

[24] Silverberg ND, Panenka WJ, and Iverson GL. Work Productivity Loss After Mild Traumatic Brain Injury. *Archives of Physical Medicine and Rehabilitation*, 99(2):250–256, 2018. doi:10.1016/j.apmr.2017.07.006.

[25] Osier ND and Dixon CE. The Controlled Cortical Impact Model: Applications, Considerations for Researchers,

and Future Directions. *Frontiers in Neurology*, 7, 2016. doi:10.3389/fneur.2016.00134.

[26] Onyszchuk G, Al-Hafez B, He Y, Bilgen M, Berman NEJ, and Brooks WM. A mouse model of sensorimotor controlled cortical impact: Characterization using longitudinal magnetic resonance imaging, behavioral assessments and histology. *Journal of Neuroscience Methods*, 160(2):187–196, 2007. doi:10.1016/j.jneumeth.2006.09.007.

[27] Pischiutta F, Micotti E, Hay JR, Marongiu I, Sammali E, Tolomeo D, Vegliante G, Stocchetti N, Forloni G, De Simoni MG, Stewart W, and Zanier ER. Single severe traumatic brain injury produces progressive pathology with ongoing contralateral white matter damage one year after injury. *Experimental Neurology*, 300(October 2017):167–178, 2018. doi:10.1016/j.expneurol.2017.11.003.

[28] Xu S, Zhuo J, Racz J, Shi D, Roys S, Fiskum G, and Gullapalli R. Early Microstructural and Metabolic Changes following Controlled Cortical Impact Injury in Rat: A Magnetic Resonance Imaging and Spectroscopy Study. *Journal of Neurotrauma*, 28(10):2091–2102, 2011. doi:10.1089/neu.2010.1739.

[29] Ajao DO, Pop V, Kamper JE, Adami A, Rudobeck E, Huang L, Vlkolinsky R, Hartman RE, Ashwal S, Obenaus A, and Badaut J. Traumatic Brain Injury in Young Rats Leads to Progressive Behavioral Deficits Coincident with Altered Tissue Properties in Adulthood. *Journal of Neurotrauma*, 29(11):2060–2074, 2012. doi:10.1089/neu.2011.1883.

[30] Turtzo LC, Budde MD, Gold EM, Lewis BK, Janes L, Yarnell A, Grunberg NE, Watson W, and Frank JA. The evolution of traumatic brain injury in a rat focal contusion model. *NMR in Biomedicine*, 26(4):468–479, 2013. doi:10.1002/nbm.2886.

[31] Long JA, Watts LT, Chemello J, Huang S, Shen Q, and Duong TQ. Multiparametric and Longitudinal MRI Characterization of Mild Traumatic Brain Injury in Rats. *Journal of Neurotrauma*, 32 (8):598–607, 2015. doi:10.1089/neu.2014.3563.

[32] Li W, Long JA, Watts L, Shen Q, Liu Y, Jiang Z, and Duong TQ. Spatiotemporal changes in diffusion, T 2 and susceptibility of white matter following mild traumatic brain injury. *NMR in Biomedicine*, 29(7):896–903, 2016. doi:10.1002/nbm.3536.

[33] Maze Engineers. Animal models of traumatic brain injury. `https://mazeengineers.com/animal-models-of-traumatic-brain-injury/`, 2017. Accessed: 2019-06-05.

[34] Lyeth BG. Historical Review of the Fluid-Percussion TBI Model. *Frontiers in Neurology*, 7(DEC):1–7, 2016. doi:10.3389/fneur.2016.00217.

[35] Liu YR, Cardamone L, Hogan RE, Gregoire MC, Williams JP, Hicks RJ, Binns D, Koe A, Jones NC, Myers DE, O'Brien TJ, and Bouilleret V. Progressive Metabolic and Structural Cerebral Perturbations After Traumatic Brain Injury: An In Vivo Imaging Study in the Rat. *Journal of Nuclear Medicine*, 51(11):1788–1795, 2010. doi:10.2967/jnumed.110.078626.

[36] Hylin MJ, Orsi SA, Zhao J, Bockhorst K, Perez A, Moore AN, and Dash PK. Behavioral and Histopathological Alterations Resulting from Mild Fluid Percussion Injury. *Journal of Neurotrauma*, 30 (9):702–715, 2013. doi:10.1089/neu.2012.2630.

[37] Cole JT, Yarnell A, Kean WS, Gold E, Lewis B, Ren M, McMullen DC, Jacobowitz DM, Pollard HB, O'Neill JT, Grunberg NE, Dalgard CL, Frank JA, and Watson WD. Craniotomy: True Sham for Traumatic Brain Injury, or a Sham of a Sham? *Journal of Neurotrauma*, 28(3):359–369, 2011. doi:10.1089/neu.2010.1427.

[38] Yu F, Shukla DK, Armstrong RC, Marion CM, Radomski KL, Selwyn RG, and Dardzinski BJ. Repetitive Model of Mild Traumatic Brain Injury Produces Cortical Abnormalities Detectable by Magnetic Resonance Diffusion Imaging, Histopathology, and Behavior. *Journal of Neurotrauma*, 34(7):1364–1381, 2017. doi:10.1089/neu.2016.4569.

[39] Sullivan GM, Mierzwa AJ, Kijpaisalratana N, Tang H, Wang Y, Song S, Selwyn R, and Armstrong RC. Oligodendrocyte Lineage and Subventricular Zone Response to Traumatic

Axonal Injury in the Corpus Callosum. *Journal of Neuropathology & Experimental Neurology*, 72(12):1106–1125, 2013. doi:10.1097/NEN.0000000000000009.

[40] Hernandez A, Donovan V, Grinberg YY, Obenaus A, and Carson MJ. Differential detection of impact site versus rotational site injury by magnetic resonance imaging and microglial morphology in an unrestrained mild closed head injury model. *Journal of Neurochemistry*, 136:18–28, 2016. doi:10.1111/jnc.13402.

[41] Maruichi K, Kuroda S, Chiba Y, Hokari M, Shichinohe H, Hida K, and Iwasaki Y. Graded model of diffuse axonal injury for studying head injury-induced cognitive dysfunction in rats. *Neuropathology*, 29(2):132–139, 2009. doi:10.1111/j.1440-1789.2008.00956.x.

[42] Shultz SR, McDonald SJ, Vonder Haar C, Meconi A, Vink R, van Donkelaar P, Taneja C, Iverson GL, and Christie BR. The potential for animal models to provide insight into mild traumatic brain injury: Translational challenges and strategies. *Neuroscience & Biobehavioral Reviews*, 76:396–414, 2017. doi:10.1016/j.neubiorev.2016.09.014.

[43] Shultz SR, Sun M, Wright DK, Brady RD, Liu S, Beynon S, Schmidt SF, Kaye AH, Hamilton JA, O'Brien TJ, Grills BL, and McDonald SJ. Tibial Fracture Exacerbates Traumatic Brain Injury Outcomes and Neuroinflammation in a Novel Mouse Model of Multitrauma. *Journal of Cerebral Blood Flow & Metabolism*, 35 (8):1339–1347, 2015. doi:10.1038/jcbfm.2015.56.

[44] Albert-Weißenberger C, Várrallyay C, Raslan F, Kleinschnitz C, and Sirén A. An experimental protocol for mimicking pathomechanisms of traumatic brain injury in mice. *Experimental & Translational Stroke Medicine*, 4(1):1, 2012. doi:10.1186/2040-7378-4-1.

[45] Marmarou A, Foda MAA, van den Brink W, Campbell J, Kita H, and Demetriadou K. A new model of diffuse brain injury in rats. *Journal of Neurosurgery*, 80(2):291–300, 1994. doi:10.3171/jns.1994.80.2.0291.

[46] Kallakuri S, Zakaria N, Shen Y, Kou Z, Zhang L, Bandaru S, Haacke EM, and Cavanaugh JM. Traumatic Brain Injury by a Closed Head Injury Device Induces Cerebral Blood Flow Changes and Microhemorrhages. *Journal of Clinical Imaging Science*, 5(1): 1–52, 2015. doi:10.4103/2156-7514.166354.

[47] Singh K, Trivedi R, Devi MM, Tripathi RP, and Khushu S. Longitudinal changes in the DTI measures, anti-GFAP expression and levels of serum inflammatory cytokines following mild traumatic brain injury. *Experimental Neurology*, 275:427–435, 2016. doi:10.1016/j.expneurol.2015.07.016.

[48] Mychasiuk R, Farran A, and Esser MJ. Assessment of an Experimental Rodent Model of Pediatric Mild Traumatic Brain Injury. *Journal of Neurotrauma*, 31(8):749–757, 2014. doi:10.1089/neu.2013.3132.

[49] Cernak I and Noble-Haeusslein LJ. Traumatic Brain Injury: An Overview of Pathobiology with Emphasis on Military Populations. *Journal of Cerebral Blood Flow & Metabolism*, 30(2):255–266, 2010. doi:10.1038/jcbfm.2009.203.

[50] Zhuo J, Keledjian K, Xu S, Pampori A, Gerzanich V, Simard JM, and Gullapalli RP. Changes in Diffusion Kurtosis Imaging and Magnetic Resonance Spectroscopy in a Direct Cranial Blast Traumatic Brain Injury (dc-bTBI) Model. *PLOS ONE*, 10(8): e0136151, 2015. doi:10.1371/journal.pone.0136151.

[51] Calabrese E, Du F, Garman RH, Johnson GA, Riccio C, Tong LC, and Long JB. Diffusion Tensor Imaging Reveals White Matter Injury in a Rat Model of Repetitive Blast-Induced Traumatic Brain Injury. *Journal of Neurotrauma*, 31(10):938–950, 2014. doi:10.1089/neu.2013.3144.

[52] Tucker LB, Velosky AG, and McCabe JT. Applications of the Morris water maze in translational traumatic brain injury research. *Neuroscience & Biobehavioral Reviews*, 88:187–200, 2018. doi:10.1016/j.neubiorev.2018.03.010.

[53] Cicerone K, Levin H, Malec J, Stuss D, and Whyte J. Cognitive Rehabilitation Interventions for Executive Function: Moving from Bench to Bedside in Patients with Traumatic Brain Injury. *Journal of Cognitive Neuroscience*, 18(7):1212–1222, 2006. doi:10.1162/jocn.2006.18.7.1212.

[54] Hallock H, Collins D, Lampit A, Deol K, Fleming J, and Valenzuela M. Cognitive Training for Post-Acute Traumatic Brain Injury: A Systematic Review and Meta-Analysis. *Frontiers in Human Neuroscience*, 10, 2016. doi:10.3389/fnhum.2016.00537.

[55] De Luca R, Calabrò RS, Gervasi G, De Salvo S, Bonanno L, Corallo F, De Cola MC, and Bramanti P. Is computer-assisted training effective in improving rehabilitative outcomes after brain injury? A case-control hospital-based study. *Disability and Health Journal*, 7(3):356–360, 2014. doi:10.1016/j.dhjo.2014.04.003.

[56] Sood N, Godfrey C, Anderson V, and Catroppa C. Rehabilitation of Executive function in Paediatric Traumatic brain injury (REPeaT): protocol for a randomized controlled trial for treating working memory and decision-making. *BMC Pediatrics*, 18(1): 362, 2018. doi:10.1186/s12887-018-1338-x.

[57] Treble-Barna A, Sohlberg MM, and Wade BE, Harn andSL. Cognitive Intervention for Attention and Executive Function Impairments in Children With Traumatic Brain Injury. *Journal of Head Trauma Rehabilitation*, 31(6):407–418, 2016. doi:10.1097/HTR.0000000000000200.

[58] Verhelst H, Vander Linden C, Vingerhoets G, and Caeyenberghs K. How to Train an Injured Brain? A Pilot Feasibility Study of Home-Based Computerized Cognitive Training. *Games for Health Journal*, 6(1):28–38, 2017. doi:10.1089/g4h.2016.0043.

[59] Bogdanova Y, Yee MK, Ho VT, and Cicerone KD. Computerized Cognitive Rehabilitation of Attention and Executive Function in Acquired Brain Injury. *Journal of Head Trauma Rehabilitation*, 31(6):419–433, 2016. doi:10.1097/HTR.0000000000000203.

[60] Fetta J, Starkweather A, and Gill JM. Computer-Based Cognitive Rehabilitation Interventions for Traumatic Brain Injury. *Journal of Neuroscience Nursing*, 49(4):235–240, 2017. doi:10.1097/JNN.0000000000000298.

[61] Bondi CO, Klitsch KC, Leary JB, and Kline AE. Environmental Enrichment as a Viable Neurorehabilitation Strategy for Experimental Traumatic Brain Injury. *Journal of Neurotrauma*, 31(10): 873–888, 2014. doi:10.1089/neu.2014.3328.

[62] Bondi CO, Semple BD, Noble-Haeusslein LJ, Osier ND, Carlson SW, Dixon CE, Giza CC, and Kline AE. Found in translation: Understanding the biology and behavior of experimental traumatic brain injury. *Neuroscience & Biobehavioral Reviews*, 58:123–146, 2015. doi:10.1016/j.neubiorev.2014.12.004.

[63] Matter AM, Folweiler KA, Curatolo LM, and Kline AE. Temporal effects of environmental enrichment-mediated functional improvement after experimental traumatic brain injury in rats. *Neurorehabilitation and Neural Repair*, 25(6):558–564, 2011. doi:10.1177/1545968310397206.

[64] de Witt BW, Ehrenberg KM, McAloon RL, Panos AH, Shaw KE, Raghavan PV, Skidmore ER, and Kline AE. Abbreviated Environmental Enrichment Enhances Neurobehavioral Recovery Comparably to Continuous Exposure After Traumatic Brain Injury. *Neurorehabilitation and Neural Repair*, 25(4):343–350, 2011. doi:10.1177/1545968310390520.

[65] Cheng JP, Shaw KE, Monaco CM, Hoffman AN, Sozda CN, Olsen AS, and Kline AE. A Relatively Brief Exposure to Environmental Enrichment after Experimental Traumatic Brain Injury Confers Long-Term Cognitive Benefits. *Journal of Neurotrauma*, 29(17): 2684–2688, 2012. doi:10.1089/neu.2012.2560.

[66] Heated circular pool/water maze (panlab). `https://www.harvardapparatus.com/heated-circular-pool-water-maze-panlab.html`, 2019. Accessed: 2019-03-01.

[67] Brayer SW, Ketcham S, Zou H, Hurwitz M, Henderson C, Fuletra J, Kumar K, Skidmore E, Thiels E, and Wagner AK. Developing a clinically relevant model of cognitive training after experimental traumatic brain injury. *Neurorehabilitation and Neural Repair*, 29 (5):483–495, 2015. doi:10.1177/1545968314550367.

[68] Edwards CM, Kumar K, Koesarie K, Brough E, Ritter AC, Brayer SW, Thiels E, Skidmore ER, and Wagner AK. Visual Priming Enhances the Effects of Nonspatial Cognitive Rehabilitation Training on Spatial Learning After Experimental Traumatic Brain Injury. *Neurorehabilitation and neural repair*, 29(9):897–906, 2015. doi:10.1177/1545968315570326.

[69] Bussey TJ, Muir JL, and Robbins TW. A novel automated touchscreen procedure for assessing learning in the rat using computer graphic stimuli. *Neuroscience Research Communications*, 15(2): 103–110, 1994. doi:10.1007/s11940-002-0004-6.

[70] Barnett JH, Blackwell AD, Sahakian BJ, and Robbins TW. The Paired Associates Learning (PAL) Test: 30 Years of CANTAB Translational Neuroscience from Laboratory to Bedside in Dementia Research. *Current Topics on Behavioural Neuroscience*, 28: 449–474, 2016. doi:10.1007/7854_2015_5001.

[71] Nichols JN, Hagan KL, and Floyd CL. Evaluation of Touchscreen Chambers To Assess Cognition in Adult Mice: Effect of Training and Mild Traumatic Brain Injury. *Journal of Neurotrauma*, 34 (17):2481–2494, 2017. doi:10.1089/neu.2017.4998.

[72] Talpos JC, Winters BD, R Dias, Saksida LM, and Bussey TJ. A novel touchscreen-automated paired-associate learning (PAL) task sensitive to pharmacological manipulation of the hippocampus: a translational rodent model of cognitive impairments in neurodegenerative disease. *Psychopharmacology*, 205(1):157–168, 2009. doi:10.1007/s00213-009-1526-3.

[73] De Rover M, Pironti VA, McCabe JA, Acosta-Cabronero J, Arana FS, Morein-Zamir S, Hodges JR, Robbins TW, Fletcher

PC, Nestor PJ, and Sahakian BJ. Hippocampal dysfunction in patients with mild cognitive impairment: a functional neuroimaging study of a visuospatial Paired Associates Learning task. *Neuropsychologia*, 49:2060–2070, 2011. doi:10.1016/j.neuropsychologia.2011.03.037.

[74] Owen AM, Milner B, Petrides M, and Evans AC. A specific role for the right parahippocampal gyrus in the retrieval of object-location: a positron emission tomography study. *Journal of Cognitive Neuroschience*, 8:588–602, 1996. doi:10.1162/jocn.1996.8.6.588.

[75] Talpos JC, Aerts N, Fellini L, and Steckler T. A touch-screen based paired-associates learning (PAL) task for the rat may provide a translatable pharmacological model of human cognitive impairment. *Pharmacology Biochemistry and Behaviour*, 122:97–106, 2014. doi:10.1016/j.pbb.2014.03.014.

[76] Riccio CA, Reynolds CR, Lowe P, and Moore J. The continuous performance test: a window on the neural substrates for attention? *Archives of Clinical Neuropsychology*, 17(3):235–272, 2002. doi:10.1016/S0887-6177(01)00111-1.

[77] Hvoslef-Eide M, Nilsson SRO, Saksida LM, and Bussey TJ. Cognitive Translation Using the Rodent Touchscreen Testing Approach. *Current Topics Behavioural Neuroscience*, 28:423–447, 2016. doi:10.1007/7854_2015_5007.

[78] Young JW, Light G, Marston HM, Sharp R, and Geyer M. The 5-Choice Continuous Performance Test: Evidence for a Translational Test of Vigilance for Mice. *PLoS ONE*, 4(1):e4227, 2009. doi:10.1371/journal.pone.0004227.

[79] Bigler ED and Maxwell WL. Neuropathology of mild traumatic brain injury: relationship to neuroimaging findings. *Brain Imaging and Behavior*, 6(2):108–136, 2012. doi:10.1007/s11682-011-9145-0.

[80] Chastain CA, Oyoyo UE, Zipperman M, Joo E, Ashwal S, Shutter LA, and Tong KA. Predicting Outcomes of Traumatic Brain Injury by Imaging Modality and Injury Distribution. *Journal of Neurotrauma*, 26(8):1183–1196, 2009. doi:10.1089/neu.2008.0650.

[81] Kou Z, Wu Z, Tong KA, Holshouser B, Benson RR, Hu J, and Haacke ME. The Role of Advanced MR Imaging Findings as Biomarkers of Traumatic Brain Injury. *Journal of Head Trauma Rehabilitation*, 25(4):267–282, 2010. doi:10.1097/HTR.0b013e3181e54793.

[82] Kuperman V. *Magnetic Resonance Imaging. Physical Principles and Applicayions*. Academic Press, 2000. ISBN 0124291503.

[83] Gould TA and Edmonds M. How mri works. `https://science.howstuffworks.com/mri1.htm`, 2019. Accessed: 2018-02-14.

[84] Hendrix A. *Magnets, Spins, and Resonances. An introduction to the basics of Magnetic Resonance*. Siemens AG Medical Solutions, Erlangen, 2003. ISBN 315279273. doi:A91100-M2200-M705-1-7600.

[85] Schild HH. *MRI made easy*. Schering AG, 1990. ISBN 3921817412.

[86] Elster AD. What is phase encoding. `https://mri-q.com/what-is-phase-encoding.html`, 2019. Accessed: 2019-08-21.

[87] Zaidi H. *Molecular Imaging of Small Animals*. Springer New York, New York, NY, 2014. ISBN 978-1-4939-0893-6. doi:10.1007/978-1-4939-0894-3.

[88] Van Hecke w, Emsell L, Sunaert S, Stieltjes B, Brunner RM, Fritzsche KH, and Laun FB. *Diffusion Tensor Imaging*. Springer, Berlin, Heidelberg, 2013. ISBN 978-3-642-20455-5. doi:10.1007/978-3-642-20456-2. URL `http://link.springer.com/10.1007/978-3-642-20456-2`.

[89] Tournier JD, Mori S, and Leemans A. Diffusion tensor imaging and beyond. *Magnetic Resonance in Medicine*, 65(6):1532–1556, 2011. doi:10.1002/mrm.22924.

[90] Jones DK, Knösche TR, and Turner R. White matter integrity, fiber count, and other fallacies: The do's and don'ts of diffusion MRI. *NeuroImage*, 73:239–254, 2013. doi:10.1016/j.neuroimage.2012.06.081.

[91] Jensen JH and Helpern JA. MRI quantification of non-Gaussian water diffusion by kurtosis analysis. *NMR in Biomedicine*, 23(7): 698–710, 2010. doi:10.1002/nbm.1518.

[92] Fieremans E, Jensen JH, and Helpern JA. White matter characterization with diffusional kurtosis imaging. *NeuroImage*, 58(1): 177–188, 2011. doi:10.1016/j.neuroimage.2011.06.006.

[93] Steven AJ, Zhuo J, and Melhem ER. Diffusion Kurtosis Imaging: An Emerging Technique for Evaluating the Microstructural Environment of the Brain. *American Journal of Roentgenology*, 202(1): W26–W33, 2014. doi:10.2214/AJR.13.11365.

[94] Novikov DS, Kiselev VG, and Jespersen SN. On modeling. *Magnetic Resonance in Medicine*, 79(6):3172–3193, 2018. doi:10.1002/mrm.27101.

[95] Jelescu IO and Budde MD. Design and Validation of Diffusion MRI Models of White Matter. *Frontiers in Physics*, 5:61, 2017. doi:10.3389/fphy.2017.00061.

[96] Raffelt DA, Smith RE, Ridgway GR, Tournier JD, Vaughan DN, Rose S, Henderson R, and Connelly A. Connectivity-based fixel enhancement: Whole-brain statistical analysis of diffusion MRI measures in the presence of crossing fibres. *NeuroImage*, 117:40–55, 2015. doi:10.1016/j.neuroimage.2015.05.039.

[97] Raffelt DA, Tournier JD, Smith RD, Vaughan DN, Jackson G, Ridgway GR, and Connelly A. Investigating white matter fibre density and morphology using fixel-based analysis. *NeuroImage*, 144:58–73, 2017. doi:10.1016/j.neuroimage.2016.09.029.

[98] Tournier JD, Calamante F, and Connelly A. Robust determination of the fibre orientation distribution in diffusion MRI: Non-negativity constrained super-resolved spherical deconvolution. *NeuroImage*, 35(4):1459–1472, 2007. doi:10.1016/j.neuroimage.2007.02.016.

[99] Asken BM, DeKosky ST, Clugston JR, Jaffee MS, and Bauer RM. Diffusion tensor imaging (DTI) findings in adult civilian,

military, and sport-related mild traumatic brain injury (mTBI): a systematic critical review. *Brain Imaging and Behavior*, 12(2): 585–612, 2018. doi:10.1007/s11682-017-9708-9.

[100] Hulkower MB, Poliak. DB, Rosenbaum SB, Zimmerman ME, and Lipton ML. A Decade of DTI in Traumatic Brain Injury: 10 Years and 100 Articles Later. *American Journal of Neuroradiology*, 34 (11):2064–2074, 2013. doi:10.3174/ajnr.A3395.

[101] Wallace EJ, Mathias JL, and Ward L. Diffusion tensor imaging changes following mild, moderate and severe adult traumatic brain injury: a meta-analysis. *Brain Imaging and Behavior*, pages 1–15, 2018. doi:10.1007/s11682-018-9823-2.

[102] Niogi SSN, Mukherjee P, Ghajar J, Johnson C, Kolster RA, Sarkar R, Lee H, Meeker M, Zimmerman RD, Manley GT, and McCandliss BD. Extent of Microstructural White Matter Injury in Postconcussive Syndrome Correlates with Impaired Cognitive Reaction Time: A 3T Diffusion Tensor Imaging Study of Mild Traumatic Brain Injury. *American Journal of Neuroradiology*, 29 (5):967–973, 2008. doi:10.3174/ajnr.A0970.

[103] Rutgers DR, Toulgoat F, Cazejust J, Fillard P, Lasjaunias P, and Ducreux D. White Matter Abnormalities in Mild Traumatic Brain Injury: A Diffusion Tensor Imaging Study. *American Journal of Neuroradiology*, 29(3):514–519, 2008. doi:10.3174/ajnr.A0856.

[104] Li S, Sun Y, Shan D, Feng B, Xing J, Duan Y, Dai J, Lei H, and Zhou Y. Temporal profiles of axonal injury following impact acceleration traumatic brain injury in rats—a comparative study with diffusion tensor imaging and morphological analysis. *International Journal of Legal Medicine*, 127(1):159–167, 2013. doi:10.1007/s00414-012-0712-8.

[105] Zhuo J, Xu S, Proctor JL, Mullins RJ, Simon JZ, Fiskum G, and Gullapalli RP. Diffusion kurtosis as an in vivo imaging marker for reactive astrogliosis in traumatic brain injury. *NeuroImage*, 59(1): 467–477, 2012. doi:10.1016/j.neuroimage.2011.07.050.

[106] Tu TW, Williams RA, Lescher JD, Jikaria N, Turtzo LC, and Frank JA. Radiological-pathological correlation of diffusion tensor and magnetization transfer imaging in a closed head traumatic brain injury model. *Annals of Neurology*, 79(6):907–920, 2016. doi:10.1002/ana.24641.

[107] Alexander DC, Dyrby TB, Nilsson M, and Zhang H. Imaging brain microstructure with diffusion MRI: practicality and applications. *NMR In Biomedicine*, 32:e3841, 2019. doi:10.1002/nbm.3841.

[108] Murphy DB. *Fundamentals of Light Microscopy and Electronic Imaging*. John Wiley & Sons, Inc, 2001.

[109] Hollricher O. Raman Instrumentation for Confocal Raman Microscopy. In *Confocal Raman Microscopy*, pages 43–60. Springer, 2011.

[110] James ML and Gambhir SS. A molecular imaging primer: modalities, imaging agents, and applications. *Physiological Reviews*, 92: 897–965, 2012. doi:10.1152/physrev.00049.2010.

[111] Smith E and Dent G. *Modern Raman spectroscopy : a practical approach*. John Wiley & Sons Ltd, 2005. ISBN 0-471-49668-5 (Cloth).

[112] Movasaghi Z, Rehman S, and Rehman IU. Raman Spectroscopy of Biological Tissues. *Applied Spectroscopy Reviews*, 42(5):493–541, 2007. doi:10.1080/05704920701551530.

[113] Desroches J, Laurence A, Jermyn M, Pinto M, Tremblay MA, Petrecca K, and Leblond F. Raman spectroscopy in microsurgery: impact of operating microscope illumination sources on data quality and tissue classification. *The Analyst*, 142(8):1185–1191, 2017. doi:10.1039/C6AN02061E.

[114] van Kempen I. Diffusie gewogen magnetische resonantie beeldvorminggebasseerde biomarker voor traumatisch hersenletsel. *Ghent University*, 2018.

[115] Dewan MC, Mummareddy N, Wellons JC, and Bonfield CM. Epidemiology of Global Pediatric Traumatic Brain Injury: Qualitative Review. *World Neurosurgery*, 91:497–509.e1, 2016. doi:10.1016/j.wneu.2016.03.045.

[116] Thurman DJ. The Epidemiology of Traumatic Brain Injury in Children and Youths: A Review of Research Since 1990. *J Child Neurol*, 31(1):20–27, 2016. doi:10.1177/0883073814544363.

[117] Li XY and Feng DF. Diffuse axonal injury: Novel insights into detection and treatment. *Journal of Clinical Neuroscience*, 16(5): 614–619, 2009. doi:10.1016/j.jocn.2008.08.005.

[118] Basser PJ, Mattiello J, and LeBihan D. MR diffusion tensor spectroscopy and imaging. *Biophysical Journal*, 66(1):259–267, 1994. doi:10.1016/S0006-3495(94)80775-1.

[119] Pierpaoli C and Basser PJ. Toward a quantitative assessment of diffusion anisotropy. *Magnetic Resonance in Medicine*, 36(6):893–906, 1996. doi:10.1002/mrm.1910360612.

[120] Bazarian JJ, Zhu T, Blyth B, Borrino A, and Zhong J. Subject-specific changes in brain white matter on diffusion tensor imaging after sports-related concussion. *Magnetic Resonance Imaging*, 30 (2):171–180, 2012. doi:10.1016/j.mri.2011.10.001.

[121] Mayer AR, Ling J, Mannell MV, Gasparovic C, Phillips JP, Doezema D, Reichard R, and Yeo RA. A prospective diffusion tensor imaging study in mild traumatic brain injury. *Neurology*, 74(8):643–650, 2010. doi:10.1212/WNL.0b013e3181d0ccdd.

[122] Grossman EJ, Ge Y, Jensen JH, Babb JS, Miles L, Reaume J, Silver JM, Grossman RI, and Inglese M. Thalamus and Cognitive Impairment in Mild Traumatic Brain Injury: A Diffusional Kurtosis Imaging Study. *Journal of Neurotrauma*, 29(13):2318–2327, 2012. doi:10.1089/neu.2011.1763.

[123] Grossman EJ, Jensen JH, Babb JS, Chen Q, Tabesh A, Fieremans E, Xia D, Inglese M, and Grossman RI. Cognitive impairment in mild traumatic brain injury: a longitudinal diffusional kurtosis

and perfusion imaging study. *AJNR Am J Neuroradiol*, 34:951–957, 2013. doi:10.3174/ajnr.A3358.

[124] Zhang S, Zhang J, Fang J, Liang M, Li J, Wang X, and Zhou Q. Preliminary Study of Diffusion Kurtosis Imaging in Mild Traumatic Brain Injury. *Iranian Journal of Radiology*, 15(3):1–10, 2018. doi:10.5812/iranjradiol.56115.Research.

[125] Hutchinson EB, Schwerin SC, Avram AV, Juliano SL, and Pierpaoli C. Diffusion MRI and the detection of alterations following traumatic brain injury. *Journal of Neuroscience Research*, 96(4):612–625, 2018. doi:10.1002/jnr.24065.

[126] Chung S, Fieremans E, Wang X, Kucukboyaci NE, Morton CJ, Babb J, Amorapanth P, Foo FYA, Novikov DS, Flanagan SR, Rath JF, and Lui YW. White Matter Tract Integrity: An Indicator of Axonal Pathology after Mild Traumatic Brain Injury. *Journal of Neurotrauma*, 35(8):1015–1020, 2018. doi:10.1089/neu.2017.5320.

[127] Grossman EJ, Kirov II, Gonen O, Novikov DS, Davitz MS, Lui YW, Grossman RI, Inglese M, and Fieremans E. N-acetylaspartate levels correlate with intra-axonal compartment parameters from diffusion MRI. *NeuroImage*, 118:334–343, 2015. doi:10.1016/j.neuroimage.2015.05.061.

[128] de Kouchkovsky I, Fieremans E, Fleysher L, Herbert J, Grossman RI, and Inglese M. Quantification of normal-appearing white matter tract integrity in multiple sclerosis: a diffusion kurtosis imaging study. *Journal of Neurology*, 263(6):1146–1155, 2016. doi:10.1007/s00415-016-8118-z.

[129] Lazar M, Miles LM, Babb JS, and Donaldson JB. Axonal deficits in young adults with High Functioning Autism and their impact on processing speed. *NeuroImage: Clinical*, 4:417–425, 2014. doi:10.1016/j.nicl.2014.01.014.

[130] Fieremans E, Benitez A, Jensen JH, Falangola MF, Tabesh A, Deardorff RL, Spampinato MVS, Babb JS, Novikov DS, Ferris SH, and Helpern JA. Novel White Matter Tract Integrity Metrics

Sensitive to Alzheimer Disease Progression. *American Journal of Neuroradiology*, 34(11):2105–2112, 2013. doi:10.3174/ajnr.A3553.

[131] Kelm ND, West KL, Carson RP, Gochberg DF, Ess KC, and Does MD. Evaluation of diffusion kurtosis imaging in ex vivo hypomyelinated mouse brains. *NeuroImage*, 124:612–626, 2016. doi:10.1016/j.neuroimage.2015.09.028.

[132] Guglielmetti C, Veraart J, Roelant E, Mai Z, Daans J, Van Audekerke J, Naeyaert M, Vanhoutte G, Delgado y Palacios R, Praet J, Fieremans E, Ponsaerts P, Sijbers J, Van der Linden A, and Verhoye M. Diffusion kurtosis imaging probes cortical alterations and white matter pathology following cuprizone induced demyelination and spontaneous remyelination. *NeuroImage*, 125: 363–377, 2016. doi:10.1016/j.neuroimage.2015.10.052.

[133] Jelescu IO, Zurek M, Winters KV, Veraart J, Rajaratnam A, Kim NS, Babb JS, Shepherd TM, Novikov DS, Kim SG, and Fieremans E. In vivo quantification of demyelination and recovery using compartment-specific diffusion MRI metrics validated by electron microscopy. *NeuroImage*, 132:104–114, 2016. doi:10.1016/j.neuroimage.2016.02.004.

[134] Veraart J, Fieremans E, and Novikov DS. Diffusion MRI noise mapping using random matrix theory. *Magnetic Resonance in Medicine*, 76(5):1582–1593, 2016. doi:10.1002/mrm.26059.

[135] Veraart J, Novikov DS, Christiaens D, Ades-aron B, Sijbers J, and Fieremans E. Denoising of diffusion MRI using random matrix theory. *NeuroImage*, 142:394–406, 2016. doi:10.1016/j.neuroimage.2016.08.016.

[136] Leemans A, Jeurissen B, Sijbers J, and Jones D. ExploreDTI: a graphical toolbox for processing, analyzing, and visualizing diffusion MR data. *Proc Intl Soc Mag Reson Med*, 17:3537, 2009.

[137] Veraart J, Sijbers J, Sunaert S, Leemans A, and Jeurissen B. Weighted linear least squares estimation of diffusion MRI parameters: strengths, limitations, and pitfalls. *NeuroImage*, 81:335–346, 2013. doi:10.1016/j.neuroimage.2015.10.052.

[138] Veraart J, Poot DHJ, Van Hecke W, Blockx I, Van der Linden A, Verhoye M, and Sijbers J. More accurate estimation of diffusion tensor parameters using diffusion kurtosis imaging. *Magnetic Resonance in Medicine*, 65(1):138–145, 2011. doi:10.1002/mrm.22603.

[139] Loening AM and Gambhir SS. AMIDE: A Free Software Tool for Multimodality Medical Image Analysis. *Molecular Imaging*, 2(3): 131–137, 2003. doi:10.1162/153535003322556877.

[140] Duricki DA, Soleman S, and Moon LDF. Analysis of longitudinal data from animals with missing values using SPSS. *Nature Protocols*, 11(6):1112–1129, 2016. doi:10.1038/nprot.2016.048.

[141] Qin Y, Xu GL, Li andXH, Sun ZY, Gu JW, and Gao FB. Brain structure alterations and cognitive impairment following repetitive mild head impact: An in vivo MRI and behavioral study in rat. *Behavioural Brain Research*, 340(9):41–48, 2018. doi:10.1016/j.bbr.2016.08.008.

[142] Yu F, Shukla DK, Armstrong RC, Marion CM, Radomski KL, Selwyn RG, and Dardzinski BJ. Repetitive Model of Mild Traumatic Brain Injury Produces Cortical Abnormalities Detectable by Magnetic Resonance Diffusion Imaging, Histopathology, and Behavior. *Journal of Neurotrauma*, 34(7):1364–1381, 2017. doi:10.1089/neu.2016.4569.

[143] Karlsen RH, Einarsen C, Moe HK, Håberg AK, Vik A, Skandsen T, and Eikenes L. Diffusion kurtosis imaging in mild traumatic brain injury and postconcussional syndrome. *Journal of Neuroscience Research*, 97(5):568–581, 2019. doi:10.1002/jnr.24383.

[144] Davenport EM, Apkarian K, Whitlow CT, Urban JE, Jensen JH, Szuch E, Espeland MA, Jung Y, Rosenbaum DA, Gioia GA, Powers AK, Stitzel JD, and Maldjian JA. Abnormalities in Diffusional Kurtosis Metrics Related to Head Impact Exposure in a Season of High School Varsity Football. *Journal of Neurotrauma*, 33(23):2133–2146, 2016. doi:10.1089/neu.2015.4267.

[145] Lancaster MA, Olson DV, McCrea MA, Nelson LD, LaRoche AA, and Muftuler LT. Acute white matter changes following sport-related concussion: A serial diffusion tensor and diffusion kurtosis

tensor imaging study. *Human Brain Mapping*, 37(11):3821–3834, 2016. doi:10.1002/hbm.23278.

[146] Lancaster MA, Meier TB, Olson DV, McCrea MA, Nelson LD, and Muftuler LT. Chronic differences in white matter integrity following sport-related concussion as measured by diffusion MRI: 6-Month follow-up. *Human Brain Mapping*, 39(11):4276–4289, 2018. doi:10.1002/hbm.24245.

[147] DeWitt DS, Perez-Polo R, Hulsebosch CE, Dash PK, and Robertson CS. Challenges in the Development of Rodent Models of Mild Traumatic Brain Injury. *Journal of Neurotrauma*, 30(9): 688–701, 2013. doi:10.1089/neu.2012.2349.

[148] Yamamoto S, Levin HS, and Prough DS. Mild, moderate and severee: terminology implications for clinical and experimental traumatic brain injury. *Current Opinion in Neurology*, 31(6):672–680, 2018. doi:10.1097/WCO.0000000000000624.

[149] Thibo Billiet, Mathieu Vandenbulcke, Burkhard Mädler, Ronald Peeters, Thijs Dhollander, Hui Zhang, Sabine Deprez, Bea R H Van den Bergh, Stefan Sunaert, and Louise Emsell. Age-related microstructural differences quantified using myelin water imaging and advanced diffusion MRI. *Neurobiology of Aging*, 36(6):2107–2121, 2015. ISSN 15581497. doi:10.1016/j.neurobiolaging.2015.02.029. URL `http://dx.doi.org/10.1016/j.neurobiolaging.2015.02.029`.

[150] Lebel C, Gee M, Camicioli R, Wieler M, Martin W, and Beaulieu C. Diffusion tensor imaging of white matter tract evolution over the lifespan. *NeuroImage*, 60(1):340–352, 2012. doi:10.1016/j.neuroimage.2011.11.094.

[151] Lebel C, Treit S, and Beaulieu C. A review of diffusion MRI of typical white matter development from early childhood to young adulthood. *NMR in Biomedicine*, page e3778, 2017. doi:10.1002/nbm.3778.

[152] De Santis S, Drakesmith M, Bells S, Assaf Y, and Jones DK. Why diffusion tensor MRI does well only some of the time:

Variance and covariance of white matter tissue microstructure attributes in the living human brain. *NeuroImage*, 89:35–44, 2014. doi:10.1016/j.neuroimage.2013.12.003.

[153] Szczepankiewicz F, Lätt J, Wirestam R, Leemans A, Sundgren P, van Westen D, Ståhlberg F, and Nilsson M. Variability in diffusion kurtosis imaging: Impact on study design, statistical power and interpretation. *NeuroImage*, 76:145–154, 2013. doi:10.1016/j.neuroimage.2013.02.078.

[154] Green REA. Editorial: Brain Injury as a Neurodegenerative Disorder. *Frontiers in Human Neuroscience*, 9(1):9–11, 2016. doi:10.3389/fnhum.2015.00615.

[155] DeKosky ST and Asken BM. Injury cascades in TBI-related neurodegeneration. *Brain Injury*, 31(9):1177–1182, 2017. doi:10.1080/02699052.2017.1312528.

[156] McDonald S, Dalton KI, Rushby JA, and Landin-Romero R. Loss of white matter connections after severe traumatic brain injury (TBI) and its relationship to social cognition. *Brain Imaging and Behaviour*, pages 1–11, 2018. doi:10.1007/s11682-018-9906-0.

[157] Haberg AK, Olson A, Moen KG, Schirmer-Mikalsen K, Visser E, Finnanger TG, Evensen KAI, Skandsen T, Vik A, and Eikenes L. White Matter Microstructure in Chronic Moderate-To-Severe Traumatic Brain Injury: Impact of Acute-Phase Injury-Related Variables and Associations With Outcome Measures. *Journal of Neuroscience Research*, pages 1109–1126, 2015. doi:10.1002/jnr.23534.

[158] Gajamange S, Raffelt D, Dhollander T, Lui E, van der Walt A, Kilpatrick T, Fielding J, Connelly A, and Kolbe S. Fibre-specific white matter changes in multiple sclerosis patients with optic neuritis. *NeuroImage: Clinical*, 17:60–68, 2018. doi:10.1016/j.nicl.2017.09.027.

[159] Mito R, Raffelt D, Dhollander T, Vaughan DN, Tournier JD, Salvado O, Brodtmann A, Rowe CC, Villemagne VL, and Connelly A. Fibre-specific white matter reductions in Alzheimer's disease

and mild cognitive impairment. *Brain*, 141(3):888–902, 2018. doi:10.1093/brain/awx355.

[160] Verhelst H. *Training-related changes in cognitive abilities and neural plasticity in children with traumatic brain injury.* PhD thesis, Ghent University, 2018.

[161] Wright DK, Johnston LA, Kershaw J, Ordidge R, O'Brien TJ, and Shultz SR. Changes in Apparent Fiber Sensity and Track-Weighted Imaging Metrics in White Matter following Experimental Traumatic Brain Injury. *Journal of Neurotrauma*, 34:2109–2118, 2017. doi:10.1089/neu.2016.4730.

[162] Dhollander T, Raffelt D, and Connelly A. Unsupervised 3-tissue response function estimation from single-shell or multi-shell diffusion mr data without a co-registered t1 image. page 5, 2016.

[163] Dhollander T, Raffelt D, and Connelly A. Accuracy of response function estimation algorithms for 3-tissue spherical deconvolution of diverse quality diffusion mri data. page 1569, 2018.

[164] Jeurissen B, Tournier JD, Dhollander T, Connelly A, and Sijbers J. Multi-tissue constrained spherical deconvolution for improved analysis of multi-shell diffusion MRI data. *NeuroImage*, 103:411–426, 2014. doi:10.1016/j.neuroimage.2014.07.061.

[165] Sinke MRT, Otte WM, Christiaens D, Schmitt O, Leemans A, van der Toorn A, Sarabdjitsingh A, Joëls M, and Dijkhuizen RM. Diffusion MRI-based cortical connectome reconstruction: dependency on tractography procedures and neuroanatomical characteristics. *Brain Structure & Function*, 223(5):2269—-2285, 2018. doi:10.1007/s00429-018-1628-y.

[166] Smith RE, Tournier JD, Calamante F, and Connelly A. SIFT: Spherical-deconvolution informed filtering of tractograms. *NeuroImage*, 67:298–312, 2013. doi:10.1016/j.neuroimage.2012.11.049.

[167] Smith RE, Tournier JD, Calamante F, and Connelly A. SIFT2: Enabling dense quantitative assessment of brain white matter

connectivity using streamlines tractography. *NeuroImage*, 119: 338–351, 2015. doi:10.1016/j.neuroimage.2015.06.092.

[168] Smith SM and Nichols TE. Threshold-free cluster enhancement: addressing problems of smoothing, threshold dependence and localisation in cluster inference. *NeuroImage*, 44(1):83–98, 2009. doi:10.1016/j.neuroimage.2008.03.061.

[169] Hunter LE, Lubin N, Glassman NR, Xue X, Spira M, and Lipton ML. Comparing Region of Interest Versus Voxel-Wise Diffusion Tensor Imaging Analytic Methods in Mild and Moderate Traumatic Brain Injury: A Systematic Review and Meta-Analysis. *Journal of Neurotrauma*, 35:1–9, 2018. doi:10.1089/neu.2018.5838.

[170] Alruwaili AR, Pannek K, Henderson RD, Gray M, Kurniawan ND, and McCombe PA. Tract integrity in amyotrophic lateral sclerosis: 6–month evaluation using MR diffusion tensor imaging. *BMC Medical Imaging*, 19:1–10, 2019. doi:10.1186/s12880-019-0319-3.

[171] Krafft C and Popp J. The many facets of Raman spectroscopy for biomedical analysis. *Analytical and Bioanalytical Chemistry*, 407 (3):699–717, 2015. doi:10.1007/s00216-014-8311-9.

[172] Jermyn M, Mok K, Mercier J, Desroches J, Pichette J, Saint-Arnaud K, Bernstein L, Guiot MC, Petrecca K, and Leblond F. Intraoperative brain cancer detection with Raman spectroscopy in humans. *Science Translational Medicine*, 7(274):27ra19, 2015. doi:10.1126/scitranslmed.aaa2384.

[173] Morisaki S, Ota C, Matsuda K, Kaku N, Fujiwara H, Oda R, Ishibashi H, Kubo T, and Kawata M. Application of Raman spectroscopy for visualizing biochemical changes during peripheral nerve injury in vitro and in vivo. *Journal of Biomedical Optics*, 18(11):116011, 2013. doi:10.1117/1.JBO.18.11.116011.

[174] Surmacki JM, Ansel-Bollepalli L, Pischiutta F, Zanier ER, Ercole A, and Bohndiek SE. Label-free monitoring of tissue biochemistry following traumatic brain injury using Raman spectroscopy. *Analyst*, 142:132–139, 2017. doi:10.1039/C6AN02238C.

[175] Paxinos G and Watson C. *The rat brain in stereotaxic coordinates*. Elsevier, 6 edition, 2007.

[176] Beleites CSV. Hyperspec: A package to handle hyperspectral data sets in r. `http://hyperspec.r-forge.r-project.org`, 2013. R package version 0.98-20130516.

[177] Eilers PHC and Boelens HFM. Baseline correction with asymmetric least squares smoothing. `https://zanran_storage.s3.amazonaws.com/www.science.uva.nl/ContentPages/443199618.pdf`, 2005.

[178] Gibb S and Strimmer K. MALDIquant: a versatile R package for the analysis of mass spectrometry data. *Bioinformatics*, 28(17): 2270–2271, 2012. doi:10.1093/bioinformatics/bts447.

[179] McDonald JH. Multiple comparisons. In *Handbook of Biological Statistics*, pages 254–263. Sparky House Publishing, 2014.

[180] Siedler DG, Chuah MI, Kirkcaldie MTK, Vickers JC, and King AE. Diffuse axonal injury in brain trauma: insights from alterations in neurofilaments. *Frontiers in Cellular Neuroscience*, 8: 1–10, 2014. doi:10.3389/fncel.2014.00429.

[181] Johnson VE, Stewart W, and Smith DH. Axonal pathology in traumatic brain injury. *Experimental Neurology*, 246:35–43, 2013. doi:10.1016/j.expneurol.2012.01.013.

[182] Burda JE, Bernstein AM, and Sofroniew MV. Astrocyte roles in traumatic brain injury. *Experimental Neurology*, 275:305–315, 2016. doi:10.1016/j.expneurol.2015.03.020.

[183] Lipton ML, Kim N, Park YK, Hulkower MB, Gardin TM, Shifteh K, Kim M, Zimmerman ME, Lipton RB, and Branch CA. Robust detection of traumatic axonal injury in individual mild traumatic brain injury patients: Intersubject variation, change over time and bidirectional changes in anisotropy. *Brain Imaging and Behavior*, 6(2):329–342, 2012. doi:10.1007/s11682-012-9175-2.

[184] Harris NG, Verley DR, Gutman BA, and Sutton RL. Bi-directional changes in fractional anisotropy after experiment TBI: Disorganization and reorganization? *NeuroImage*, 133:129–143, 2016. doi:10.1016/j.neuroimage.2016.03.012.

[185] Shandra O, Winemiller AR, Heithoff BP, Munoz-Ballester C, and Robel S. Repetitive Diffuse Mild Traumatic Brain Injury Causes an Atypical Astrocyte Response and Spontaneous Recurrent Seizures. *The Journal of Neuroscience*, 39(10):1944 –1963, 2019.

[186] Wang J, Lin K, Zheng W, Ho KY, Teh M, Yeoh KG, and Huang Z. Simultaneous fingerprint and high- wavenumber fiber-optic Raman spectroscopy improves in vivo diagnosis of esophageal squamous cell carcinoma at endoscopy. *Scientific Reports*, 5:12957, 2015. doi:10.1038/srep12957.

[187] Korley FK, Kelen GD, Jones CM, and Diaz-Arrastia R. Emergency Department Evaluation of Traumatic Brain Injury in the United States, 2009–2010. *Journal of Head Trauma Rehabilitation*, 31(6):379–387, 2016. doi:10.1097/HTR.0000000000000187.

[188] Peeters W, van den Brande R, Polinder S, Brazinova A, Steyerberg EW, Lingsma HF, and Maas AIR. Epidemiology of traumatic brain injury in Europe. *Acta Neurochirurgica*, 157(10):1683–1696, 2015. doi:10.1007/s00701-015-2512-7.

[189] Castaño Leon AM, Cicuendez M, Navarro B, Munarriz PM, Cepeda S, Paredes I, Hilario A, Ramos A, Gómez PA, and Lagares A. What Can Be Learned from Diffusion Tensor Imaging from a Large Traumatic Brain Injury Cohort?: White Matter Integrity and Its Relationship with Outcome. *Journal of Neurotrauma*, 2376:neu.2018.5691, 2018. doi:10.1089/neu.2018.5691.

[190] Leunissen I, Coxon JP, Caeyenberghs K, Michiels K, Sunaert S, and Swinnen SP. Task switching in traumatic brain injury relates to cortico-subcortical integrity. *Human Brain Mapping*, 35(5): 2459–2469, 2014. doi:10.1002/hbm.22341.

[191] Caeyenberghs K, Leemans A, Leunissen I, Gooijers J, Michiels K, Sunaert S, and Swinnen SP. Altered structural networks and executive deficits in traumatic brain injury patients. *Brain Structure and Function*, 219(1):193–209, 2014. doi:10.1007/s00429-012-0494-2.

[192] Kim J, Parker D, Whyte J, Hart T, Pluta J, Ingalhalikar M, Coslett HB, and Verma R. Disrupted Structural Connectome Is Associated with Both Psychometric and Real-World Neuropsychological Impairment in Diffuse Traumatic Brain Injury. *Journal of the International Neuropsychological Society*, 20(9):887–896, 2014. doi:10.1017/S1355617714000812.

[193] Solmaz B, Tunç B, Parker D, Whyte J, Hart T, Rabinowitz A, Rohrbach M, Kim J, and Verma R. Assessing connectivity related injury burden in diffuse traumatic brain injury. *Human Brain Mapping*, 38(6):2913–2922, 2017. doi:10.1002/hbm.23561.

[194] Cicerone KD, Dahlberg C, Malec JF, Langenbahn DM, Felicetti T, Kneipp S, Ellmo W, Kalmar K, Giacino JT, Harley JP, Morse L, Laatschand PA, and Catanese J. Evidence-based cognitive rehabilitation: updated review of the literature from 1998 through 2002. *Archives of physical medicine and rehabilitation*, 86(8):1681–92, 2005. doi:10.1016/j.apmr.2005.03.024.

[195] Radabaugh HL, LaPorte MJ, Greene AM, Bondi CO, Lajud N, and Kline AE. Refining environmental enrichment to advance rehabilitation based research after experimental traumatic brain injury. *Experimental Neurology*, 294:12–18, 2017. doi:10.1016/j.expneurol.2017.04.013.

[196] Blumenfeld-Katzir T, Pasternak O, Dagan M, and Assaf Y. Diffusion MRI of Structural Brain Plasticity Induced by a Learning and Memory Task. *PLoS ONE*, 6(6):e20678, 2011. doi:10.1371/journal.pone.0020678.

[197] Sagi Y, Tavor I, Hofstetter S, Tzur-Moryosef S, Blumenfeld-Katzir B, and Assaf Y. Learning in the Fast Lane: New Insights into Neuroplasticity. *Neuron*, 73(6):1195–1203, 2012. doi:10.1016/j.neuron.2012.01.025.

[198] Hofstetter S, Tavor I, Tzur Moryosef S, and Assaf Y. Short-term learning induces white matter plasticity in the fornix. *The Journal of neuroscience : the official journal of the Society for Neuroscience*, 33(31):12844–50, 2013. doi:10.1523/JNEUROSCI.4520-12.2013.

[199] Hofstetter S and Assaf Y. The rapid development of structural plasticity through short water maze training: A DTI study. *NeuroImage*, 155:202–208, 2017. doi:10.1016/j.neuroimage.2017.04.056.

[200] Scholz J, Niibori Y, Franklandl PW, and JP Lerch. Rotarod training in mice is associated with changes in brain structure observable with multimodal MRI. *NeuroImage*, 107:182–189, 2015. doi:10.1016/j.neuroimage.2014.12.003.

[201] Sampaio-Baptista C, Khrapitchev AA, Foxley S, Schlagheck T, Scholz J, Jbabdi S, DeLuca GC, Miller KL, Taylor A, Thomas N, Kleim J, Sibson NR, Bannerman D, and Johansen-Berg H. Motor Skill Learning Induces Changes in White Matter Microstructure and Myelination. *Journal of Neuroscience*, 33(50):19499–19503, 2013. doi:10.1523/JNEUROSCI.3048-13.2013.

[202] Bussey TJ, Padain TL, Skillings EA, Winters BD, Morton AJ, and Saksida LM. The touchscreen cognitive testing method for rodents: how to get the best out of your rat. *Learning & memory (Cold Spring Harbor, N.Y.)*, 15(7):516–523, 2008. doi:10.1101/lm.987808.

[203] Salmond CH, Menon DK, Chatfield DA, Williams GB, Pena A, Sahakian BJ, and Pickard JD. Diffusion tensor imaging in chronic head injury survivors: correlations with learning and memory indices. *NeuroImage*, 29(1):117–124, 2006. doi:10.1016/j.neuroimage.2005.07.012.

[204] Kim CH, Heath CJ, Kent BA, Bussey TJ, and Saksida LM. The role of the dorsal hippocampus in two versions of the touchscreen automated paired associates learning (PAL) task for mice. *Psychopharmacology*, 232(21-22):3899–3910, 2015. doi:10.1007/s00213-015-3949-3.

[205] Mychasiuk R, Hehar H, and Esser MJ. A mild traumatic brain injury (mTBI) induces secondary attention-deficit hyperactivity disorder-like symptomology in young rats. *Behavioural Brain Research*, 286:285–292, 2015. doi:10.1016/j.bbr.2015.03.010.

[206] Vonder Haar C, Lam FCW, Adams WK, Riparip LK, Kaur S, Muthukrishna M, Rosi S, and Winstanley CA. Frontal Traumatic Brain Injury in Rats Causes Long-Lasting Impairments in Impulse Control That Are Differentially Sensitive to Pharmacotherapeutics and Associated with Chronic Neuroinflammation. *ACS Chemical Neuroscience*, 7(11):1531–1542, 2016. doi:10.1021/acschemneuro.6b00166.

[207] Bussey TJ, Holmes A, Lyon L, Mar AC, McAllister KAL, Nithianantharajah J, Oomen CA, and Saksida LM. New translational assays for preclinical modelling of cognition in schizophrenia: the touchscreen testing method for mice and rats. *Neuropharmacology*, 62(3):1191–203, 2012. doi:10.1016/j.neuropharm.2011.04.011.

[208] Shepherd A, Tyebji S, Hannan AJ, and Burrows EL. Translational Assays for Assessment of Cognition in Rodent Models of Alzheimer's Disease and Dementia. *Journal of Molecular Neuroscience*, 60(3):371–382, 2016. doi:10.1007/s12031-016-0837-1.

[209] Campden Instruments. 89541R- Paired Associates Learning (PAL) Task for Rat Touch Screen Systems and ABET II. In *Instruction Manual*, pages 1–49. Lafayette Instrument Company, Lafayette, IN, 2011.

[210] Campden Instruments. 89551-R - The Continuous Performance Test with images (image CPT / rCPT) for Rat Touch Screen Systems and ABET II. In *Instruction Manual*, pages 1–93. Lafayette Instrument Company, Lafayette, IN, 2013.

[211] Bari A, Dalley JW, and Robbins TW. The application of the 5-choice serial reaction time task for the assessment of visual attentional processes and impulse control in rats. *Nature protocols*, 3(5):759–767, 2008. doi:10.1038/nprot.2008.41.

[212] Mar AC, Horner AE, Nilsson SRO, Alsiö J, Kent BA, Kim CH, Holmes A, Saksida LM, and Bussey TJ. The touchscreen operant platform for assessing executive function in rats and mice. *Nature protocols*, 8(10):1985–2005, 2013. doi:10.1038/nprot.2013.123.

[213] Kellner E, Dhital B, Kiselev VG, and Reisert M. Gibbs-ringing artifact removal based on local subvoxel-shifts. *Magnetic Resonance in Medicine*, 76(5):1574–1581, 2016. doi:10.1002/mrm.26054.

[214] Braeckman K, Descamps B, Pieters L, Vral A, Caeyenberghs K, and Vanhove C. Dynamic changes in hippocampal diffusion and kurtosis metrics following experimental mTBI correlate with glial reactivity. *NeuroImage: Clinical*, 21:101669, 2019. doi:10.1016/j.nicl.2019.101669.

[215] Metzler-Baddeley C, Foley S, de Santis S, Charron C, Hampshire A, Caeyenberghs K, and Jones DK. Dynamics of White Matter Plasticity Underlying Working Memory Training: Multimodal Evidence from Diffusion MRI and Relaxometry. *Journal of Cognitive Neuroscience*, 29(2):1509–1520, 2017. doi:10.1162/jocn_a_01127.

[216] de Lange AG, ACS Brathen, Rohani DA, Grydeland H, Fjell AM, and Walhovd KB. The Effects of Memory Training on Behavioral and Microstructural Plasticity in Young and Older Adults. *Human Brain Mapping*, 38:5666–5680, 2017. doi:10.1002/hbm.23756.

[217] Bonzano L, Tacchino A, Brichetto G, Roccatagliata L, Dessypris A, Feraco P, Lopes De Carvalho ML, Battaglia MA, Mancardi GL, and Bove M. Upper limb motor rehabilitation impacts white matter microstructure in multiple sclerosis. *NeuroImage*, 90:107–116, 2014. doi:10.1016/j.neuroimage.2013.12.025.

[218] Chung S, Fieremans E, Kucukboyaci NE, Wang X, Morton CJ, Novikov DS, Rath JF, and Lui YW. Working Memory And Brain Tissue Microstructure: White Matter Tract Integrity Based On Multi-Shell Diffusion MRI. *Scientific Reports*, 8:3175, 2018. doi:10.1038/s41598-018-21428-4.

[219] Chudasama Y, Passetti F, Rhodes SEV, Lopian D, Desai A, and Robbins TW. Dissociable aspects of performance on the 5-choice serial reaction time task following lesions of the dorsal anterior cingulate, infralimbic and orbitofrontal cortex in the rat: differential effects on selectivity, impulsivity and compulsivity. *Behavioural Brain Research*, 146:105–119, 2003. doi:10.1016/j.bbr.2003.09.020.

[220] Hvoslef-Eide M, Nilsson SRO, Hailwood JM, Robbins TW, Saksida LM, Mar AC, and Bussey TJ. Effects of anterior cingulate cortex lesions on a continuous performance task for mice. *Brain and Neuroscience Advances*, 2:1–12, 2018. doi:10.1177/2398212818772962.

[221] Barbelivien A, Ruotsalainen S, and Sirvio J. Metabolic Alterations in the Prefrontal and Cingulate Cortices are Related to Behavioral Deficits in a Rodent Model of Attention-deficit Hyperactivity Disorder. *Cerebral Cortex*, 11:1056–1063, 2001. doi:10.1093/cercor/11.11.1056.

[222] Han K, Chapman SB, and Krawczyk DC. Neuroplasticity of cognitive control networks following cognitive training T for chronic traumatic brain injury. *NeuroImage : Clinical*, 18:262–278, 2018. doi:10.1016/j.nicl.2018.01.030.

[223] Yuan W, Treble-Barna A, Sohlberg MM, Harn B, and Wade SL. Changes in Structural Connectivity Following a Cognitive Intervention in Children With Traumatic Brain Injury: A Pilot Study. *Neurorehabilitation and Neural Repair*, 31(2):190–201, 2017. doi:10.1177/1545968316675430.

[224] Fan Y, Lin K, Liu H, Chen Y, and Wu C. Changes in structural integrity are correlated with motor and functional recovery after post-stroke rehabilitation. *Restorative Neurology and Neuroscience*, 33:835–844, 2015. doi:10.3233/RNN-150523.

[225] Bhandari J, Daya R, and Mishra RK. Improvements and important considerations for the 5-choice serial reaction time task - An effective measurement of visual attention in rats. *Journal of Neuroscience Methods*, 270:17–29, 2016. doi:10.1016/j.jneumeth.2016.06.002.

[226] Hyder AA, Wunderlich CA, Puvanachandraa P, Gururajc G, and Kobusingye OC. The impact of traumatic brain injuries: A global perspective. *Neurorehabilitation*, 22:341—353, 2007. doi:10.1007/s00429-018-1628-y.

[227] Tosetti P, Hicks RR, Theriault E, Phillips A, Koroshetz W, and Draghia-Akli R. Toward an International Initiative for Traumatic Brain Injury Research. *Journal of Neurotrauma*, 30:1211—1222, 2013. doi:10.1089/neu.2013.2896.

[228] Project overview. `https://www.center-tbi.eu/project/overview`, 2019. Accessed: 2019-05-09.

[229] Meconi A, Wortman RC, Wright DK, Neale KJ, Clarkson M, Shultz SR, and Christie BR. Repeated mild traumatic brain injury can cause acute neurologic impairment without overt structural damage in juvenile rats. *PLoS ONE*, 13(5):e0197187, 2018. doi:10.1371/journal.pone.0197187.

[230] Archer DP, McCann SK, Walker AM, Premji ZA, Rogan KJ, Hutton MJH, and Gray LJ. Neuroprotection by anaesthetics in rodent models of traumatic brain injury: a systematic review and network meta-analysis. *British Journal of Anaesthesia*, 121(6): 1272e1281, 2018. doi:10.1016/j.bja.2018.07.024.

[231] Palacios EM, Martin AJ, Boss MA, Ezekiel F, Chang YS, Yuh EL, Vassar MJ, Schnyer DM, MacDonald CL, Crawford KL, Irimia A, Toga AW, and P Mukherjee. Toward Precision and Reproducibility of Diffusion Tensor Imaging: A Multicenter Diffusion Phantom and Traveling Volunteer Study. *American Journal of Neuroradiology*, 38:537–545. doi:10.3174/ajnr.A5025.

[232] Veenith TV, Carter E, Grossac J, Newcombe VFJ, Outtrim JG, Lupson V, Williams GB, Menon DK, and Coles JP. Inter Subject Variability and Reproducibility of Diffusion Tensor Imaging within and between Different Imaging Sessions. *Plos ONE*, 8:e65941. doi:10.1371/journal.pone.0065941.

[233] Brander A, Kataja A, Saastamoinen A, Ryymin P, Huhtala H, J Ohman, Soimakallio S, and Dastidar P. Diffusion tensor imaging

of the brain in a healthy adult population: Normative values and measurement reproducibility at 3 T and 1.5 T. *Acta Neuroradiologica*, pages 800–807, 2013. doi:10.3109/02841851.2010.495351.

[234] de la Rosa E, Sima DM, Vande Vyvere T, Kirschke JS, and Menze B. A radiomics approach to traumatic brain injury prediction in ct scans. 11 2018.